Prediction of oxide spallation during high temperature oxidation of alloys by using machine learning

Jularak Rojsanga

Teeratat Promchan

Advisor

Asst. Prof. Dr. Patthranit Wongpromrat

A Report Submitted in Partial Fulfillment of the Requirement for the Degree of Bachelor of Engineering (Petrochemical Engineering) Department of Chemical Engineering, School of Engineering, King Mongkut's Institute of Technology Ladkrabang Academic Year 2022

การทำนายการหลุดร่อนของออกไซด์ระหว่างการเกิดออกซิเดชันที่อุณหภูมิสูงของโลหะผสมโดยใช้การเรียนรู้ของเครื่อง

จุฬารักษ์ โรจน์สง่า

ธีรทัต พรมจรรย์

ผศ.ดร.ภัทรานิษฐ์ วงศ์พร้อมรัตน์

ปริญญานิพนธ์นี้เป็นส่วนหนึ่งของการศึกษาตามหลักสูตร

วิศวกรรมศาสตรบัณฑิต สาขาวิชาวิศวกรรมปิโตรเคมี

ภาควิชาวิศวกรรมเคมี คณะวิศวกรรมศาสตร์

สถาบันเทคโนโลยีพระจอมเกล้าเจ้าคุณทหารลาดกระบัง

ปีการศึกษา 2565

Title	Prediction of oxide spallation during high temperature oxidation of alloys using machine learning
By	Julark Rojsanga Teeratat Promchan
Field of study	Petrochemical Engineering
Advisor	Asst. Prof. Dr. Patthranit Wongpromrat
Co-advisor	Asst. Prof. Dr. Amata Anantpinijwatna

Accepted by the Faculty of Engineering, King Mongkut's Institute of Technology Ladkrabang in Partial Fulfillment of the Requirements for the Degree of Bachelor of Engineering (Petrochemical Engineering).

Thesis Committee

_____ Chairman

(Asst. Prof. Dr. Patthranit Wongpromrat)

_____ Committee

(Asst. Prof. Dr. Natthanon Phaiboonsilpha)

_____ Committee

(Asst. Prof. Dr. Pornsawan Assawasaengrat)

Report Title	Prediction of oxide spallation during high temperature oxidation of alloys by using machine learning
By	Julark Rojsanga Teeratat Promchan
Degree	Bachelor of Engineering
Program	Petrochemical Engineering
Year	2022
Advisor	Asst. Prof. Dr. Patthranit Wongpromrat
Co-advisor	Asst. Prof. Dr. Amata Anantpinijwatna

Abstract

High-temperature corrosion of alloy is a main problem in many industries. One of the failure form is the cracking or spallation of self-protective oxide film due to the stress development from the oxidation process and thermal stress from the different thermal expansion of oxide and alloy. Conventionally, Pilling-Bedworth ratio (PBR) which has been developed to describe the effect of the difference between the volume changes of oxides and metals during the oxidation, is used to predict the cracking of self-protective oxide film. However, the crystal structures and the formation of oxides of alloy are different from metals: Applying the PBR in alloy causes an inaccuracy of the prediction of self-protective oxide film stress generation. The problem of the PBR ratio led to this work that focuses on using machine learning to predict the cracking of the self-protective oxide films of alloys at the temperatures between 200-1200 °C under various atmospheres. The model uses alloys' compositions, oxidation's conditions, and oxidation periods as the inputs to predict the oxidation rate of oxide films, the thermal expansion coefficient of the oxide films and alloys, and the spallation of the self-protective oxide films as the outputs.

เรื่อง	การทำนายการหลุดร่อนของออกไซด์ระหว่างการเกิดออกซิเดชันที่อุณหภูมิสูงของโลหะผสมโดยใช้การเรียนรู้ของเครื่อง
โดย	จุฬารักษ์ โรจน์สง่า
	ธีรทัต พรมจรรย์
ปริญญา	วิศวกรรมศาสตรบัณฑิต
สาขาวิชา	วิศวกรรมปิโตรเคมี
ปีการศึกษา	2565
อาจารย์ที่ปรึกษา	ผศ.ดร.ภัทรานิษฐ์ วงศ์พร้อมรัตน์
อาจารย์ที่ปรึกษาร่วม	ผศ.ดร.อมตะ อนันต์พินิจวัฒนา

บทคัดย่อ

การกัดกร่อนที่อุณหภูมิสูงของโลหะผสมเป็นปัญหาหลักในอุตสาหกรรมมากมาย หนึ่งในปัญหาที่เกิดขึ้นคือการแตกหรือการหลุดร่อนของชั้นออกไซด์ที่ปกป้องตัวเอง (self-protective film) เนื่องจากเกิดความเครียดจากกระบวนการเกิดออกซิเดชันและการเกิดความเครียดทางความร้อนจากความแตกต่างของการขยายตัวทางความร้อนของออกไซด์และโลหะผสม โดยปกติแล้วอัตราส่วน Pilling-Bedworth ใช้อธิบายผลของความแตกต่างระหว่างปริมาตรที่เปลี่ยนแปลงของออกไซด์และโลหะผสมระหว่างเกิดออกซิเดชัน ซึ่งใช้ทำนายการแตกของชั้นออกไซด์ที่ปกป้องตัวเอง อย่างไรก็ตามด้วยโครงร่างผลึกและการเกิดออกไซด์ของโลหะผสมแตกต่างจากโลหะบริสุทธิ์ การนำเอาอัตราส่วน Pilling-Bedworth มาใช้กับโลหะผสมทำให้เกิดความไม่แม่นยำในการทำนายการเกิดความเครียดของชั้นออกไซด์ที่ปกป้องตัวเอง ดังนั้นปัญหาของอัตราส่วน Pilling-Bedworth นำไปสู่งานวิจัยนี้ซึ่งจะเจาะจงไปที่การใช้การเรียนรู้ของเครื่องเพื่อทำนายการแตกของชั้นออกไซด์ที่ปกป้องตัวเองของโลหะผสมที่อุณหภูมิ 200-1200 องศาเซลเซียส ภายใต้สภาวะที่หลากหลาย แบบจำลองจะป้อนข้อมูลองค์ประกอบของโลหะผสม สภาวะการเกิดออกซิเดชันและระยะเวลาออกซิเดชันเพื่อที่จะทำนายอัตราการเกิดออกซิเดชันของชั้นออกไซด์ ค่าสัมประสิทธิ์การขยายตัวทางความร้อนของชั้นออกไซด์และโลหะผสม และการหลุดร่อนของชั้นออกไซด์ที่ปกป้องตัวเอง

Acknowledgements

With the deepest gratitude, the author wishes to express their sincere gratefulness to Asst. Prof. Dr. Patthranit Wongpromrat and Asst. Prof. Dr. Amata Anantpinijwatna, Department of Chemical Engineering, School of Engineering for their fruitful guidance and perpetual supervision throughout this research. Their willingness to give their time so generously have been very much appreciated.

The author would also like to express their gratitude to their gratitude to Assist. Prof. Dr. Natthanon Phaiboonsilpha and Assist. Prof. Dr. Pornsawan Assawasaengrat for their valuable discussions, time, and great assistance with experiment guidelines and analysis of experimental results in this research, as well as for their helpful corrections for the final report.

I would like to thank the Department of Chemical Engineering at King Mongkut's Institute of Technology Ladkrabang for supporting the equipment, workspace, and other facility.

Finally, I am most grateful to my parents, my family, and my friends in the Department of Petrochemical Engineering for their suggestion, advice, support, and all the help they have provided throughout the period of this thesis.

Table of contents

List of Figures

List of Tables

Chapter 1
Introduction

1.1 Backgrounds of the research and its significant

Alloy is a composite material whose major component is metal. It has been used in various ways in industrials [1]. The alloy usually deploys at high-temperature conditions because of their resistance to high-temperature deteriorations. The high-temperature resistant properties of alloys come from the oxidation of some elements resulting in the production of the self-protective oxide film that prevents the metals from the environment. The contact between metals and the environments may leads to the corrosion of materials which leads to the cracks of the metals and alloys [1].

Spallation is breaking of the oxide film, cracking through the thickness of the oxide film. It occurs from changing temperatures during cooling and also from the differences of thermal expansion coefficients of oxide and metal or alloy that are mismatched, leading to cracking [2].

From the occurred spallation previously mentioned, the prediction of protection performance of the oxide films could be predicted by the Pilling-Bedworth ratio (PBR) expressed as the oxide and the metal volumes ratio. The volume change due to the formation of the oxide generates stress that may cause the oxide film cracking which leads to spallation of the oxide film. The PBR has been used to predict the stress development during the oxidation process since 1923 [3].

Originally PBR was established for the formation of a single type of oxide during the oxidation of metals which can be described by the simple kinetic equation, known as the parabolic rate law [4]. By considering the assumptions includes: 1) the oxide growth occurs by uncharged particles, 2) the diffusion coefficient is independent of the concentration, 3) the concentrations C(0) and C(L) in the interface regions (metal-oxide and oxide-gas, respectively) are independent of the film thickness, 4) film growth is a steady state phenomenon [5], 5) the metal oxides grow by diffusion of oxygen inward through the oxide layer to the metal, and 6) the possibility of plastic flow by the oxide or metal was not considered.

Although many investigators have shown that the oxidation of the protective materials follow a parabolic rate law over a wide range of temperatures for both pure metals and alloys [4]. Typically, the kinetics of oxidation during the early stages are parabolic behavior, but, after a period of time they are also possible to be logarithm or linear behavior above a certain thickness [6] which implies the cracking and then spallation of self-protection film. It was found that the PBR for the oxidation of alloys is not the same as those of metals. The PBR for the alloys are significantly different to the PBR for the metals because the oxidation of alloys is influenced by the crystal structure and lattice constants of the alloys [3]. When using this PBR with alloys that have many compositions, many types of oxide are possible to occur with different oxidation behavior. Also, not only the parabolic kinetics of oxidations, but also the

linear and logarithmic rates could be occurred. So, this PBR method is not practical for alloys with many compositions.

From various research in the field of high-temperature oxidation, there are many factors that cause spallation of oxide, such as alloy compositions, the conditions that the alloy is exposed, and time, these factors affect the rate of formation of oxide on the metal surface while expansions of the metal and the oxide due to high temperature operations are promoted. With a large number of independent variables, machine learning can be applied to this work and able to predict certain factors including predicting spallation as well as being able to analyze the importance of the prevailing variables. Machine learning algorithms are used to predict dependent variables using multiple independent variables as input datasets which can also describe the importance of each independent variable to the dependent variable. Therefore, we apply machine learning to this work.

In this study, applying machine learning to create a new prediction model to predict the oxide spallation during high temperature oxidation of alloys precisely. The experiment data is used from reliable sources. The modeling method from machine learning is studied before developing models for the prediction of parabolic rate constant, the type of oxide form on alloy surface, the thermal expansion coefficient of oxide and alloy, and the oxide spallation's of alloys.

1.2 Objectives

1) To predict the oxide spallation of alloy at high temperature with machine learning.
2) To predict the thermal expansion coefficient of alloy and oxide at high temperature with machine learning.
3) To find the value of the difference of thermal expansion coefficient of oxide and alloy that can cause spallation of oxide.

1.3 Scopes of work

1) To collect 5 types of alloys consisting of iron-based, nickel-based, cobalt-based, copper-based and titanium-based alloys which compose of up to 24 elements and collect the thermal expansion coefficients of alloys and oxides.
2) To predict the oxide spallation from the alloy surface at temperatures higher than 500 °C in oxidizing atmospheric condition by using machine learning model.
3) To predict of the thermal expansion coefficients of alloys and their oxides formed at the temperatures higher than 500 °C in oxidizing atmospheric condition by using machine learning model.
4) To study the prediction models, both classification and regression models, by using 4 machine learning algorithms including k-nearest neighbor, decision trees, random forest, and multi-layer perceptron.

5) To train and create the machine learning algorithm prediction models by using a python programming language from open-source data analysis library, Scikit-learn.

6) To evaluate performance of prediction model using coefficient of determination (R^2), mean absolute percentage error (MAPE), accuracy, and f1 score.

1.4 Expected outputs

1) A new prediction method that is able to predicts the spallation of oxide more accurately than the pilling bed-worth ratio method.

2) The value of the difference of thermal expansion coefficient of oxide and alloy that can cause spallation of oxide is attained.

Chapter 2
Theory and literature reviews

2.1 Alloy

Alloy is a metal mixture of chemical compositions. To be called alloy, it must contain at least 2 compositions or more. Alloy has great properties in strength, toughness, and hardness. It can endure high temperature operations more than pure metal. It has been used in various ways in industrial. And it is always used in various serious environment [1]. For example, brass is an alloy of copper and zine elements which can be corrosion resistant.

2.2 High temperature oxidation of alloy

In high temperature applications, the uses of alloy are more suitable than pure metal. At high temperature, oxidation can occur along various oxidation environments where the alloy can be destroyed, cracked and scale spalled [2].

2.2.1 Mechanical of oxidation reaction

Oxidation reaction occurs between metal or alloy and oxygen gas is shown in Eq. 2.1, where M is metal element and O is oxygen.

$$xM(s) + yO(g) = M_xO_y(s) \quad (2.1)$$

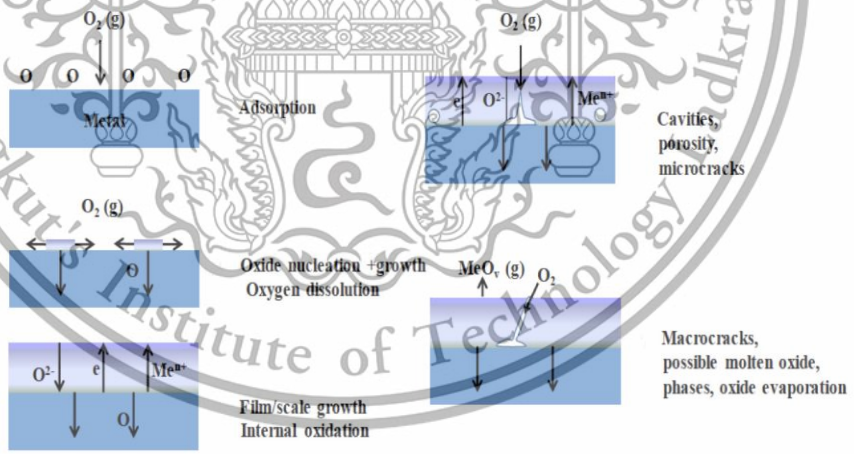

Figure 2.1 Illustration high temperature oxidation of metal and alloy **[7]**.

Oxidation reaction start with the adsorption of oxygen atom on the metal surface. Then, oxide film is formed on metal surface. In the growing of oxide film, porosity and microcrack are occurred which lead to the cracking and spallation. [8]

2.2.2 Kinetics of oxidation

To study the oxidation reaction, it is important to know kinetics of oxidation. Oxide scale can be formed on every surface of metal or alloy. Due to different oxide forming, it is necessary to consider kinetics of reaction that can reveal oxidation

behavior of the materials [2]. The oxidation kinetics can be categorized into 3 types which are logarithmic rate equation. Parabolic rate equation and linear rate equation.

2.2.2.1 Logarithmic rate equation

Commonly, this type of the kinetics is consistent to log temperature oxidation. To study the kinetics of logarithmic behavior, the metal is heated at low temperature around 300-400 °C. At the beginning, the reaction rate rises very fast and then slowdown [2]. The equations related to this type of oxidation are shown in Eqs. 2.2 and 2.3 where x is oxide thickness or weight gain per unit area, t, K and K_1 are time and rate constants for direct logarithmic and inverse logarithmic respectively.

Direct logarithmic $$x = K\log t + A \quad (2.2)$$

Inverse logarithmic $$\frac{1}{x} = B + K_1 \log t \quad (2.3)$$

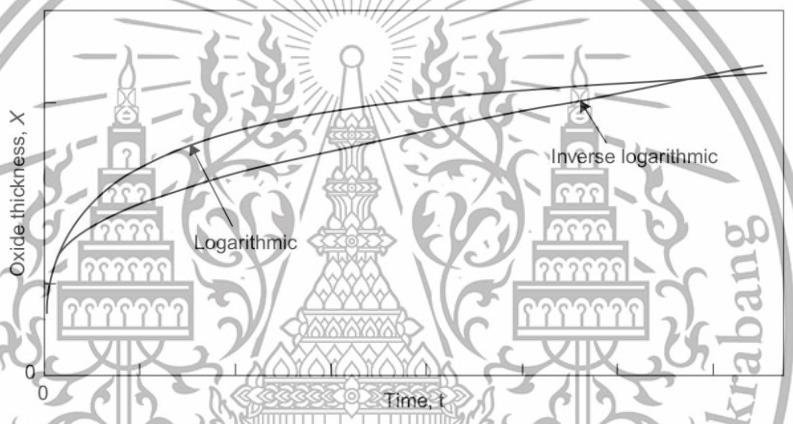

Figure 2.2 The logarithmic kinetics of oxidation.

2.2.2.2 Parabolic rate equation

Oxidation behaviors of several metals and alloys at high temperatures are parabolic as shown in Figure 2.3 [2]. The reaction rates decreases when oxide scale grows and the thickness of scale is increased. Parabolic rate can be equated into this equation.

$$\frac{dx}{dt} = \frac{k_p}{x} \quad (2.4)$$

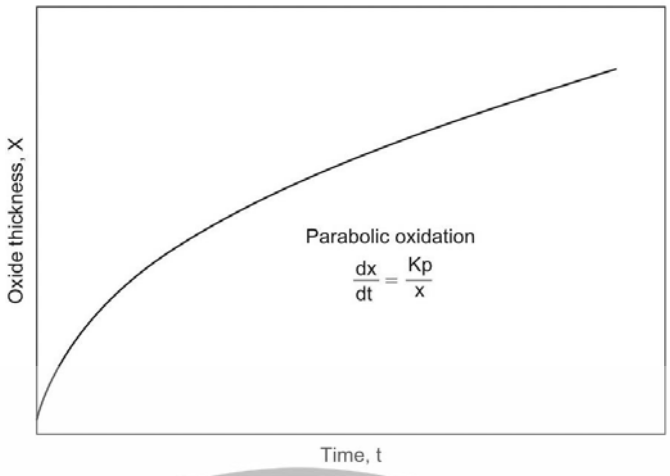

Figure 2.3 the kinetic of parabolic oxidation

After integrating, the equation will be

$$X^2 = k_p + C \tag{2.5}$$

where K_p is parabolic rate constant which implies the oxidation rate. From the Figure 2.3, the slope of graph and the rate of forming oxide film decrease when the time increases. The parabolic relation reveals the oxide protective diffusion formation and prevent further oxidation.

2.2.2.3 Linear rate equation

The linear equation is shown below [2].

$$X = kt \tag{2.6}$$

where k is linear rate constant. The oxidation rate is consistent with the linear relation. This oxidation behavior reveals that the preceding oxide formed cannot decelerate the further oxidation, hence it is not protective.

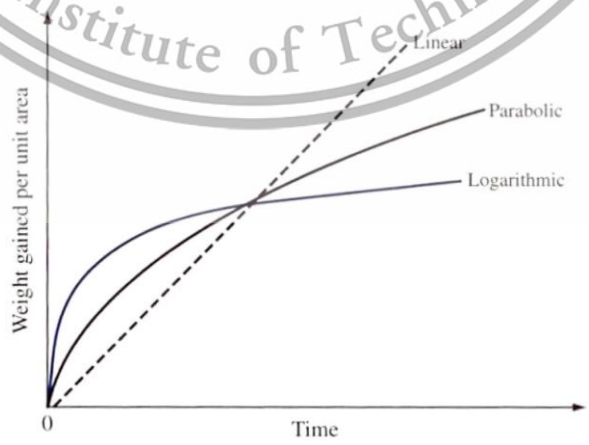

Figure 2.4 the kinetic of logarithmic, parabolic, and linear oxidation

2.2.3 Spallation

Spallation is breaking of the oxide film, cracking through the thickness of the oxide film. The main reason in spallation is stress generation. Generally, there are 2 types of stress. They are growth stress and thermal stress [3]. For growth stress, during occurring oxidation the thickness of scale increase, it leads to the crack. For thermal stress, when the metal is cooled from high temperature. It occurs thermal stress. The development of the stress are from many factors such as,

- Adequate difference in the molar volumes of metal and oxide scale form on it.
- The adequate difference in the thermal expansion coefficient of oxide and metal [2].

2.3 Development of stress

In high temperature oxidation, the thickness of oxide film increases leading to the development of stress. And the development of stress from thermal contraction when the metal is cooled. In general, there are 2 types of stress as previous mention. Hence, the oxide film will decohesion itself under compression with buckling, spalling, and cracking [9].

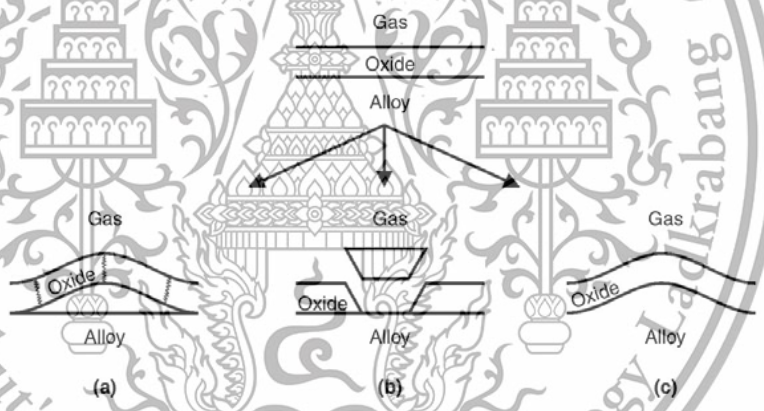

Figure 2.5 The possibilities of the oxide under load in compression. (a) buckling of the oxide, (b) shear cracking of the oxide, and (c) plastic deformation of the oxide and alloy **[9]**.

2.4 Coefficient of thermal expansion (CTE)

The coefficient of thermal expansion is thermal expanding value depending on the temperature. The equation is as follows, [10]

$$\frac{\Delta L}{L_0} = \alpha \Delta T \tag{2.7}$$

Where ΔL is changing of length
L_0 is initial length
ΔT is changing of temperature (K)
α is thermal expansion coefficient (K^{-1})

2.5 Pilling-Bedworth ratio

The Pilling-Bedworth ratio (PBR) is the volume change due to the formation of the oxide which occurs when an oxide forms at the metal/oxide interface. [3]

$$PBR_{metal} = \frac{Volume\ of\ oxide}{Volume\ of\ metal} \tag{2.8}$$

The PBR indicates whether the volume of the corrosion product is greater or less than the volume of the metal from which the corrosion product formed. If PBR < 1, the volume of the corrosion product is less than the volume of the metal from which the product formed. A film of such a corrosion product would be expected to contain cracks and pores due to tensile stress development in the oxide scale and be relatively nonprotective. On the other hand, if PBR > 1, the volume of the corrosion product scale is greater than the volume of the metal from which the scale formed, so that the scale is in compression and be protective of the underlying metal. If PBR >> 1, the scale that forms may buckle and detach (spallation) from the surface because of the higher stress that develops. [6]

The exceptions of the PBR theory are numerous. The main flaw of the PBR is the assumptions that include: 1) the oxide growth occurs by uncharged particles, 2) the diffusion coefficient is independent of the concentration, 3) the concentrations C(0) and C(L) in the interface regions (metal-oxide and oxide-gas, respectively) are independent of the film thickness, 4) film growth is a steady state phenomenon [5], 5) the metal oxides grow by diffusion of oxygen inward through the oxide layer to the metal. In fact, it is much more common for metal ions to diffuse outward through the oxide to the gas. 6) the possibility of plastic flow by the oxide of metal was not considered. [6]

Although the PBR is between 1-2 which means a protective scale would be predicted, at high temperatures the rapid growth of oxide may cause compressive stresses to become so great that the scale spalls. Typically, several oxides are protective during the early stages of oxidation, but it becomes nonprotective above a certain thickness. [6]

In addition, protection by an oxide depends on the adherence of the oxide to the substrate, low vapor pressure and high melting temperature of the oxide, slow oxide growth rate, and high thermodynamic stability. The growth mechanism of the oxide is also relevant to oxide protection. For example, if the scale is formed at the metal–oxide interface by migration of oxide ions, then compressive stresses can develop because the new oxide will be constrained by the substrate metal and the existing oxide layer. On the other hand, scale that is formed at the oxide–gas interface by migration of metal ions outward is not constrained to occupy the volume of the metal that was oxidized. Under these conditions, protective scales are expected. [6]

2.6 Machine learning

Machine learning is the field of study that gives computers the ability to learn without being explicitly programmed [11]. It is a branch of artificial intelligence (AI) and computer science. Through the use of the statistical method, algorithms are trained to make classifications or predictions.

2.6.1 Classification of machine learning based on the nature of the learning

Machine learning implementation are classified into four major categories based on the nature of the learning.

2.6.1.1 Supervised learning

Supervised learning is use of labeled datasets to train algorithms to classify data (classification) or predict outcomes (regression) accurately.

2.6.1.2 Unsupervised learning

Unsupervised learning is the use of unlabeled datasets to train algorithms to draw inferences or discover hidden patterns from datasets.

2.6.1.3 Reinforcement learning

Reinforcement learning is similar to supervised learning, but the algorithm is not trained using sample data. This model learns as it goes by using trial and error. The model automatically determines a sequence of successful outcomes that will be reinforced to develop the best recommendation.

2.6.1.4 Semi-supervised learning

Semi-supervised learning falls between supervised learning and unsupervised learning. It is suitable for a situation when incomplete datasets are given or do not have enough labeled data for a supervised learning algorithm. Semi-supervised learning combines a small amount of labeled data with a large amount of unlabeled data during training.

2.6.2 Categorization of machine learning based on required output

Machine learning task are categorized into three categories based on required output.

2.6.2.1 Classification

The output variable is a category, such as “yes” and “no” or “spallation occurs” and “no spallation occurs”. Classification model can be categorized in two groups: Binary classification and Multiclass classification.

2.6.2.2 Regression

The output variable is a numeric value or continuous value.

2.6.2.3 Clustering

Clustering is basically a type of unsupervised learning. It is the task of diving the data point into groups in which members or data points in the same group are similar.

2.6.3 Machine learning data preprocessing, training, and model evaluation

Firstly, the collected datasets are transformed and prepared to apply and feeding it to the algorithm, this process is known as data preprocessing. Eliminating the missing value, analyzing the collected datasets, and then constructing a new dataset for further processing and exploration can help the algorithm easily interpret the data's features [11]. Secondly, the prepared collected datasets are passed into algorithms to your machine learning algorithm to find patterns and make predictions, this process is known as training model. Before that, the prepared collected datasets are split into two groups including 1) a training set is a dataset that we pass to our algorithm to learn potential underlying patterns and relationships. and 2) a test set is a dataset that we use to approximate our model's unbiased accuracy. Thirdly, this process is known as model evaluation. This is done by testing the performance of the model on previously unseen data that is test set data. The prediction value obtained from training set and test set is then used for the performance analysis of models using the performance matrix such as accuracy, f1-score, coefficient of determination (R^2), and root mean squared error (RMSE). If the model's performance is acceptable, a classification model with high accuracy and low f1-score, a regression model with the nearest value 1 of coefficient of determination and low root mean squared error, we can consider an algorithm to be a predictive model that can be implemented in various applications. But if not, an improvement of the model is required by collecting a greater number of datasets or changing the algorithm [12].

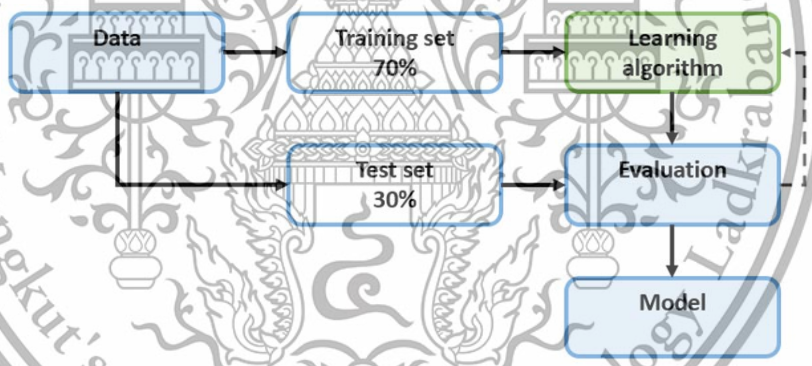

Figure 2.6 Block diagram of supervised learning

2.6.4 Machine learning (ML) algorithms

Algorithm means “A set of rules to be followed in calculations or other problem-solving operations” Or “A procedure for solving a mathematical problem in a finite number of steps that frequently by recursive operations” [13]. In machine learning, algorithms are program that is trained to predict the predicted variable or output. In this study, the algorithms that we used include:

2.6.4.1 K-Nearest Neighbors

K-nearest neighbors are unsupervised and supervised neighbors-methods used for both classification and regression. It classifies data points based on the closest distance to other available data or nearest neighbors. Euclidean distance is used as a metric measure to measure the distance between the new point and available data. Then, algorithms assign a category to a new point based on the most frequent category or average value of nearest neighbors for the amount K points. For

classification, a class label is assigned by using a majority vote. The class label of the new point is assigned to be a class label that is most frequently represented around its nearest neighbor. For regression, the data labels are continuous variables. A label is assigned by computed based on the mean of the labels of its nearest neighbor.

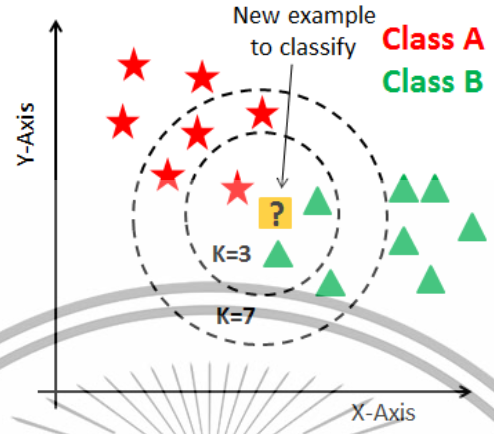

Figure 2.7 An illustration of K nearest neighbor model. [14]

2.6.4.2 Decision Trees

Decision trees are a supervised learning method used for both classification and regression. Decision trees predict the value of a target variable by using simple decision rules inferred from the data feature. It contained a series of binary decisions, each decision split the data into 2 possibilities according to a certain parameter. These 2 possibilities lead to another decision or lead to a prediction value. By defining each decision as a decision node and a possibility that leads to a prediction value as a leaf node, the structure of decision trees is shown in Figure 2.8.

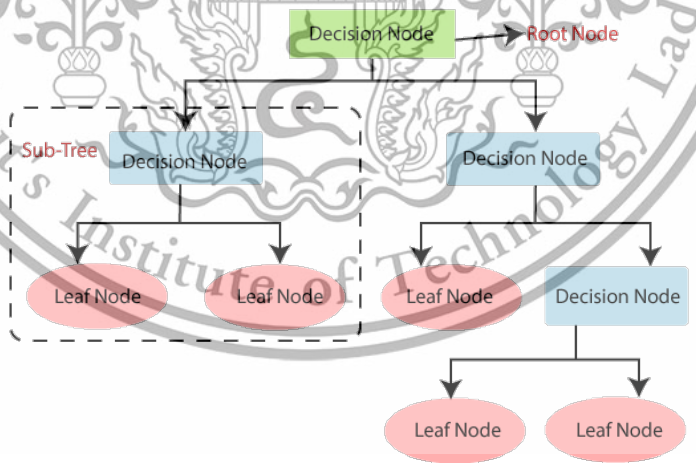

Figure 2.8 Diagram of decision trees model

The main drawback of decision trees is typically exhibit high variance and tend to overfit which can easily observe as show in Figure 2.9 [15].

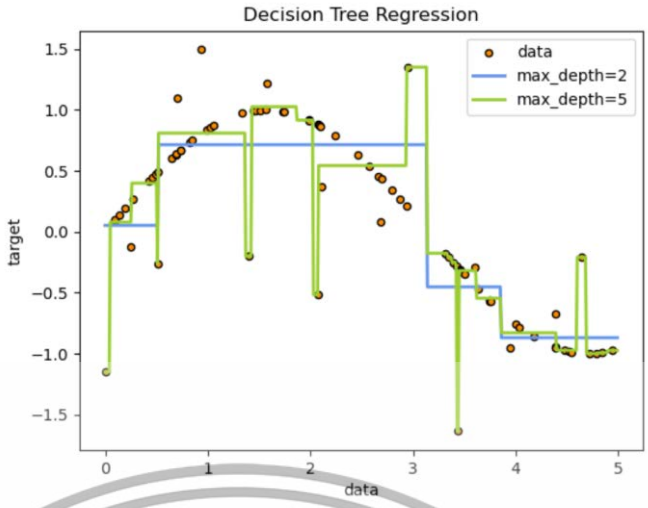

Figure 2.9 Results plot of decision tree model in data analysis

2.6.4.3 Random Forest

Random Forest is a supervised learning method used for both classification and regression. It consists of many decision trees to establish the outcome based on the predictions of the decision trees. The prediction value of random forest is the average of the prediction value from various trees. So, the greater number of trees in the forest leads to higher accuracy and prevents the problem of overfitting [15].

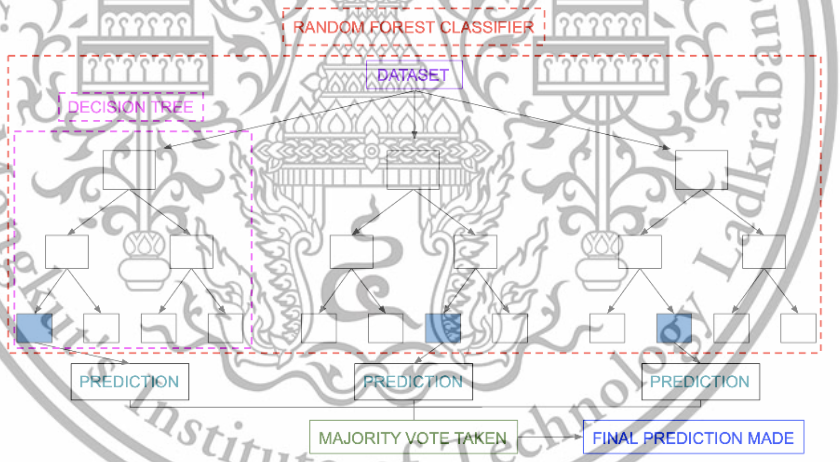

Figure 2.10 Diagram of random forest model.

2.6.4.4 Multi-layer Perceptron

Multi-layer Perceptron (MLP) is a supervised learning algorithm. Multi-layer Perceptron is a feedforward artificial neural network model that maps sets of input data onto a set of appropriate outputs. It's like the neuron network of a human brain, the input data enter the layer of the nodes or hidden layer which contained an activation function to produce output. The output is sent as input for the next layer of the nodes to produce another output. During the training process, the output is sent back to the previous layer which is called backpropagation. So, the training process of MLP contains both forward pass and backward pass of data to improve the performance of the algorithm. MLP is capable to learn non-linear data and sensitive to feature scaling.

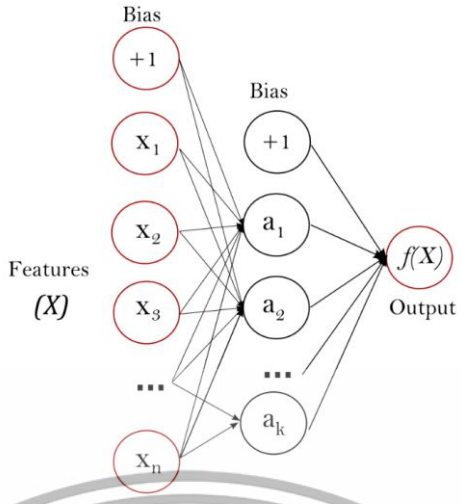

Figure 2.11 Diagram of one hidden layer MLP

2.6.5 Explaining the prediction of model

Interpretability and explainability of the prediction are necessary for descript the prediction model to make other people understand the model. So, the tool used for interpreting and explaining is required to help other people understand easily. In this study, the tool used to interpret and explain the prediction model include.

2.6.5.1 Feature importance

Feature importance is used to describe how much each input feature contributes to predicting a target variable. It determines the score of the usefulness of a specific variable for a current model and prediction.

In the machine learning model, the more features a model contains for the training of the algorithm, the more complex it is, therefore the more sensitive the model is to errors due to variance. So, feature importance is required to eliminate features. It is useful for selecting the minimum required features to produce a valid model.

2.6.5.2 SHAP (Shapley Additive exPlanations)

SHAP is a method used to explain individual predictions by visualizing their output. SHAP explains the prediction of a model by computing the contribution of each feature to the prediction. The computed value from the SHAP explanation method is the Shapley values. These values are related to the game theory which assumes that each feature value of a model is a "player" in a game where the prediction value is the payout. From this situation, the Shapley values tell us how to fairly distribute the "payout" among the features. The interpretation of model by using the Shapley value are suitable for both classification and regression model.

2.6.5.3 The coefficient of determination (R^2)

The coefficient of determination, denoted as R^2, is a statistical measure that quantifies the proportion of the variation in the dependent variable that is predicted from the independent variable(s). It can be used to measure how well a statistical model predicts an outcome. The lowest possible value of the coefficient of determination is 0, and the highest possible value is 1. However, in some cases, R^2 can

yield negative values. A value of 0 indicates that the model does not predict the outcome, while a value between 0 and 1 indicates that the model partially predicts the outcome, and a value of 1 indicates that the model perfectly predicts the outcome.

2.6.5.4 Root means square error (RMSE)

RMSE is the standard deviation of the residuals, or prediction errors. Residuals are a measure of how far data points are from the regression line. RMSE is calculated by taking the square root of the average of the squared differences between the predicted values and the actual values. It provides a measure of the average deviation between the predicted values and the actual values, with a lower RMSE indicating better accuracy and a higher RMSE indicating greater error.

2.6.5.5 Accuracy

Accuracy is a common evaluation metric used to measure the performance of a classification model. It is calculated by dividing the number of correct predictions made by the model by the total number of predictions. It provides a measure of how well a classification model is performing. However, it can be misleading in some cases. For example, if a classification model is only trained on a very small dataset, it may have a high accuracy even if it is not actually very good at making predictions. For these reasons, it is important to use other evaluation metrics in addition to accuracy when evaluating classification models.

2.6.5.6 The F1 score

The F1 score is a common evaluation metric used to measure the performance of a classification model. It combines precision and recall into a single measure to provide a balanced assessment of a model's performance.

Precision represents the ability of a classifier to correctly identify positive instances out of the total instances it predicted as positive. It is calculated as the ratio of true positive predictions to the sum of true positive and false positive predictions.

Recall, also known as sensitivity or true positive rate, measures the ability of a classifier to correctly identify positive instances out of the total actual positive instances. It is calculated as the ratio of true positive predictions to the sum of true positive and false negative predictions.

The F1 score is the harmonic mean of precision and recall, which gives equal weight to both metrics. It ranges from 0 to 1, with 1 being the best score indicating perfect precision and recall, and 0 being the worst score indicating poor performance. It helps in evaluating the model's performance by considering both false positives and false negatives and can be a good overall measure when both precision and recall are important.

2.7 Literature reviews

The Pilling-Bedworth Ratio (PBR) describe the volume change of oxide during formation of metal oxide, is used in prediction magnitude of growth stress of metal since 1923.

J. Stringer (1970) has studied stress generation and relief in growing oxide film. This review suggest that plastic flow takes place during the oxidation process and consideration of plastic flow is important for several reasons. For example, dislocations are climbing in thin scales, oxide-metal adhesion during the oxidation of alloys could only be maintained by large plastic flow, removal of an atom from a step on the metal surface requires a readjustment of the oxide equivalent to the movement of one edge dislocation in order to maintain adhesion. One of assumption of PBR is the possibility of plastic flow by the oxide of metal was not considered. So, this assumption is main flaw of the PBR. From this review, it is acknowledged that there is no direct relation between PBR and the level of stress in the scale. This means that the stress generation and release mechanisms are complicated, and the effects of PBR are not simple and well understood.

C. Xu and W. Gao (2000) has developed a method to calculate PBR for the oxidation of alloy. It was found that PBR for oxidation of alloys is not the same as oxidation of pure metal due to the crystal structure and lattice constant of alloys affects the volume of alloy. The result shows great difference in PBR of metal and alloy. The results indicated that the PBR for alloys are significantly different to the PBR for pure metal.

Trent et al. (2016) has studied the comparison of corrosion performance of grade 316 and grade 347H stainless steels in molten nitrate salt and reported that spallation of oxide scales on stainless steel surface. The scale delamination and/or spallation during cooled to room temperature due to the coefficient of thermal expansion (CTE) mismatch between the oxide and metal. Because there is no research that has been conducted to find the exact mismatch value of CTE. So, these are the considerations that will be used in further studies in our research.

John, R.C. et al. (2004) has developed mathematical models via thermochemical calculations to predict equipment lifetimes with high-temperature corrosion data. The elements of alloy considered for calculation are W-La-Mo-Nb-Cu-Ni-Co-Fe-Mn-Cr-Ti-Ar-Cl-S-Si-Al-F-O-N-C-H. Exposure times ranged up to nearly 24,000 hr. with variations in the O_2 concentrations from 0.1 to 100% in O_2-N_2 gases and temperatures of 200 – 1200 °C. The mathematic model has the capability to predict the corrosion formation of the basic types of corrosion products and the capability to predict alloy corrosion kinetics for wide range of conditions.

Chapter 3
Research methodology

3.1 Collecting and preparing data

3.1.1 Collecting data

In this study, the data were collected from the experiments of many types of alloys. There were 3 data sets. The first data set was, the data consists of %chemical composition of alloys in each type of alloys, temperature, oxidation time, partial pressure of oxygen, partial pressure of water, parabolic rate constant, types of oxide film formed and spallation state. The collected data were composed of 56 types of alloys which consist of 43 types of iron based alloys, 6 types of nickel based alloys, 3 types of cobalt based alloys, 2 types of copper based alloys and 2 types of titanium based alloy. The total first data set provided 240 points. The second data set was, the data consists of %chemical composition of alloys in each type of alloys, temperature range and coefficient of thermal expansion (CTE). The collected data were composed of 75 types of alloys which consist of 68 types of iron based alloys and 7 types of nickel based alloys. The total second data set gave 216 points. The third data set was, the data consists of chemical composition of oxide film, temperature range and coefficient of thermal expansion (CTE). The collected data were composed of 40 types of oxide films. The total third data set have 52 points. All data was studied along scope of work mentioned before. The amounts of alloy data, CTEs of alloy and oxide collected are summarized in Tables 3.1, 3.2 and 3.3 respectively.

Table 3.1 The amount of alloy data and references

Types of alloys	Amount	References
Iron based alloy	212	[16] [17] [18] [19] [20] [21] [22] [23] [24] [25] [26] [27] [28] [29] [30]
Nickel based alloy	9	[31] [32] [33] [34]
Cobalt based alloy	6	[35] [36]
Copper based alloy	4	[37]
Titanium based alloy	9	[38] [39]

Table 3.2 The amount of CTE of alloy data and references

CTE of alloys	Amount	References
Iron based alloy	209	[40] [41] [42] [43] [44] [45]
Ni based alloy	7	[46]

Table 3.3 The amount of CTE of oxide data and references

CTE of oxide	Amount	References
TiO_2	1	[47]
Al_2O_3	2	[47] [48]
Cr_2O_3	1	[49]
FeO	2	[49] [50]
NiO	1	[49]
Fe_2O_3	2	[49] [50]
CoO	1	[49]
Cu_2O	1	[51]
SiO_2	3	[52] [48]
$Y_2Si_2O_7$	1	[52]
$Y_3Al_5O_{12}$	1	[52]
$Si_2Al_6O_{13}$	1	[52]
CuO	2	[53] [54]
$NiCr_2O_4$	1	[55]
$MnCr_2O_4$	1	[55]
$CoCr_2O_4$	1	[55]
$Mn_{1.5}Co_{1.5}O_4$	1	[56]
Co_2MnO_4	1	[57]
$MgAl_2O_4$	2	[58]
$MnAl_2O_4$	1	[58]
$CoAl_2O_4$	1	[58]
$NiAl_2O_4$	1	[58]
$ZnAl_2O_4$	2	[58]
$MgCr_2O_4$	2	[58]
$CoCr_2O_4$	1	[58]
$ZnCr_2O_4$	1	[58]
Mn_3O_4	1	[58]
$NiMn_2O_4$	1	[58]
$Cu_{1.4}Mn_{1.6}O_4$	1	[58]
$MgFe_2O_4$	2	[58]
$CoFe_2O_4$	1	[58]
Co_3O_4	1	[58]
Ta_2O_5	1	[48]
Nb_2O_5	1	[48]
Al_2TiO_5	1	[59]
$ZrTiO_4$	1	[59]
Fe_2SiO_4	1	[50]
Fe_3O_4	1	[50]
WO_3	3	[60] [61]
$CoWO_4$	1	[62]

3.1.2 Preparing data

For the preparing data step, all data are brought into excel file to be analyzed with Python. The input and output variables were then defined. For the first data set, input variables were %chemical composition of alloys, temperature, oxidation time, partial pressure of oxygen and partial pressure of water in the experimental environments. Output variable were parabolic rate, types of oxide film, spallation state. For the second data set, input variables were %chemical composition of alloys. Output variable was thermal expansion coefficient of alloys. For the third data set, input variable was chemical composition of oxide film. Output variable was thermal expansion coefficient of oxide film.

3.2 Creating model and selection of algorithm for prediction

In this study, our model was created by using Python. The collected data were imported into python, including the independent variable (x) for input datasets and the dependent variable (y) for output datasets or predicted value. The collected data were structured data with 49 column that consist of 17 columns of independent variable which include the chemical composition of the alloy, environment composition, oxidation time, temperature, and pressure, and 32 columns of dependent variables which includes the parabolic rate constant, types of oxide formed on alloy surface, oxide spallation state, and thermal expansion coefficient of oxide and alloy. The lists of variables from collected data are shown in Table 3.4.

Table 3.4 the lists of independent variable and dependent variable

Independent variable (x)	Dependent variable (y)
The chemical composition of the alloy	Types of oxide formed on alloy surface
Environmental composition	Oxide spallation state
Oxidation time	Thermal expansion coefficient of alloy
Temperature	Thermal expansion coefficient of oxide
Pressure	

Each dependent variable was categorized into 4 groups as shown in Table 3.4. Then, by splitting the collected data into 2 sets that were training set and test set which is a ratio of 0.7 and 0.3 respectively, the training set data was used as input datasets to train the algorithms. Algorithms in this study include K-nearest neighbor (KNN), Decision trees, Random Forest, and Multi-layer perceptron. Algorithms that were trained with a training set data were classified as models. The models obtained from this study are shown in Table 3.5.

Table 3.5 the categorization of dependent variables for training algorithms

Dependent variable (y)	Types of algorithms	Models
Types of oxide form on alloy surface	Classification algorithm	Model for predicting the type of oxide form on alloy surface.
Oxide spallation state	Classification algorithm	Model for predicting the type of oxide form on alloy surface.
Thermal expansion coefficient of alloy	Regression algorithm	Model for predicting thermal expansion coefficient of alloy.
Thermal expansion coefficient of oxide	Regression algorithm	Model for predicting thermal expansion coefficient of oxide.

Then, a test set data was used as input datasets for models to predict the output datasets from a test set data. The prediction results or output datasets of the algorithm from a training set data and a test set data were then statistically analyzed by using the performance matrix which is mentioned in the next section. To obtain a high-performance prediction model, it is necessary to improve the performance of the model by increasing the number of input datasets or changing of machine learning (ML) algorithm.

3.3 Model performance analysis

The prediction performance of each model in this study was evaluated. The most common method to estimate the performance of the model is by using performance metrics. The type of performance metrics used depends on the type of algorithm used to create the model.

The model for predicting the thermal expansion coefficient of oxide and alloy is a regression model. The performance metrics for regression models in this study are coefficient of determination (R^2) and root mean squared error (RMSE) which show in Eqs. 3.1 and 3.2 respectively.

$$R^2 = 1 - \frac{\sum_{i=1}^{n}\left(y_i - y_p\right)^2}{\sum_{i=1}^{n}\left(y_i - \bar{y}\right)^2} \tag{3.1}$$

$$RMSE = \sqrt{\frac{1}{n}\sum_{i=1}^{n}\left(y_p - y_i\right)^2} \tag{3.2}$$

Where n is total number of data
y_i is the target value
y_p is the prediction value
$\bar{y}$ is the mean of the target data

The model for predicting the type of oxide formed on alloy surface and oxide spallation state was a classification model. The performance metrics for classification models in this study were accuracy and F1-score which show in Eqs. 3.3 and 3.4 respectively.

$$Accuracy = \frac{correct\ predicted\ value}{all\ predicted\ value} \tag{3.3}$$

$$F1\ score = \frac{2 \times (Recall \times Precision)}{(Recall + Precision)} \tag{3.4}$$

The recall and precision used to calculate F1-score can be obtained from Eqs. 3.5 and 3.6 respectively.

$$Recall = \frac{TP}{TP + FN} \tag{3.5}$$

$$Precision = \frac{TP}{TP + FP} \tag{3.6}$$

Where TP is true positive - the correctly predicted positive value
FP is false positive - actual class is no but predicted class is yes
FN is false negative - actual class is yes but predicted class is no

3.4 Comparing the prediction performance of each model

By comparing the models that were created from different algorithms using metrics, the prediction models with acceptable efficiency were obtained. The prediction model was analyzed and compared to the other prediction models that predicted another variable: 1) types of oxide formed on alloy surface, 2) the oxide spallation state, 3) the thermal expansion coefficient of alloy, and 4) the thermal expansion coefficient of oxide. Then, we find the relationship between each predicted variable and improve the efficiency of each model further.

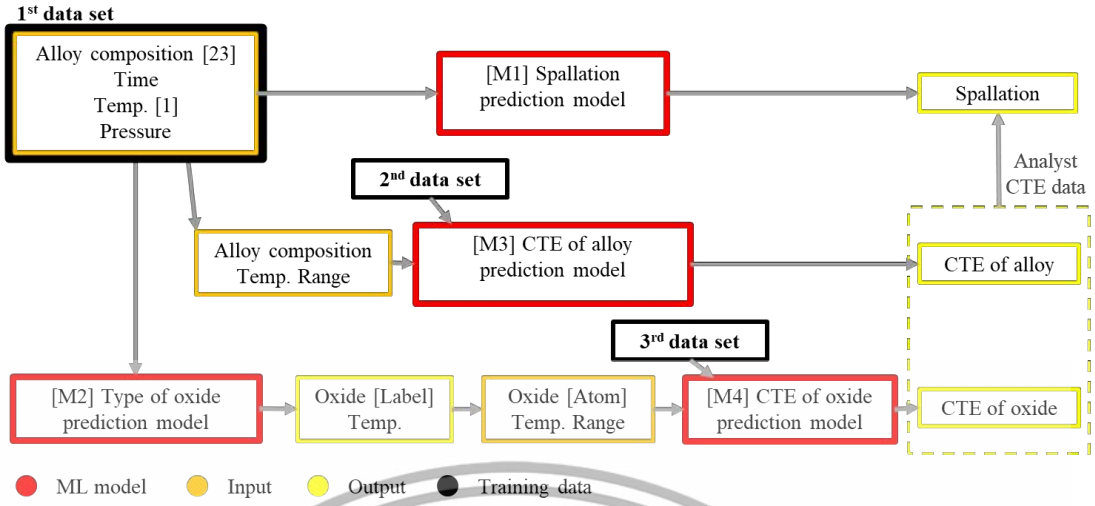

Figure 3.1 The overviews of assemble model; M1 is the spallation prediction model, M2 is the types of oxide prediction model, M3 is the thermal expansion coefficient (CTE) of alloy prediction model, and M4 is the thermal expansion coefficient (CTE) of oxide prediction model.

3.5 Calculate the Pilling-Bedworth ratio for comparing the machine learning.

From the first data set, they are calculated the Pilling-Bedworth ratio (PBR) to compare the performance with the machine learning. The PBR is the volume of oxide divided by the volume of metal or alloy. The equation of PBR is shown as Eq 3.7. If PBR is less than 1, the oxide film is too less which the oxide film can crack. If the PBR is more than 1 but less than 2, the oxide film is protective. And if the PBR is more than 2, the oxide film is formed too much which it generates the stress and cracks. After calculation, the PBR is compared with the experiment spallation state which is from the first data set. Then, calculating the accuracy and compare the performance with the machine learning.

$$PBR_{metal} = \frac{Volume\ of\ oxide}{Volume\ of\ metal} \tag{3.7}$$

Chapter 4
Results and Discussion

4.1 Data collection and preparation

The data including the percentages of chemical composition of alloy, the environmental conditions at which the alloy is exposed, the formation of different types of oxides at different environmental conditions, spallation of alloys at that condition, and thermal expansion coefficients (CTE) of alloy and oxide from all reference sources gathered by the authors are presented in the Appendix. These data were provided to train each algorithm. The arrangement and preparation of the data to prepare for training the algorithm differed depending on what dependent variables we want to predict.

Data collected from reference sources were prepared for training algorithms that aimed to predict oxide spallation, type of oxide formed on the alloy surface, thermal expansions (CTE) of alloy and oxide by categorizing and transforming the data into the format shown in Tables 4.1, 4.2, 4.3, and 4.4 respectively.

Table 4.1 Example of data prepared to train the algorithm for predicting oxide spallation.

Type	Chemical compositions of alloys					Environmental condition				Spallation
	C	Mn	Si	...	Fe	t	T	pO_2	pH_2O	
AISI 630	0.04	0.6	0.3	...	73.96	500	650	41.45	0	0
AISI 630	0.04	0.6	0.3	...	73.96	1000	650	41.45	0	0
AISI 347 H	0.07	1.28	0.66	...	70.69	500	650	41.45	0	1

Table 4.2 Example of data prepared to train the algorithm for predicting type of oxide form on the alloy surface.

Type	Chemical compositions of alloys					Environment that alloys exposed				Types of oxide				
	C	Mn	Si	...	Fe	t	T	pO_2	pH_2O	Fe_2O_3	Fe_3O_4	Cr_2O_3	...	$(Mn, Cr)_3O_4$
AISI 630	0.04	0.6	0.3	...	73.96	500	650	41.45	0	0	0	1	...	0
AISI 630	0.04	0.6	0.3	...	73.96	1000	650	41.45	0	0	0	1	...	0
AISI 347 H	0.07	1.28	0.66	...	70.69	500	650	41.45	0	0	0	1	...	0

Table 4.3 Example of data prepared to train the algorithm for predicting thermal expansion coefficient (CTE) of alloy.

Alloy	Chemical compositions of alloys						Temperature range		CTE
	C	Mn	P	S	...	Fe	T_{in} (°C)	T_{fi} (°C)	(× 10^{-5} °C^{-1})
S20100	0.15	6.5	0.06	0.03	...	70.51	0	100	1.57
S20100	0.15	6.5	0.06	0.03	...	70.51	0	315	1.75
S20100	0.15	6.5	0.06	0.03	...	70.51	0	538	1.84
S20100	0.15	6.5	0.06	0.03	...	70.51	0	650	1.89

Table 4.4 Example of data prepared to train the algorithm for predicting thermal expansion coefficient (CTE) of oxide.

Oxide	Chemical compositions of alloys						Temperature range		CTE
	Ti	Al	Cr	Fe	...	Mg	T_{in} (°C)	T_{fi} (°C)	(× 10^{-5} °C^{-1})
TiO_2	2	0	0	0	...	0	20	600	0.7
Al_2O_3	0	2	0	0	...	0	20	1000	0.84
Cr_2O_3	0	0	2	0	...	0	100	1000	0.73
FeO	0	0	0	1	...	0	100	1000	1.22

The data gathered to train algorithms for predicting the thermal expansion coefficient of oxides consist of the empirical formula of oxides, the temperature range and the thermal expansion coefficient of oxides. These data were transformed by replacing the empirical formula of oxides with the number of atoms of each element in the empirical formula. This information was then organized into a new data table that contains the number of atoms of each element in the empirical formula of the respective oxide, as shown in Table 4.4.

4.2 Analysis of the performance of spallation prediction and type of oxide prediction model

The main goal of this study was to develop the most accurate machine learning model for predicting the type of oxide formed on alloy surface and spallation of oxide on alloy surface. Among the machine learning algorithms, the decision tree algorithm was found to produce the best performance with the highest accuracy and F1 score compared to other algorithms in this study.

The performance matrixes were used to compare the performance of different algorithms. For spallation prediction models, which were the classification models, the performance matrixes used to compare models were accuracy and F1 score. The performance analysis of all four algorithms, including k-nearest neighbor, decision tree, random forest, and multi-layer perceptron, is presented based on 3 datasets: training set, test set and overall data, as shown in Table 4.5 and Figure 4.1. Upon analyzing the training set data, the decision tree and random forest algorithms were found to be the best algorithms for predicting oxide spallation, achieving the accuracy of 100% and the F1 score of 1, followed by multi-layer perceptron with the accuracy of 95.71% and the F1 score of 0.9559, and k-nearest neighbor with the accuracy of 93.25% and the F1 score of 0.9238. When considering the test set data, the decision tree algorithm was

found to be the best algorithm for predicting oxide spallation. It achieved the accuracy of 90.14% and the F1 score of 0.8948. The random forest algorithm came in second with the accuracy of 88.73% and the F1 score of 0.8826. The k-nearest neighbor algorithm came in third with the accuracy of 85.92% and the F1 score of 80.59. The multi-layer perceptron algorithm came in last with the accuracy of 83.10% and the F1 score of 0.8033. Finally, when analyzing the overall data, the decision tree algorithm was found to be the best algorithm for predicting oxide spallation with the accuracy of 97.01% and the F1 score of 0.9695. The random forest algorithm came in second with the accuracy of 96.58% and the F1 score of 0.9654. The multi-layer perceptron algorithm came in third with the accuracy of 91.88% and the F1 score of 0.9137. The k-nearest neighbor algorithm came in last with the accuracy of 91.03% and the F1 score of 0.8933.

So, the decision tree algorithm gave the highest accuracy and F1 score, which means that it is the most accurate and precise model for predicting oxide spallation.

Table 4.5 Summary of performance matrix analysis for spallation prediction model.

Performance matrix		K-nearest neighbor	Decision tree	Random forest	Multi-layer perceptron
Accuracy (%)	Training set	93.25	100.00	100.00	95.71
	Test set	85.92	90.14	88.73	83.10
	Overall data	91.03	97.01	96.58	91.88
F1 score	Training set	0.9238	1.0000	1.0000	0.9559
	Test set	0.8059	0.8948	0.8826	0.8033
	Overall data	0.8933	0.9695	0.9654	0.9137

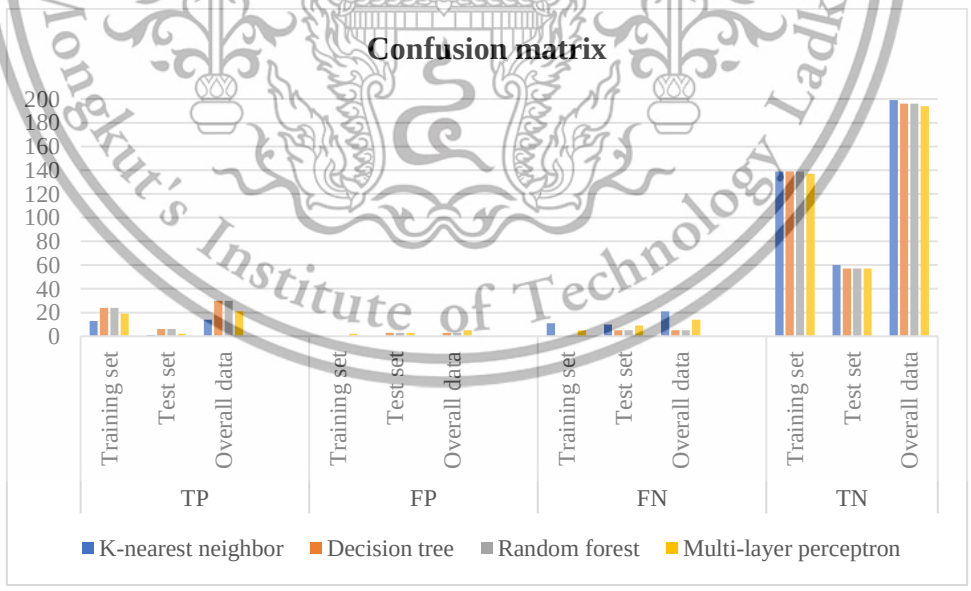

Figure 4.1 The confusion matrix consists of four basic characteristics obtained from the spallation prediction model that is used to calculate the performance matrix of the model.

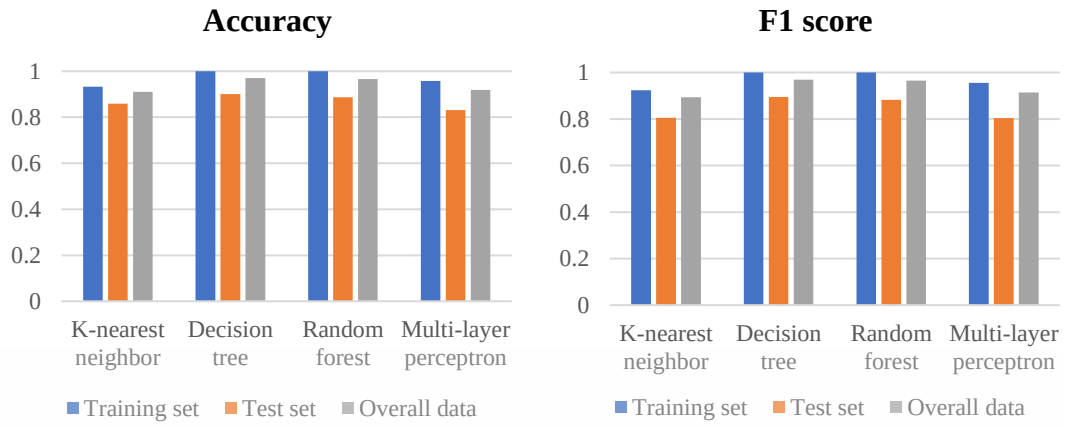

Figure 4.2 Chart of summary of performance matrix analysis for spallation prediction model

For the type of oxide prediction model, the performance matrixes were used in the same way as the spallation prediction model to compare the performance of different algorithms on 3 data sets, as shown in Table 4.6 and Figure 4.2. Upon analyzing the training set data, the decision tree and random forest algorithms were found to be the best algorithms for predicting the type of oxide formed on the alloy surface, achieving the equal accuracies of 99.39% and F1 scores of 0.9816 and 0.9877 respectively, followed by multi-layer perceptron with the accuracy of 78.53% and the F1 score of 0.9441, and the k-nearest neighbor with the accuracy of 73.62% and the F1 score of 0.8770. When considering the test set data, the decision tree and random forest algorithms were found to be the best algorithms for predicting the type of oxide formed on the alloy surface with the equal accuracies of 78.87% and F1 scores of 0.9816 and 0.9877 respectively, followed by multi-layer perceptron with the accuracy of 54.93% and the F1 score of 0.8257, and k-nearest neighbor with the accuracy of 56.34% and the F1 score of 0.7515. In this case, multi-layer perceptron had a significantly higher F1 score than k-nearest neighbor. On the other hand, k-nearest neighbor had a higher accuracy than multi-layer perceptron, but not by much when compared to the F1 score. Therefore, multi-layer perceptron is better than k-nearest neighbor, but still not as good as decision tree and random forest. Finally, when analyzing the overall data, the decision tree and random forest algorithms were found to be the best algorithms for predicting the type of oxide formed on an alloy surface, with the equal accuracies of 93.16% and F1 scores of 0.9572 and 0.9622, respectively. Multi-layer perceptron follows with the accuracy of 71.37% and the F1 score of 0.9082, while k-nearest neighbor has the accuracy of 68.38% and the F1 score of 0.8389.

So, the decision tree and random forest algorithms provided the highest accuracy and F1 score, which means that they are the most accurate and precise models for predicting the type of oxide formed on an alloy surface.

Table 4.6 Summary of performance matrix analysis for type of oxide prediction model.

Performance matrix		K-nearest neighbor	Decision tree	Random forest	Multi-layer perceptron
Accuracy (%)	Training set	73.62	99.39	99.39	78.53
	Test set	56.34	78.87	78.87	54.93
	Overall data	68.38	93.16	93.16	71.37
F1 score	Training set	0.8770	0.9816	0.9877	0.9441
	Test set	0.7515	0.9012	0.9036	0.8257
	Overall data	0.8389	0.9572	0.9622	0.9082

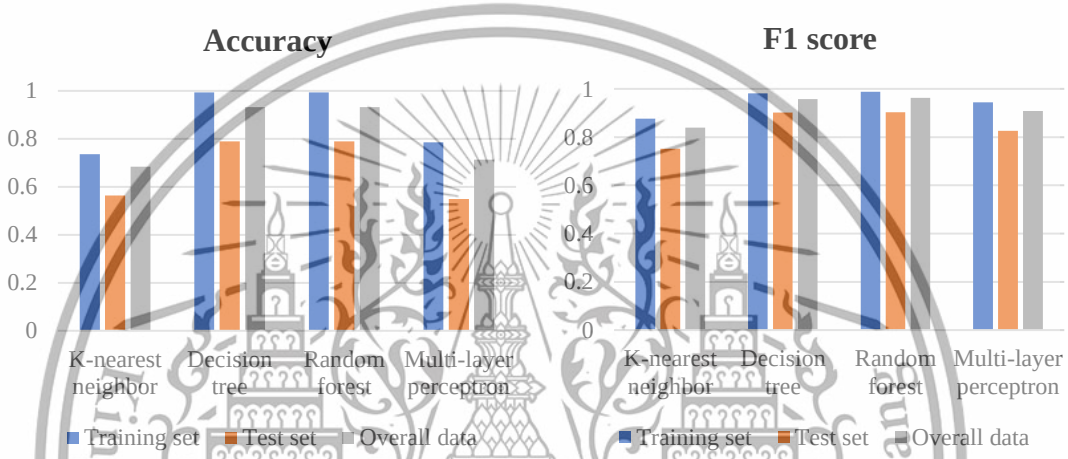

Figure 4.3 Chart of summary of performance matrix analysis for type of oxide prediction model.

4.3 Analysis of the performance of thermal expansion coefficient (CTE) of alloy and oxide prediction model

For thermal expansion coefficient (CTE) prediction models, which were regression models, the performance matrixes used to compare models were the mean absolute percentage error (MAPE) and the coefficient of determination (R^2). The performance analyses of all four algorithms, including k-nearest neighbor, decision tree, random forest, and multi-layer perceptron, were presented based on 3 datasets: training set, test set, and overall data. The results are shown in Table 4.7 and Figure 4.3, which is similar to the spallation prediction model and the type of oxide prediction model.

For the thermal expansion coefficient (CTE) of alloy prediction model, when considered the training set data, the decision tree algorithm was found to be the best algorithm for predicting thermal expansion coefficient of alloy with the MAPE of 0% and the R^2 of 1. The random forest algorithm came in second with the MAPE of 1.37% and the R^2 of 0.9891. The k-nearest neighbor algorithm came in third with the MAPE of 2.98% and the R^2 of 0.9260. The deep learning algorithm was the worst with the MAPE of 75.50% and the R^2 of 0.5530. When considering the test set data, the random forest algorithm was found to be the best algorithm for predicting thermal expansion coefficient of alloy with the MAPE of 3.16% and the R^2 of 0.9609, followed by the

decision tree and k-nearest neighbor with MAPE of 4.71% and 4.44% respectively, and R^2 with 0.8854 and 0.8831 respectively. The deep learning algorithm was the worst with the MAPE of 86.80% and the R^2 of 0.4160. Finally, when considered overall data, the decision tree and random forest algorithms were found to be the best algorithms for predicting thermal expansion coefficient of alloy with MAPE of 1.42% and 1.91% respectively, and R^2 of 0.9615 and 0.9796 respectively, followed by the k-nearest neighbor with the MAPE of 3.42% and the R^2 of 0.9115. The deep learning algorithm was the worst with the MAPE of 77.70% and the R^2 of 0.5050.

So, the decision tree and random forest algorithms gave the lowest MAPE and highest R^2, which means that they are the most accurate and precise models for predicting thermal expansion coefficient of alloy.

Table 4.7 Summary of performance matrix analysis for thermal expansion coefficient (CTE) of alloy prediction model.

Performance matrix		K-nearest neighbor	Decision tree	Random forest	Deep learning
MAPE (%)	Training set	2.98	0.00	1.37	75.50
	Test set	4.44	4.71	3.16	86.80
	Overall data	3.42	1.42	1.91	77.70
R^2	Training set	0.9260	1.0000	0.9891	0.5330
	Test set	0.8831	0.8854	0.9609	0.4160
	Overall data	0.9115	0.9615	0.9796	0.5050

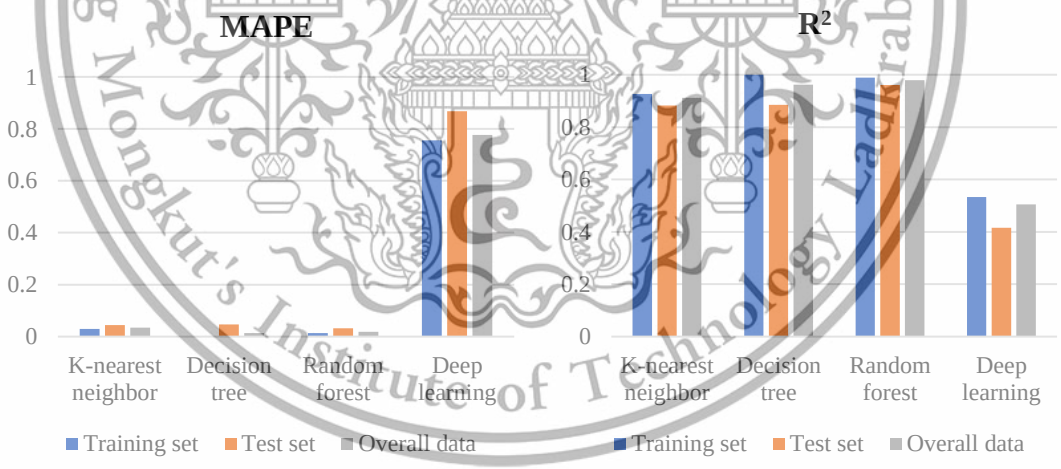

Figure 4.4 Chart of summary of performance matrix analysis for thermal expansion coefficient (CTE) of alloy prediction model.

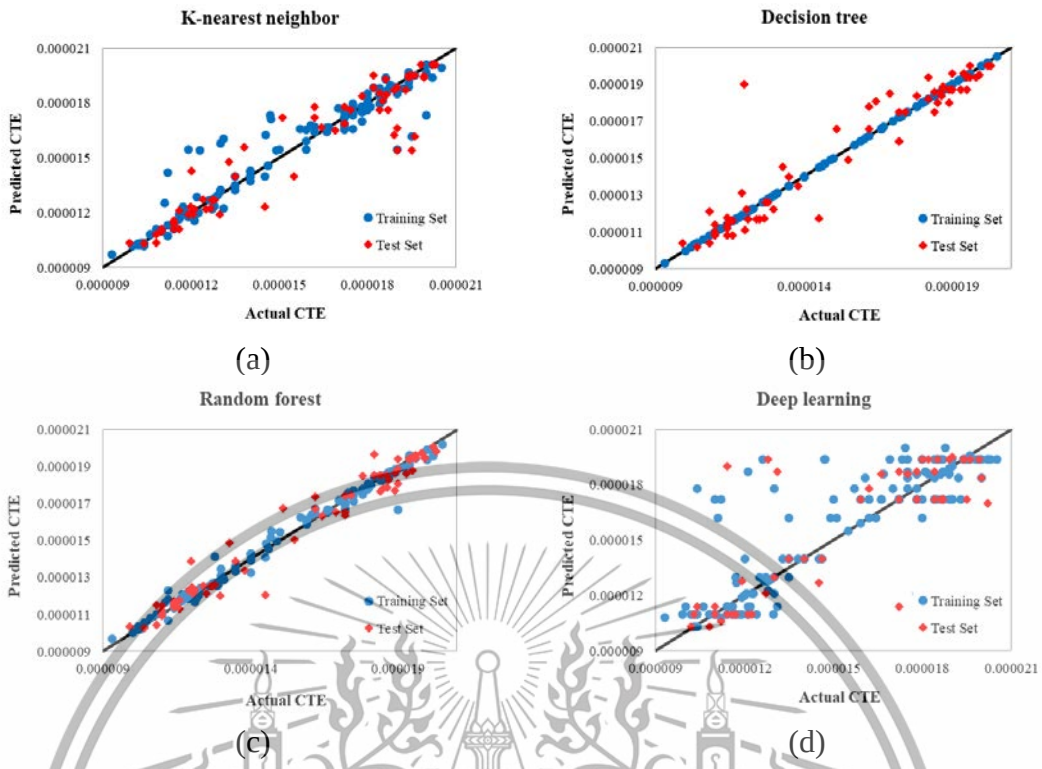

Figure 4.5 Thermal expansion coefficient of alloy predicted from (a) the k-nearest neighbor algorithm, (b) the decision tree algorithm, (c) the random forest algorithm, and (d) the deep learning algorithm compared to actual value.

For the thermal expansion coefficient (CTE) of oxide prediction model, the performance matrixes were used in the same way as the thermal expansion coefficient (CTE) of alloy prediction model to compare the performance of different algorithms on 3 data sets. Considering the training set data, the decision tree algorithm was found to be the best algorithm for predicting the thermal expansion coefficient of oxides with the MAPE of 0% and the R^2 of 1. The random forest algorithm came in second with the MAPE of 25.66% and the R^2 of 0.9277. The k-nearest neighbor algorithm came in third with the MAPE of 32.23% and the R^2 of 0.7598. The deep learning algorithm was the worst with the MAPE of 55.80% and the R^2 of 0.2920. When considering the test set data, the random forest algorithm was found to have the lowest MAPE of 26.33%, but a poor R^2 of -0.0173. This is similar to the decision tree algorithm with the MAPE of 34.99% and the R^2 of -0.3230, and the k-nearest neighbor algorithm with the MAPE of 36.29% and the R^2 of -0.1760. All three of these algorithms had negative value of R^2 for the test set data. On the other hand, the deep learning algorithm had the highest R^2 of 0.2090 but a poor MAPE of 95.50%. Finally, when considering overall data, the decision tree and random forest algorithms were found to be the best algorithms for predicting the thermal expansion coefficient of oxides with MAPE of 10.77% and 25.86% respectively, and R^2 of 0.4279 and 0.5225 respectively, followed by the k-nearest neighbor with the MAPE of 33.48% and the R^2 of 0.3665. The deep learning algorithm was the worst with the MAPE of 60.70% and the R^2 of 0.2800.

Due to the thermal expansion coefficient of oxide data were limited. So, the further data are needed in order to prove these findings. However, the results reveal that

the decision tree and random forest algorithms are promising approaches for predicting the thermal expansion coefficient of oxides.

Table 4.8 Summary of performance matrix analysis for thermal expansion coefficient (CTE) of oxide prediction model.

Performance matrix		K-nearest neighbor	Decision tree	Random forest	Deep learning
MAPE (%)	Training set	32.23	0.00	25.66	55.80
	Test set	36.29	34.99	26.33	95.50
	Overall data	33.48	10.77	25.86	60.70
R^2	Training set	0.7598	1.0000	0.9277	0.2920
	Test set	-0.1760	-0.3230	-0.0173	0.2090
	Overall data	0.3665	0.4279	0.5225	0.2800

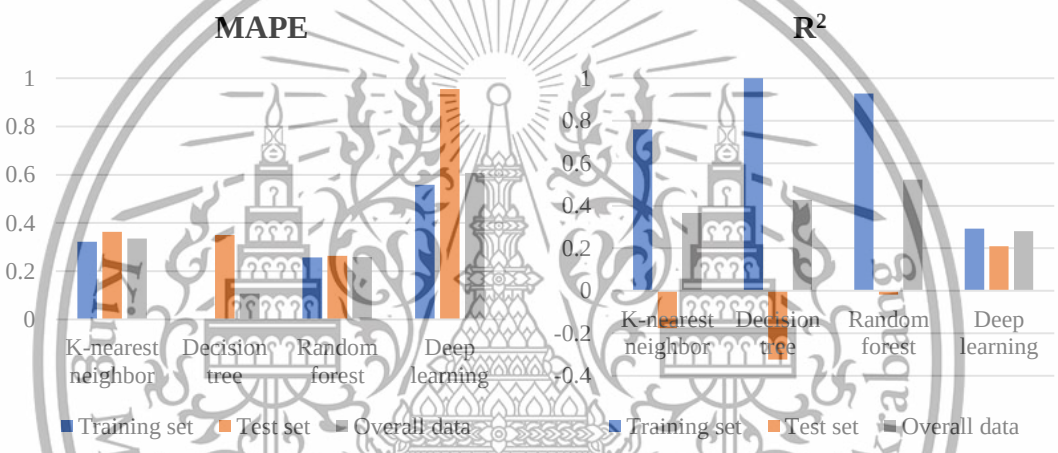

Figure 4.6 Chart of summary of performance matrix analysis for thermal expansion coefficient (CTE) of oxide prediction model.

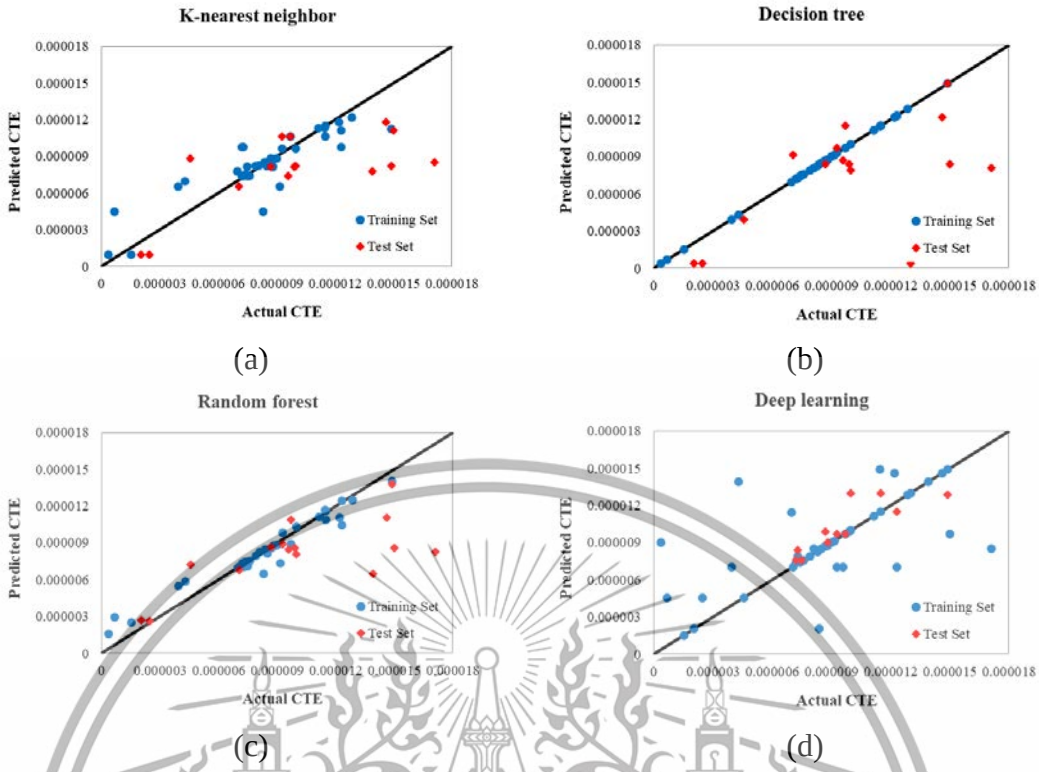

Figure 4.7 Thermal expansion coefficient of oxide predicted from (a) the k-nearest neighbor algorithm, (b) the decision tree algorithm, (c) the random forest algorithm, and (d) the deep learning algorithm compared to actual value.

4.4 Evaluation of the representative value of thermal expansion coefficient of alloys and oxides using machine learning prediction model.

After developing a model to predict the thermal expansion coefficient of alloys and oxides, we applied these models to the dataset used for training the models to predict the spallation of oxide on alloy surface and the types of oxide formed on alloy surface. We obtained the representative thermal expansion coefficient of alloys and oxides for each condition of experiment that was gathered. Many possible oxides may occur, so the representative thermal expansion coefficient (CTE) of oxide was the lowest value, which represents the worst expanding oxide when compared to each oxide that occurred on that alloy surface. The lower value of the representative CTE of oxide compared to the higher value of the CTE of alloy means a greater difference between the two CTEs, which can be used to identify the spallation of oxide formed on the alloy surface. Note that the representative values of thermal expansion coefficient for both alloy and oxide are not the actual values. They are predicted values obtained from the thermal expansion coefficient prediction model for alloy and oxide. The thermal expansion coefficient prediction model for alloy was the random forest algorithm with the MAPE of 1.91% and the R^2 of 0.9796. The thermal expansion coefficient prediction model for oxide was the random forest algorithm with the MAPE of 25.86% and the R^2 of 0.5225. The representative value of thermal expansion coefficient includes the error from the prediction model. This means that the value may not be absolutely accurate.

Table 4.9 Example of thermal expansion coefficient data obtained from thermal expansion coefficient (CTE) of alloys and oxides prediction model.

No.	Type of alloy	CTE alloy ($\times 10^{-5}$ °C^{-1})	CTE oxide ($\times 10^{-6}$ °C^{-1})
0	AISI 430	1.23	7.5936
1	AISI 430	1.23	7.5936
2	AISI 630	1.3	7.5936
3	AISI 630	1.3	7.5936
4	AISI 347 H	1.31	13.6198
5	AISI 347 H	1.31	13.6198
6	AISI 316 LN	1.75	13.6198
7	AISI 316 LN	1.75	13.6198
8	Fe22Cr	1.22	7.5936
9	Fe22Cr	1.22	7.5936
10	Fe22Cr	1.22	7.5936

4.5 Calculation of the mismatch value of the thermal expansion coefficient between alloy and oxide.

We used the representative thermal expansion coefficient of alloys and oxides obtained from machine learning prediction model to calculate the difference in thermal expansion coefficient between alloys and oxides that formed on them. This difference was analyzed to determine the mismatch value of the thermal expansion coefficient between alloy and oxide. This mismatch value caused the alloy and oxide to expand unsuitably, leading to spallation of oxides. The results are shown in Figure 4.8.

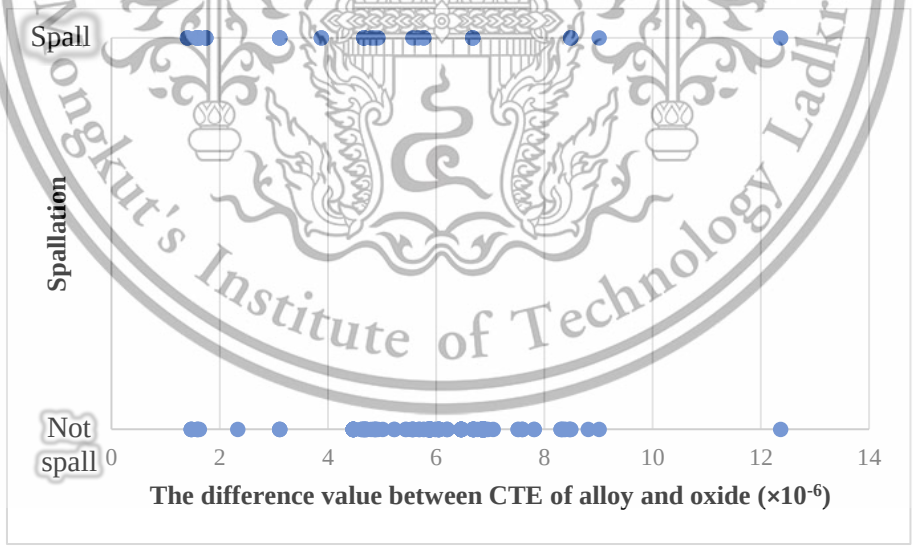

Figure 4.8 The relationship of the difference between the thermal expansion coefficients of alloy and oxide and the spallation of oxide.

Figure 4.8 shows that there is no significant difference in the thermal expansion coefficient between alloy and oxide that causes spallation of oxide. Spallation can occur at any difference in the thermal expansion coefficient between alloy and oxide. So, the thermal expansion coefficient of alloy and oxide does not affect the spallation of oxide film on alloy surface.

4.6 Analysis the spallation prediction performance between the Pilling-Bedworth ratio (BPR) and machine learning.

Analyzing the spallation prediction performance between the Pilling-Bedworth ratio (PBR) and machine learning. The PBR is the volume of oxide divided by the volume of the metal. The PBR values were calculated from the first data set which was collected as mentioned before. In PBR calculation, PBR is less than 1 and more than 2 as spallation. And PBR is between 1-2 as not spallation. Then define the spallation value of No and Yes mean the crack and spallation did not occur and occurred, respectively. These values were used to represent the spallation state obtained from the experiment. They were compared between spallation state from experiment and calculation from PBR. The PBR can right predict of 18 from 43 situations which was calculation to be the accuracy of 41.86%. So, the machine learning performance was much better than PBR. From the best model results, the accuracy of 80%-90% while the accuracy of PBR was 41.86%. Machine learning can perform twice as better than PBR. Due to the machine learning using the experimental data, including chemical composition of alloy, oxidation condition, oxidation time temperature and spallation state, in prediction, this is the reason that the machine learning is more reliable.

Table 4.10 Example of data for the PBR calculation and compared to experiment data to find accuracy of the PBR.

Type	t (hr)	T (°C)	pO_2 (atm)	pH_2O (atm)	Metal volume / surface area (mm)	Oxide volume/ surface area (mm)	PBR	Spallation from experiment	Spallation from PBR
Fe22Cr	100	700	0.21	0	0.35	0.4	1.1428	No	No
AISI430	2000	650	0.21	0	0.0003	0.0006	2	No	No
AISI441	2000	750	0.21	0	0.0003	0.0007	2.3333	No	Yes
Crofer22H	2000	700	0.21	0	0.0003	0.0005	1.6667	No	No
Fe11Cr0.5Ti	100	900	0.21	0	1.2	0.74	0.6167	Yes	Yes
								Accuracy	41.86 %

Chapter 5
Conclusion and Recommendation

5.1 Conclusion

This study aims to develop the most accurate machine-learning model for predicting the type of oxide formed on alloy surface, spallation of oxide on alloy surface, and thermal expansion coefficients of alloy and oxide to estimate the value of the difference in thermal expansion coefficient of oxide and alloy that can cause spallation of oxide.

From studying, starting with collecting the data of alloy, spallation of oxide on alloy, thermal expansion coefficient of alloy and oxide which were 3 data sets. The first data set contained 240 points. The second data set had 216 points while the third data set comprised 52 points. After that, the data were prepared in excel for analyzing in machine learning.

The preparing data were defined as input and output. After that, they were spitted into 2 sets of data that were training set data and test set data which is a ratio of 0.7 and 0.3 respectively, the training set data is used as input datasets to train the algorithm. Algorithms in this study included K-nearest neighbor (KNN), Decision trees, Random Forest, and Multi-layer perceptron. Then, the test set data was used to analyze the performance of each algorithm. For the model predicting the types of oxides that were formed on alloy surfaces, a random forest algorithm was used to create the prediction model. The model achieved the accuracy of 93.16% and the F1 score of 0.9622. The model predicts the types of oxides based on data on the composition of the alloy and the environment in which it was exposed. For a prediction model for oxide spallation, a decision tree algorithm was used to create a prediction model. The model achieved the accuracy of 97.01% and the F1 score of 0.9695. The model predicts spallation of oxide on the alloy surface based on data on the composition of the alloy and the environment in which it was exposed. Compared to the conventional method of the Pilling-Bedworth ratio, which had an accuracy of 41.86%, this machine learning prediction model gave twice of accuracy. For a prediction model for the coefficient of thermal expansion (CTE) of alloys, a decision tree and a random forest were used to create the prediction model. The model achieved the highest R^2 values of 0.9615 and 0.9796, respectively, and the lowest MAPE values of 1.42% and 1.91%, respectively. This model can be used to predict the thermal expansion coefficient of alloys for specific alloy types which contain most of the 18 elements of chemical composition such as C, Mn, P, S, Si, Cr, Ni, Mo, N, Ti, Al, La, Nb, V, Cu, W, Se, and Fe. Take in to account the prediction model for the coefficient of thermal expansion (CTE) of oxides, the decision tree and the random forest were used to create a prediction model for the coefficient of thermal expansion (CTE) of oxides. The model achieved the lowest MAPE values of 10.77% and 25.86%, respectively, and the highest R^2 values of 0.4279 and 0.5225, respectively. The model still needs the improvement due to the low R^2 value and high MAPE value, overfitting problem of the model, and limited data on oxide composition to train the algorithm. The model can be used to predict the CTE of

oxide for specific oxide types that only contain specific elements such as Ti, Al, Cr, Fe, Ni, Co, Cu, Si, Y, Mn, Zn, Ta, Nb, Zr, W, and Mg.

The difference in the thermal expansion coefficient values of alloy and oxide used in this study was obtained from the prediction model for the thermal expansion coefficient of alloy and oxide. The low accuracy of the oxide thermal expansion coefficient prediction model leads to inaccuracy of the difference of the thermal expansion coefficient values of alloy and oxide. By calculating the difference between the thermal expansion coefficient value of alloy and oxide predicted from the prediction model the inaccurate difference in the thermal expansion coefficient value of alloy and oxide was obtained. So, when analyzing these differences in the thermal expansion coefficient values of alloy and oxide, we reached two conclusions: (1) The exact mismatch value of thermal expansion coefficient causing the crack and spallation cannot be estimated; (2) The thermal expansion coefficient of alloy and oxide does not affect the spallation of oxide film on alloy surface.

5.2 Recommendation

The prediction model for the CTE of oxides still needs improvement due to low R^2 value and high MAPE value, overfitting problem of model, and it is only able to predict the CTE of oxides for specific oxide types that only contain specific elements. These can be solved by collecting more thermal expansion coefficient of oxide data to training more accurate model, use a combination of machine learning algorithms to improve the accuracy of the model, or use a different approach to predicting the CTE of oxides.

References

[1] C. Zhou, R. Pan, H. Ma, H. Zhang, X. Guan, N. Mao and F. Sun, "oxidation kinetic research under the condition of compressive loading," *IOP*, 2018.

[2] A. Khanna, High temperature oxidation, Bombay, India, 2012.

[3] Chunhua Xu and Wei Gao, "Pilling-Bedworth ratio for oxidation of alloys," *Mat Res Innovat*, vol. 3, pp. 231-235, 2000.

[4] S. Mrowec and A. Stoklosa, "Calculations of Parabolic Rate Constants for Metal Oxidation," *Oxidation of Metals*, vol. 8, 1973.

[5] A. T. Fromhold, Theory of Metal Oxidation, Amsterdam: North Holland Publishing Company, 1976.

[6] R. Winston Revie, Herbert H. Uhlig, Corrosion and Corrosion Control: An Introduction to Corrosion Science and Engineering, Hoboken, N.J: Wiley-Interscience, 2008.

[7] N. Lin, R. Xie, J. Zhou, J. Qin, Y. Wang, S. Yuan, D. Li, L. Zhao, L. Zhang, Z. Wang, Y. Ma, P. Han, W. Tian, X. Liu, Z. Wang and B. Tang, "Surface damage mitigation of titanium and its alloy via thermal oxidation: A brief review," *De gruyter*, pp. 132-146, 2019.

[8] D. j. young, High temperature oxidation and corrosion of metals, Amsterdam, The Netherlands, 2008.

[9] N. Birks, G. H. Meier and F. S. Pettit, "oxidation of alloys," in *introduction to the high temperature oxidation of metals*, Cambridge university press, 2006, pp. 101-162.

[10] s. A. Bradley, B. Hindin, U. U. Kattner, J. G. Kaufman, C. A. Parker and H. W. Sizek, Thermal properties of metals, ASM international, 2002.

[11] "Machine Learning," 2022. [Online]. Available: https://www.geeksforgeeks.org/machine-learning/?ref=shm. [Accessed 29 November 2022].

[12] M. Banoula, "Machine Learning Steps: A Complete Guide!," 15 Nov 2022. [Online]. Available: https://www.simplilearn.com/tutorials/machine-learning-tutorial/machine-learning-steps. [Accessed 10 Dec 2022].

[13] "Algorithms," 2022. [Online]. Available: https://www.geeksforgeeks.org/fundamentals-of-algorithms/#AnalysisofAlgorithms. [Accessed 29 November 2022].

[14] A. Navlani, "KNN Classification Tutorial using Scikit-learn," 2018. [Online]. Available: https://www.datacamp.com/tutorial/k-nearest-neighbor-classification-scikit-learn. [Accessed 28 November 2022].

[15] "scikit-learn 1.2.0 Supervised learning," [Online]. Available: https://scikit-learn.org/stable/supervised_learning.html. [Accessed 29 Dec 2022].

[16] M. Palcut, L. Mikkelsen, K. Neufeld, M. Chen, R. Knibbe and P. V. Hendriksen, "Corrosion stability of ferritic stainless steels for solid oxideelectrolyser cell interconnects," *Corrosion Science*, pp. 3309-3320, 2010.

[17] H. Buscail, C. Issartel, F. Riffard, R. Rollanda, S. Perrier and A. Fleurentin, "Influence of various gaseous environments on SiO2formation on the 330Cb(Fe-35Ni-18Cr-1Nb-2.15Si) alloy at 900°C," *Corrosion Science*, pp. 535-541, 2012.

[18] D. Koszelow, M. Makowska, F. Marone, J. Karczewski, P. Jasinski and S. Molin, "High temperature corrosion evaluation and lifetime prediction of porous," *Corrosion Science*, 2021.

[19] E. Stefan, C. Denonville, Y. Larring, M. Stange and R. Haugsrud, "Oxidation Study of Porous Metal Substrates for Metal Supported ProtonCeramic Electrolyzer Cells," *Corrosion Science*, 2019.

[20] J. Yuan, W. Wang, S. Zhu and F. Wang, "Comparison between the oxidation of iron in oxygen and in steamat 650–750°C," *Corrosion Science*, pp. 309-317, 2013.

[21] B. Talic, V. Venkatachalam, P. V. Hendriksen and R. Kiebach, "Comparison of MnCo2O4 coated crofer 22H, 441, 430 as interconnects for intermediate-temperature solid oxide fuel stacks," *Journal of alloys and compounds*, 2019.

[22] S. Chandra-ambhorn, T. Thublaor and P. Wiman, "High temperature oxidation of AISI 430 stainless steel in Ar-H2O at 800 °C," *Case studies in fire safety*, 2020.

[23] T. Roy, L. Latu-Romain, I. Guillotte, B. Latouche and Y. Wouters, "Modeling of Trilayered oxide thermally grown on 441 ferritic stainless steel at 900 °C in synthetic air," *oxidation of metals*, 2021.

[24] K. Bawane, K. Lu, Q. Li and R. Bordia, "High temperature oxidation behaviors of SiON coated AISI 441 in Ar+ O2, Ar+H2O, and Ar+ CO2 atmospheres," *Case studies in fire safety*, 2019.

[25] M. de Fatima Salgado, I. S. Carvalho, R. S. Santos, J. Alberto Santos Porto, O. Correa, L. Ramanathan, A. de Sa Brandim and V. F.C. Lins, "Effect of oxygen partial pressure on oxidation behavior of ferritic stainless AISI 441 at high temperature," *Engineering Failure Analysis*, pp. 215-226, 2019.

[26] X. Jiang, X. Che, Z. Zhang, S. Yin, H. Wang and L. Chen, "High temperature oxidation behavior and mechanism of FeXCr0.5Ti ferritic stainless steels," *Materials Research Express*, 2021.

[27] A. Claret Soares Sabioni, A.-M. Huntz, E. Conceicao da Luz, M. Mantel and C. Haut, "Comparative study of high temperature oxidation behavior in AISI 304 and AISI 439 stainless steels," *Materials Research*, pp. 179-185, 2003.

[28] S. Chandra-Ambhorn, Y. Wouters, L. Antoni, F. Toscan and A. Galerie, "Adhesion of oxide scales grown on ferritic stainless steels in solid oxide fuel cells temperature and atmosphere conditions," *Journal of power sources*, pp. 688-695, 2007.

[29] A. M. Avelar, C. Giovedi, Y. A. Abe and M. B. Mourao, "Oxidation of AISI 304L and 348 stainless steels in water at high temperature," *Materials research*, 2020.

[30] L. Intiso, L. Johansson, J. Sevensson and M. Halvarsson, "oxidation of sanicro 25 (42Fe22Cr25NiWCuNbN) in O2 and O2+H2O environments at 600-750 °C," *Oxidation of metals*, pp. 367-391, 2015.

[31] J. Brenneman, J. Wei, Z. Sun, L. Liu, G. Zou and Y. Zhou, "Oxidation behavior of GTD111 Ni-based superalloy at900◦Cinai," *Corrosion Science*, pp. 267-274, 2015.

[32] G. Jia, W. Xu, M. Ouyang, H. Wang, L. Wang and X. Xiao, "Oxidation behavior of Ni-25Cr-10Fe-3Si-χNb alloys at 1000 °C in ambient air: Role of Laves phase," *Corrosion Science*, 2021.

[33] C. T. Liu, J. Ma and X. F. Sun, "Oxidation behavior of a single-crystal Ni-base superalloy between 900 and1000◦C in air," *Jornal of Alloys and Compounds*, pp. 522-526, 2010.

[34] M. Li, X. Sun, J. Li, Z. Zhang, T. Jin, H. Guan and Z. Hu, "Oxidation Behavior of a Single-Crystal Ni-Base Superalloy in Air. I: At 800 and 900 °C," *Oxidation of Meatals*, pp. 591-605, 2003.

[35] L. Klein, M. S. Killian and S. Virtanen, "The effect of nickel and silicon addition on some oxidation properties of novelCo-based high temperature alloys," *Corrosion Science*, pp. 43-49, 2013.

[36] L. Klein, A. Bauer, S. Neumeier, M. Göken and S. Virtanen, "High temperature oxidation of γ/γ'-strengthened Co-base superalloys," *Corrosion Science*, pp. 2027-2034, 2011.

[37] Y. Niu, Z. L. Zhao, F. Gesmundo and M. Al-Omary, "The air oxidation of two Cu±Ni±Ag alloys at 600±700°C," *Corrosion Science*, pp. 1541-1556, 2001.

[38] H. L. Du, A. Aljarany, P. K. Datta and J. S. Burnell-Gray, "Oxidation behaviour of Ti–46.7Al–1.9W–0.5Si in air and Ar–20%O2 between 750 and 950°C," *Corrosion Science*, pp. 1706-1723, 2005.

[39] K. Aniolek, M. Kupka, M. Luczuk and A. Barylski, "Isothermal oxidation of Ti-6Al-7Nb alloy," *Vacuum*, pp. 114-118, 2015.

[40] S. D. Cramer, B. S. Covino and J. , ASM handbook volume 13B, corrosion: materials, The United States of America: ASM International, 2005.

[41] F. Cverna, ASM Ready Refernce-Thermal Properties of Matals, Ther United States of America: ASM International, 2002.

[42] X. Montero, F. Tietz, D. Sebold, H. Buchkremer, A. Ringuede, M. Cassir, A. Laresgoiti and I. Villarreal, "MnCo1.9Fe0.1O4 spinel protection layer on commercial ferritic steels for interconnect applications in solid oxide fuel cells," *Journal of Power Sources*, pp. 172-179, 2008.

[43] H. Zhai, W. Guan, Z. Chen Xu and W. Wang, "Research on performance of LSM coating on interconnect materials for SOFCs," *Journal of Korean Ceramic Society*, pp. 77-781, 2008.

[44] V. m. A. c. o. ACERINOX, "VDM Crofer 22 APU," March 2022. [Online]. Available: https://www.vdm-metals.com/fileadmin/user_upload/Downloads/Data_Sheets/Data_Sheet_VDM_Crofer_22_APU.pdf. [Accessed January 2023].

[45] A. Werner Bredvei Skibred and R. Haugsrud, "Sandvik Sanergy HT- A potential interconnect material for LaNbO4-based proton ceramic fuel cells," *Journal of Power Sources*, pp. 70-76, 2012.

[46] G. M. Valentino, J. A.Krogstad, T. P.Weihs and K. J.Hemker, "Tailoring the coefficient of thermal expansion of ternary nickel alloys through compositional control and non-contact measurements," *Journal of Alloys and Compounds*, 2020.

[47] G. Samsonov, The oxide handbook, London: Plenum Press, 1973.

[48] C.-L. Tien, C.-C. Lee and K.-P. Chuang, "Improved interometric method for the determination of the mechanical properties of metal oxide films," *Proceedings of SPIE - The International Society for Optical Engineering*, pp. 445-455, 2000.

[49] D. J. Young, High temperature oxidation and corrosion of metals, Elsevier, 2008.

[50] M. Takeda, T. Onishi, S. Nakakubo and S. Fujimoto, "Physical properties of Iron-oxide scale on Si-containing Steels at high temperature," *Materials Transactions*, pp. 2242-2246, 2009.

[51] A. Khanna, "Chapter 6 - High temperature oxidation," in *Handbook of environmental degradation of materials*, Bombay, India, Corrosion Science and Engineering, Indian Institute of Technology, Bombay, India, 2005, pp. 105-152.

[52] M. Wang, Q. Zheng, A. Chen, Y. Li, X. Zhang, D. Zhang, S. Jin, D. Xiong and W. Deng, "Crystallization, thermal expansion and hardness of Y2O3-Al2O3-SiO2 glasses," *Ceramics International*, pp. 25059-25066, 2021.

[53] A. Tsuruta, K. Nomura, M. Mikami, Y. Kinemuchi, I. Terasaki, N. Murayama and W. Shin, "Unsually small thermal expansion of ordered perovkite oxide CaCu3Ru4O12 with high conductivity," *Materials*, 2018.

[54] G. H.Meier, "8-Adhesion," in *Thermodynamics of surfaces and interfaces*, Cambridge, Cambridge University , 2014, pp. 210-236.

[55] W. Qu, L. Jian, J. M.Hill and D. G.Ivey, "Electrical and microstructural characterization of spinel phases as potential coatings for SOFC metallic interconnects," *Journal of Power Sources*, pp. 114-124, 2006.

[56] C. Jia, Y. Wang, S. Molin, Y. Zhang, M. Chen and M. Han, "High temperature oxidation behavior of SUS430 SOFC interconnects with Mn-Co spinel coating in air," *Journal of Alloys Compounds*, pp. 1327-1335, 2019.

[57] M. V.F.Schlupp, J. W. Kim, A. Brevet, C. Rado, K. Couturier, U. F.Vogt, F. Lefebvre-Joud and A. Zuttel, "Avoiding chromium transport from stainless steel interconnects into contact layers and oxygen electrodes in intermediate temperature solid oxide electrolysis stacks," *Journal of Power Sources*, pp. 587-593, 2014.

[58] A. Petric and H. Ling, "Electrical conductivity and thermal expansion of spinels at elevated temperature," *Journal of the American Ceramic Society*, pp. 1515-1520, 2007.

[59] I. J. Kim and G. Cao, "Low thermal expansion behavior and thermal durability of ZrTiO4-Al2TiO5-Fe2O3 ceramics between 750 and 1400 °C," *Journal of the European Ceramic Society*, pp. 2627-2632, 2002.

[60] J.-H. Koh, E. Sorge, T.-C. Wen and D. K.Shetty, "Thermal expansion behaviors of yttrium tungstates in the WO3-Y2O3 system," *Creanics International*, pp. 8421-8427, 2013.

[61] C. Rosen, E. Banks and E. Post, "The thermal expansion and phase transitions of WO3," *Acta Crystallopraphica*, pp. 475-476, 1956.

[62] L. Gan, T. Nishimura, S. A. Sheikh, I. Saeki and H. Murakami, "Thermal stability of CoWO4 layer fored on ferritic stainless steel," *Corrosion Science*, 2020.

[63] B. Klein, "Neural Networks with Scikit," 2022. [Online]. Available: https://python-course.eu/machine-learning/neural-networks-with-scikit.php. [Accessed 29 November 2022].

[64] R.C. John, A.D. Pelton, A.L. Young, W.T. Thompson, and I. G. Wright, "Predicting Equipment Lifetimes with High Temperature Corrosion Data," *Materials Science Forum,* Vols. 461-464, pp. 599-610, 2004.

[65] A. Gomes, M. Navas, N. Uranga, T. Paiva, I. Figueira, and T.C. Diamantino, "High-temperature corrosion performance of austenitic stainless steels type," *Solar Energy,* vol. 177, pp. 408-419, 2019.

[66] C. Xu and W. Gao, "Pilling-Bedworth ratio for oxidation of alloys," *material reseach innovations,* pp. 231-235, 2000.

[67] J. Davis, ASM Specialty Handbook: Heat-Resistant Materials, ASM International, 1997.

Appendix

Appendix A

Table A.1 The first data set is collected for prediction.

Type	C	Mn	Si	P	S	Cr	Ni	Mo	Nb	Ti	Cu	V	O	N	Al	W	Ag	B	Re	Ta	Co	La	Se	Fe
AISI 430	0.05	0.82	0.47	0	0	17.8	0.8	0	0	0	0	0	0	0	0	0	0	0	0	0	0	0	0	80.06
AISI 430	0.05	0.82	0.47	0	0	17.8	0.8	0	0	0	0	0	0	0	0	0	0	0	0	0	0	0	0	80.06
AISI 630	0.04	0.6	0.3	0	0	17.1	4.2	0	0.3	0	3.5	0	0	0	0	0	0	0	0	0	0	0	0	73.96
AISI 630	0.04	0.6	0.3	0	0	17.1	4.2	0	0.3	0	3.5	0	0	0	0	0	0	0	0	0	0	0	0	73.96
AISI 347 H	0.07	1.28	0.66	0	0	18.3	8.6	0	0.4	0	0	0	0	0	0	0	0	0	0	0	0	0	0	70.69
AISI 347 H	0.07	1.28	0.66	0	0	18.3	8.6	0	0.4	0	0	0	0	0	0	0	0	0	0	0	0	0	0	70.69
AISI 316 LN	0.03	1.93	0.63	0	0	18.9	13.9	2.78	0.16	0	0	0	0	0	0	0	0	0	0	0	0	0	0	61.67
AISI 316 LN	0.03	1.93	0.63	0	0	18.9	13.9	2.78	0.16	0	0	0	0	0	0	0	0	0	0	0	0	0	0	61.67
Fe22Cr	0.04	0.23	0.08	0	0.01	22	0.03	0.01	0.02	0	0.02	0	0.58	0.07	0	0	0	0	0	0	0	0	0	76.91
Fe22Cr	0.04	0.23	0.08	0	0.01	22	0.03	0.01	0.02	0	0.02	0	0.58	0.07	0	0	0	0	0	0	0	0	0	76.91
Fe22Cr	0.04	0.23	0.08	0	0.01	22	0.03	0.01	0.02	0	0.02	0	0.58	0.07	0	0	0	0	0	0	0	0	0	76.91
Fe22Cr	0.04	0.23	0.08	0	0.01	22	0.03	0.01	0.02	0	0.02	0	0.58	0.07	0	0	0	0	0	0	0	0	0	76.91
Fe22Cr	0.04	0.23	0.08	0	0.01	22	0.03	0.01	0.02	0	0.02	0	0.58	0.07	0	0	0	0	0	0	0	0	0	76.91
330Cb	0.05	0.69	2.15	0.015	0.005	21.14	33.81	0.22	1.02	0	0.22	0	0	0	0	0	0	0	0	0	0	0	0	40.68
0.12B	0	0	0	0	0	0	0	0	0	0	0	0	0	0	8.8	9.3	0	0.12	0	0	81.78	0	0	0
0.12B	0	0	0	0	0	0	0	0	0	0	0	0	0	0	8.8	9.3	0	0.12	0	0	81.78	0	0	0
0.12B2Si	0	0	2.3	0	0	0	0	0	0	0	0	0	0	0	8.1	9.4	0	0.12	0	0	80.08	0	0	0
0.12B2Si	0	0	2.3	0	0	0	0	0	0	0	0	0	0	0	8.1	9.4	0	0.12	0	0	80.08	0	0	0
0.12B2Si	0	0	2.3	0	0	0	0	0	0	0	0	0	0	0	8.1	9.4	0	0.12	0	0	80.08	0	0	0
0.12B9Ni	0	0	0	0	0	0	9.3	0	0	0	0	0	0	0	9.6	9.6	0	0.12	0	0	71.38	0	0	0
DD32	0	0	0	0	0	4.5	61.4	1	1.6	0	0	0	0	0	6	8.5	0	0	4	4	9	0	0	0
DD32	0	0	0	0	0	4.5	61.4	1	1.6	0	0	0	0	0	6	8.5	0	0	4	4	9	0	0	0
ANSI 310	0.018	1.79	0.65	0	0	25.8	19.33	0	0	0	0	0	0	0	0	0	0	0	0	0	0	0	0	52.412
ANSI 310	0.018	1.79	0.65	0	0	25.8	19.33	0	0	0	0	0	0	0	0	0	0	0	0	0	0	0	0	52.412
ANSI 310	0.018	1.79	0.65	0	0	25.8	19.33	0	0	0	0	0	0	0	0	0	0	0	0	0	0	0	0	52.412
GTD111	0.1	0	0	0	0	14	61.66	1.5	0	4.9	0	0	0	0	3	3.8	0	0.015	0	2.8	9.5	0	0	0.225
GTD111	0.1	0	0	0	0	14	61.66	1.5	0	4.9	0	0	0	0	3	3.8	0	0.015	0	2.8	9.5	0	0	0.225
Ti36.7Al1.9W0.5Si	0	0	0.5	0	0	0	0	0	0	50.9	0	0	0	0	46.7	1.9	0	0	0	0	0	0	0	0
Ti36.7Al1.9W0.5Si	0	0	0.5	0	0	0	0	0	0	50.9	0	0	0	0	46.7	1.9	0	0	0	0	0	0	0	0
Ti36.7Al1.9W0.5Si	0	0	0.5	0	0	0	0	0	0	50.9	0	0	0	0	46.7	1.9	0	0	0	0	0	0	0	0
Ti36.7Al1.9W0.5Si	0	0	0.5	0	0	0	0	0	0	50.9	0	0	0	0	46.7	1.9	0	0	0	0	0	0	0	0
Ti36.7Al1.9W0.5Si	0	0	0.5	0	0	0	0	0	0	50.9	0	0	0	0	46.7	1.9	0	0	0	0	0	0	0	0
Ti36.7Al1.9W0.5Si	0	0	0.5	0	0	0	0	0	0	50.9	0	0	0	0	46.7	1.9	0	0	0	0	0	0	0	0
Ferritic ss	0.06	0.03	0.08	0	0.01	20.6	0.01	0.01	0	0	0	0.61	0	0.05	0	0	0	0	0	0	0	0	0	78.54
Ferritic ss	0.06	0.03	0.08	0	0.01	20.6	0.01	0.01	0	0	0	0.61	0	0.05	0	0	0	0	0	0	0	0	0	78.54
Ferritic ss	0.06	0.03	0.08	0	0.01	20.6	0.01	0.01	0	0	0	0.61	0	0.05	0	0	0	0	0	0	0	0	0	78.54
Ferritic ss	0.06	0.03	0.08	0	0.01	20.6	0.01	0.01	0	0	0	0.61	0	0.05	0	0	0	0	0	0	0	0	0	78.54
Ferritic ss	0.06	0.03	0.08	0	0.01	20.6	0.01	0.01	0	0	0	0.61	0	0.05	0	0	0	0	0	0	0	0	0	78.54
Ferritic ss	0.06	0.03	0.08	0	0.01	20.6	0.01	0.01	0	0	0	0.61	0	0.05	0	0	0	0	0	0	0	0	0	78.54
Ferritic ss	0.06	0.03	0.08	0	0.01	20.6	0.01	0.01	0	0	0	0.61	0	0.05	0	0	0	0	0	0	0	0	0	78.54
iron	0.011	0.035	0.028	0.05	0.0094	0.009	0.018	0.004	0.004	0	0.023	0	0	0	0.015	0	0	0	0	0	0	0	0	99.7936
iron	0.011	0.035	0.028	0.05	0.0094	0.009	0.018	0.004	0.004	0	0.023	0	0	0	0.015	0	0	0	0	0	0	0	0	99.7936
iron	0.011	0.035	0.028	0.05	0.0094	0.009	0.018	0.004	0.004	0	0.023	0	0	0	0.015	0	0	0	0	0	0	0	0	99.7936
F 20 T	0	0.252	0.013	0.0259	0	19.5	0.14	0.025	0.002	0.33	0.0389	0	0	0	0.124	0	0	0	0	0	0.0224	0	0	79.5268
F 20 T	0	0.252	0.013	0.0259	0	19.5	0.14	0.025	0.002	0.33	0.0389	0	0	0	0.124	0	0	0	0	0	0.0224	0	0	79.5268

Table A.1 The first data set is collected for prediction (continue).

Type	C	Mn	Si	P	S	Cr	Ni	Mo	Nb	Ti	Cu	V	O	N	Al	W	Ag	B	Re	Ta	Co	La	Se	Fe
F 20 T	0	0.252	0.013	0.0259	0	19.5	0.14	0.025	0.002	0.33	0.0389	0	0	0	0.124	0	0	0	0	0	0.0224	0	0	79.5268
F 20 T	0	0.252	0.013	0.0259	0	19.5	0.14	0.025	0.002	0.33	0.0389	0	0	0	0.124	0	0	0	0	0	0.0224	0	0	79.5268
F 20 T	0	0.252	0.013	0.0259	0	19.5	0.14	0.025	0.002	0.33	0.0389	0	0	0	0.124	0	0	0	0	0	0.0224	0	0	79.5268
F 20 T	0	0.252	0.013	0.0259	0	19.5	0.14	0.025	0.002	0.33	0.0389	0	0	0	0.124	0	0	0	0	0	0.0224	0	0	79.5268
F 20 T	0	0.252	0.013	0.0259	0	19.5	0.14	0.025	0.002	0.33	0.0389	0	0	0	0.124	0	0	0	0	0	0.0224	0	0	79.5268
F 20 T	0	0.252	0.013	0.0259	0	19.5	0.14	0.025	0.002	0.33	0.0389	0	0	0	0.124	0	0	0	0	0	0.0224	0	0	79.5268
F 20 T	0	0.252	0.013	0.0259	0	19.5	0.14	0.025	0.002	0.33	0.0389	0	0	0	0.124	0	0	0	0	0	0.0224	0	0	79.5268
F 20 T	0	0.252	0.013	0.0259	0	19.5	0.14	0.025	0.002	0.33	0.0389	0	0	0	0.124	0	0	0	0	0	0.0224	0	0	79.5268
F 20 T	0	0.252	0.013	0.0259	0	19.5	0.14	0.025	0.002	0.33	0.0389	0	0	0	0.124	0	0	0	0	0	0.0224	0	0	79.5268
F 20 T	0	0.252	0.013	0.0259	0	19.5	0.14	0.025	0.002	0.33	0.0389	0	0	0	0.124	0	0	0	0	0	0.0224	0	0	79.5268
F 20 T	0	0.252	0.013	0.0259	0	19.5	0.14	0.025	0.002	0.33	0.0389	0	0	0	0.124	0	0	0	0	0	0.0224	0	0	79.5268
F 20 T	0	0.252	0.013	0.0259	0	19.5	0.14	0.025	0.002	0.33	0.0389	0	0	0	0.124	0	0	0	0	0	0.0224	0	0	79.5268
F 20 T	0	0.252	0.013	0.0259	0	19.5	0.14	0.025	0.002	0.33	0.0389	0	0	0	0.124	0	0	0	0	0	0.0224	0	0	79.5268
TUS 220M	0	0.101	0.058	0.0258	0	22	0.089	1.67	0.316	0.157	0.0182	0	0	0	0.018	0	0	0	0	0	0.024	0	0	75.523
TUS 220M	0	0.101	0.058	0.0258	0	22	0.089	1.67	0.316	0.157	0.0182	0	0	0	0.018	0	0	0	0	0	0.024	0	0	75.523
TUS 220M	0	0.101	0.058	0.0258	0	22	0.089	1.67	0.316	0.157	0.0182	0	0	0	0.018	0	0	0	0	0	0.024	0	0	75.523
TUS 220M	0	0.101	0.058	0.0258	0	22	0.089	1.67	0.316	0.157	0.0182	0	0	0	0.018	0	0	0	0	0	0.024	0	0	75.523
TUS 220M	0	0.101	0.058	0.0258	0	22	0.089	1.67	0.316	0.157	0.0182	0	0	0	0.018	0	0	0	0	0	0.024	0	0	75.523
TUS 220M	0	0.101	0.058	0.0258	0	22	0.089	1.67	0.316	0.157	0.0182	0	0	0	0.018	0	0	0	0	0	0.024	0	0	75.523
TUS 220M	0	0.101	0.058	0.0258	0	22	0.089	1.67	0.316	0.157	0.0182	0	0	0	0.018	0	0	0	0	0	0.024	0	0	75.523
TUS 220M	0	0.101	0.058	0.0258	0	22	0.089	1.67	0.316	0.157	0.0182	0	0	0	0.018	0	0	0	0	0	0.024	0	0	75.523
TUS 220M	0	0.101	0.058	0.0258	0	22	0.089	1.67	0.316	0.157	0.0182	0	0	0	0.018	0	0	0	0	0	0.024	0	0	75.523
TUS 220M	0	0.101	0.058	0.0258	0	22	0.089	1.67	0.316	0.157	0.0182	0	0	0	0.018	0	0	0	0	0	0.024	0	0	75.523
TUS 220M	0	0.101	0.058	0.0258	0	22	0.089	1.67	0.316	0.157	0.0182	0	0	0	0.018	0	0	0	0	0	0.024	0	0	75.523
TUS 220M	0	0.101	0.058	0.0258	0	22	0.089	1.67	0.316	0.157	0.0182	0	0	0	0.018	0	0	0	0	0	0.024	0	0	75.523
TUS 220M	0	0.101	0.058	0.0258	0	22	0.089	1.67	0.316	0.157	0.0182	0	0	0	0.018	0	0	0	0	0	0.024	0	0	75.523
TUS 220M	0	0.101	0.058	0.0258	0	22	0.089	1.67	0.316	0.157	0.0182	0	0	0	0.018	0	0	0	0	0	0.024	0	0	75.523
TUS 220M	0	0.101	0.058	0.0258	0	22	0.089	1.67	0.316	0.157	0.0182	0	0	0	0.018	0	0	0	0	0	0.024	0	0	75.523
AL 453	0	0.184	0.02	0.0248	0	22.1	0.131	0.01	0.001	0.003	0.0172	0	0	0	0.696	0	0	0	0	0	0.0261	0.0086	0	76.7783
AL 453	0	0.184	0.02	0.0248	0	22.1	0.131	0.01	0.001	0.003	0.0172	0	0	0	0.696	0	0	0	0	0	0.0261	0.0086	0	76.7783
AL 453	0	0.184	0.02	0.0248	0	22.1	0.131	0.01	0.001	0.003	0.0172	0	0	0	0.696	0	0	0	0	0	0.0261	0.0086	0	76.7783
AL 453	0	0.184	0.02	0.0248	0	22.1	0.131	0.01	0.001	0.003	0.0172	0	0	0	0.696	0	0	0	0	0	0.0261	0.0086	0	76.7783
AL 453	0	0.184	0.02	0.0248	0	22.1	0.131	0.01	0.001	0.003	0.0172	0	0	0	0.696	0	0	0	0	0	0.0261	0.0086	0	76.7783
AL 453	0	0.184	0.02	0.0248	0	22.1	0.131	0.01	0.001	0.003	0.0172	0	0	0	0.696	0	0	0	0	0	0.0261	0.0086	0	76.7783
AL 453	0	0.184	0.02	0.0248	0	22.1	0.131	0.01	0.001	0.003	0.0172	0	0	0	0.696	0	0	0	0	0	0.0261	0.0086	0	76.7783
AL 453	0	0.184	0.02	0.0248	0	22.1	0.131	0.01	0.001	0.003	0.0172	0	0	0	0.696	0	0	0	0	0	0.0261	0.0086	0	76.7783
AL 453	0	0.184	0.02	0.0248	0	22.1	0.131	0.01	0.001	0.003	0.0172	0	0	0	0.696	0	0	0	0	0	0.0261	0.0086	0	76.7783
AL 453	0	0.184	0.02	0.0248	0	22.1	0.131	0.01	0.001	0.003	0.0172	0	0	0	0.696	0	0	0	0	0	0.0261	0.0086	0	76.7783
AL 453	0	0.184	0.02	0.0248	0	22.1	0.131	0.01	0.001	0.003	0.0172	0	0	0	0.696	0	0	0	0	0	0.0261	0.0086	0	76.7783
AL 453	0	0.184	0.02	0.0248	0	22.1	0.131	0.01	0.001	0.003	0.0172	0	0	0	0.696	0	0	0	0	0	0.0261	0.0086	0	76.7783
AL 453	0	0.184	0.02	0.0248	0	22.1	0.131	0.01	0.001	0.003	0.0172	0	0	0	0.696	0	0	0	0	0	0.0261	0.0086	0	76.7783
AL 453	0	0.184	0.02	0.0248	0	22.1	0.131	0.01	0.001	0.003	0.0172	0	0	0	0.696	0	0	0	0	0	0.0261	0.0086	0	76.7783
AL 453	0	0.184	0.02	0.0248	0	22.1	0.131	0.01	0.001	0.003	0.0172	0	0	0	0.696	0	0	0	0	0	0.0261	0.0086	0	76.7783
Crofer 22 APU	0	0.526	0.016	0	0	22.4	0.022	0.003	0.002	0.052	0.0086	0	0	0	0.008	0	0	0	0	0	0.003	0.0573	0	76.9021
Crofer 22 APU	0	0.526	0.016	0	0	22.4	0.022	0.003	0.002	0.052	0.0086	0	0	0	0.008	0	0	0	0	0	0.003	0.0573	0	76.9021

Table A.1 The first data set is collected for prediction (continue)**.**

Type	C	Mn	Si	P	S	Cr	Ni	Mo	Nb	Ti	Cu	V	O	N	Al	W	Ag	B	Re	Ta	Co	La	Se	Fe
Crofer 22 APU	0	0.526	0.016	0	0	22.4	0.022	0.003	0.002	0.052	0.0086	0	0	0	0.008	0	0	0	0	0	0.003	0.0573	0	76.9021
Crofer 22 APU	0	0.526	0.016	0	0	22.4	0.022	0.003	0.002	0.052	0.0086	0	0	0	0.008	0	0	0	0	0	0.003	0.0573	0	76.9021
Crofer 22 APU	0	0.526	0.016	0	0	22.4	0.022	0.003	0.002	0.052	0.0086	0	0	0	0.008	0	0	0	0	0	0.003	0.0573	0	76.9021
Crofer 22 APU	0	0.526	0.016	0	0	22.4	0.022	0.003	0.002	0.052	0.0086	0	0	0	0.008	0	0	0	0	0	0.003	0.0573	0	76.9021
Crofer 22 APU	0	0.526	0.016	0	0	22.4	0.022	0.003	0.002	0.052	0.0086	0	0	0	0.008	0	0	0	0	0	0.003	0.0573	0	76.9021
Crofer 22 APU	0	0.526	0.016	0	0	22.4	0.022	0.003	0.002	0.052	0.0086	0	0	0	0.008	0	0	0	0	0	0.003	0.0573	0	76.9021
Crofer 22 APU	0	0.526	0.016	0	0	22.4	0.022	0.003	0.002	0.052	0.0086	0	0	0	0.008	0	0	0	0	0	0.003	0.0573	0	76.9021
Crofer 22 APU	0	0.526	0.016	0	0	22.4	0.022	0.003	0.002	0.052	0.0086	0	0	0	0.008	0	0	0	0	0	0.003	0.0573	0	76.9021
Crofer 22 APU	0	0.526	0.016	0	0	22.4	0.022	0.003	0.002	0.052	0.0086	0	0	0	0.008	0	0	0	0	0	0.003	0.0573	0	76.9021
Crofer 22 APU	0	0.526	0.016	0	0	22.4	0.022	0.003	0.002	0.052	0.0086	0	0	0	0.008	0	0	0	0	0	0.003	0.0573	0	76.9021
Crofer 22 APU	0	0.526	0.016	0	0	22.4	0.022	0.003	0.002	0.052	0.0086	0	0	0	0.008	0	0	0	0	0	0.003	0.0573	0	76.9021
Crofer 22 APU	0	0.526	0.016	0	0	22.4	0.022	0.003	0.002	0.052	0.0086	0	0	0	0.008	0	0	0	0	0	0.003	0.0573	0	76.9021
Crofer 22 APU	0	0.526	0.016	0	0	22.4	0.022	0.003	0.002	0.052	0.0086	0	0	0	0.008	0	0	0	0	0	0.003	0.0573	0	76.9021
Crofer 22 H	0	0.418	0.022	0.0101	0	22.9	0.299	0.011	0.293	0.012	0.0153	0	0	0	0.015	1.66	0	0	0	0	0.038	0.096	0	74.2106
Crofer 22 H	0	0.418	0.022	0.0101	0	22.9	0.299	0.011	0.293	0.012	0.0153	0	0	0	0.015	1.66	0	0	0	0	0.038	0.096	0	74.2106
Crofer 22 H	0	0.418	0.022	0.0101	0	22.9	0.299	0.011	0.293	0.012	0.0153	0	0	0	0.015	1.66	0	0	0	0	0.038	0.096	0	74.2106
Crofer 22 H	0	0.418	0.022	0.0101	0	22.9	0.299	0.011	0.293	0.012	0.0153	0	0	0	0.015	1.66	0	0	0	0	0.038	0.096	0	74.2106
Crofer 22 H	0	0.418	0.022	0.0101	0	22.9	0.299	0.011	0.293	0.012	0.0153	0	0	0	0.015	1.66	0	0	0	0	0.038	0.096	0	74.2106
Crofer 22 H	0	0.418	0.022	0.0101	0	22.9	0.299	0.011	0.293	0.012	0.0153	0	0	0	0.015	1.66	0	0	0	0	0.038	0.096	0	74.2106
Crofer 22 H	0	0.418	0.022	0.0101	0	22.9	0.299	0.011	0.293	0.012	0.0153	0	0	0	0.015	1.66	0	0	0	0	0.038	0.096	0	74.2106
Crofer 22 H	0	0.418	0.022	0.0101	0	22.9	0.299	0.011	0.293	0.012	0.0153	0	0	0	0.015	1.66	0	0	0	0	0.038	0.096	0	74.2106
Crofer 22 H	0	0.418	0.022	0.0101	0	22.9	0.299	0.011	0.293	0.012	0.0153	0	0	0	0.015	1.66	0	0	0	0	0.038	0.096	0	74.2106
Crofer 22 H	0	0.418	0.022	0.0101	0	22.9	0.299	0.011	0.293	0.012	0.0153	0	0	0	0.015	1.66	0	0	0	0	0.038	0.096	0	74.2106
Crofer 22 H	0	0.418	0.022	0.0101	0	22.9	0.299	0.011	0.293	0.012	0.0153	0	0	0	0.015	1.66	0	0	0	0	0.038	0.096	0	74.2106
Crofer 22 H	0	0.418	0.022	0.0101	0	22.9	0.299	0.011	0.293	0.012	0.0153	0	0	0	0.015	1.66	0	0	0	0	0.038	0.096	0	74.2106
Crofer 22 H	0	0.418	0.022	0.0101	0	22.9	0.299	0.011	0.293	0.012	0.0153	0	0	0	0.015	1.66	0	0	0	0	0.038	0.096	0	74.2106
Crofer 22 H	0	0.418	0.022	0.0101	0	22.9	0.299	0.011	0.293	0.012	0.0153	0	0	0	0.015	1.66	0	0	0	0	0.038	0.096	0	74.2106
Crofer 22 H	0	0.418	0.022	0.0101	0	22.9	0.299	0.011	0.293	0.012	0.0153	0	0	0	0.015	1.66	0	0	0	0	0.038	0.096	0	74.2106
Sanergy HT	0	0.288	0.107	0.0263	0	21.3	0.488	1.09	0.688	0.04	0.0143	0	0	0	0.014	0	0	0	0	0	0.023	0.0001	0	75.9213
Sanergy HT	0	0.288	0.107	0.0263	0	21.3	0.488	1.09	0.688	0.04	0.0143	0	0	0	0.014	0	0	0	0	0	0.023	0.0001	0	75.9213
Sanergy HT	0	0.288	0.107	0.0263	0	21.3	0.488	1.09	0.688	0.04	0.0143	0	0	0	0.014	0	0	0	0	0	0.023	0.0001	0	75.9213
Sanergy HT	0	0.288	0.107	0.0263	0	21.3	0.488	1.09	0.688	0.04	0.0143	0	0	0	0.014	0	0	0	0	0	0.023	0.0001	0	75.9213
Sanergy HT	0	0.288	0.107	0.0263	0	21.3	0.488	1.09	0.688	0.04	0.0143	0	0	0	0.014	0	0	0	0	0	0.023	0.0001	0	75.9213
Sanergy HT	0	0.288	0.107	0.0263	0	21.3	0.488	1.09	0.688	0.04	0.0143	0	0	0	0.014	0	0	0	0	0	0.023	0.0001	0	75.9213
Sanergy HT	0	0.288	0.107	0.0263	0	21.3	0.488	1.09	0.688	0.04	0.0143	0	0	0	0.014	0	0	0	0	0	0.023	0.0001	0	75.9213
Sanergy HT	0	0.288	0.107	0.0263	0	21.3	0.488	1.09	0.688	0.04	0.0143	0	0	0	0.014	0	0	0	0	0	0.023	0.0001	0	75.9213
Sanergy HT	0	0.288	0.107	0.0263	0	21.3	0.488	1.09	0.688	0.04	0.0143	0	0	0	0.014	0	0	0	0	0	0.023	0.0001	0	75.9213
Sanergy HT	0	0.288	0.107	0.0263	0	21.3	0.488	1.09	0.688	0.04	0.0143	0	0	0	0.014	0	0	0	0	0	0.023	0.0001	0	75.9213
Sanergy HT	0	0.288	0.107	0.0263	0	21.3	0.488	1.09	0.688	0.04	0.0143	0	0	0	0.014	0	0	0	0	0	0.023	0.0001	0	75.9213
Sanergy HT	0	0.288	0.107	0.0263	0	21.3	0.488	1.09	0.688	0.04	0.0143	0	0	0	0.014	0	0	0	0	0	0.023	0.0001	0	75.9213
Sanergy HT	0	0.288	0.107	0.0263	0	21.3	0.488	1.09	0.688	0.04	0.0143	0	0	0	0.014	0	0	0	0	0	0.023	0.0001	0	75.9213
Sanergy HT	0	0.288	0.107	0.0263	0	21.3	0.488	1.09	0.688	0.04	0.0143	0	0	0	0.014	0	0	0	0	0	0.023	0.0001	0	75.9213
Sanergy HT	0	0.288	0.107	0.0263	0	21.3	0.488	1.09	0.688	0.04	0.0143	0	0	0	0.014	0	0	0	0	0	0.023	0.0001	0	75.9213
E-Brite	0	0.045	0.063	0.0123	0.0111	25.7	0.121	1	0.096	0.001	0.006	0	0	0	0.006	0	0	0	0	0	0.0203	0	0	72.9183
E-Brite	0	0.045	0.063	0.0123	0.0111	25.7	0.121	1	0.096	0.001	0.006	0	0	0	0.006	0	0	0	0	0	0.0203	0	0	72.9183

Table A.1 The first data set is collected for prediction (continue)**.**

Type	C	Mn	Si	P	S	Cr	Ni	Mo	Nb	Ti	Cu	V	O	N	Al	W	Ag	B	Re	Ta	Co	La	Se	Fe
E-Brite	0	0.045	0.063	0.0123	0.0111	25.7	0.121	1	0.096	0.001	0.006	0	0	0	0.006	0	0	0	0	0	0.0203	0	0	72.9183
E-Brite	0	0.045	0.063	0.0123	0.0111	25.7	0.121	1	0.096	0.001	0.006	0	0	0	0.006	0	0	0	0	0	0.0203	0	0	72.9183
E-Brite	0	0.045	0.063	0.0123	0.0111	25.7	0.121	1	0.096	0.001	0.006	0	0	0	0.006	0	0	0	0	0	0.0203	0	0	72.9183
E-Brite	0	0.045	0.063	0.0123	0.0111	25.7	0.121	1	0.096	0.001	0.006	0	0	0	0.006	0	0	0	0	0	0.0203	0	0	72.9183
E-Brite	0	0.045	0.063	0.0123	0.0111	25.7	0.121	1	0.096	0.001	0.006	0	0	0	0.006	0	0	0	0	0	0.0203	0	0	72.9183
E-Brite	0	0.045	0.063	0.0123	0.0111	25.7	0.121	1	0.096	0.001	0.006	0	0	0	0.006	0	0	0	0	0	0.0203	0	0	72.9183
E-Brite	0	0.045	0.063	0.0123	0.0111	25.7	0.121	1	0.096	0.001	0.006	0	0	0	0.006	0	0	0	0	0	0.0203	0	0	72.9183
E-Brite	0	0.045	0.063	0.0123	0.0111	25.7	0.121	1	0.096	0.001	0.006	0	0	0	0.006	0	0	0	0	0	0.0203	0	0	72.9183
E-Brite	0	0.045	0.063	0.0123	0.0111	25.7	0.121	1	0.096	0.001	0.006	0	0	0	0.006	0	0	0	0	0	0.0203	0	0	72.9183
E-Brite	0	0.045	0.063	0.0123	0.0111	25.7	0.121	1	0.096	0.001	0.006	0	0	0	0.006	0	0	0	0	0	0.0203	0	0	72.9183
E-Brite	0	0.045	0.063	0.0123	0.0111	25.7	0.121	1	0.096	0.001	0.006	0	0	0	0.006	0	0	0	0	0	0.0203	0	0	72.9183
E-Brite	0	0.045	0.063	0.0123	0.0111	25.7	0.121	1	0.096	0.001	0.006	0	0	0	0.006	0	0	0	0	0	0.0203	0	0	72.9183
E-Brite	0	0.045	0.063	0.0123	0.0111	25.7	0.121	1	0.096	0.001	0.006	0	0	0	0.006	0	0	0	0	0	0.0203	0	0	72.9183
AL 29 4C	0	0.055	0.06	0.0173	0.0207	28.2	0.101	3.85	0.014	0.0003	0.0082	0	0	0	0.008	0	0	0	0	0	0.0153	0	0	67.6502
AL 29 4C	0	0.055	0.06	0.0173	0.0207	28.2	0.101	3.85	0.014	0.0003	0.0082	0	0	0	0.008	0	0	0	0	0	0.0153	0	0	67.6502
AL 29 4C	0	0.055	0.06	0.0173	0.0207	28.2	0.101	3.85	0.014	0.0003	0.0082	0	0	0	0.008	0	0	0	0	0	0.0153	0	0	67.6502
AL 29 4C	0	0.055	0.06	0.0173	0.0207	28.2	0.101	3.85	0.014	0.0003	0.0082	0	0	0	0.008	0	0	0	0	0	0.0153	0	0	67.6502
AL 29 4C	0	0.055	0.06	0.0173	0.0207	28.2	0.101	3.85	0.014	0.0003	0.0082	0	0	0	0.008	0	0	0	0	0	0.0153	0	0	67.6502
AL 29 4C	0	0.055	0.06	0.0173	0.0207	28.2	0.101	3.85	0.014	0.0003	0.0082	0	0	0	0.008	0	0	0	0	0	0.0153	0	0	67.6502
AL 29 4C	0	0.055	0.06	0.0173	0.0207	28.2	0.101	3.85	0.014	0.0003	0.0082	0	0	0	0.008	0	0	0	0	0	0.0153	0	0	67.6502
AL 29 4C	0	0.055	0.06	0.0173	0.0207	28.2	0.101	3.85	0.014	0.0003	0.0082	0	0	0	0.008	0	0	0	0	0	0.0153	0	0	67.6502
AL 29 4C	0	0.055	0.06	0.0173	0.0207	28.2	0.101	3.85	0.014	0.0003	0.0082	0	0	0	0.008	0	0	0	0	0	0.0153	0	0	67.6502
AL 29 4C	0	0.055	0.06	0.0173	0.0207	28.2	0.101	3.85	0.014	0.0003	0.0082	0	0	0	0.008	0	0	0	0	0	0.0153	0	0	67.6502
AL 29 4C	0	0.055	0.06	0.0173	0.0207	28.2	0.101	3.85	0.014	0.0003	0.0082	0	0	0	0.008	0	0	0	0	0	0.0153	0	0	67.6502
AL 29 4C	0	0.055	0.06	0.0173	0.0207	28.2	0.101	3.85	0.014	0.0003	0.0082	0	0	0	0.008	0	0	0	0	0	0.0153	0	0	67.6502
AL 29 4C	0	0.055	0.06	0.0173	0.0207	28.2	0.101	3.85	0.014	0.0003	0.0082	0	0	0	0.008	0	0	0	0	0	0.0153	0	0	67.6502
AL 29 4C	0	0.055	0.06	0.0173	0.0207	28.2	0.101	3.85	0.014	0.0003	0.0082	0	0	0	0.008	0	0	0	0	0	0.0153	0	0	67.6502
AL 29 4C	0	0.055	0.06	0.0173	0.0207	28.2	0.101	3.85	0.014	0.0003	0.0082	0	0	0	0.008	0	0	0	0	0	0.0153	0	0	67.6502
AL 29 4C	0	0.055	0.06	0.0173	0.0207	28.2	0.101	3.85	0.014	0.0003	0.0082	0	0	0	0.008	0	0	0	0	0	0.0153	0	0	67.6502
Cu15Ni15Ag	0	0	0	0	0	0	15	0	0	0	70	0	0	0	0	0	15	0	0	0	0	0	0	0
Cu15Ni15Ag	0	0	0	0	0	0	15	0	0	0	70	0	0	0	0	0	15	0	0	0	0	0	0	0
Cu25Ni25Ag	0	0	0	0	0	0	25	0	0	0	50	0	0	0	0	0	25	0	0	0	0	0	0	0
Cu25Ni25Ag	0	0	0	0	0	0	25	0	0	0	50	0	0	0	0	0	25	0	0	0	0	0	0	0
NCFS	0	0	3.06	0	0	24.95	62.02	0	0	0	0	0	0	0	0	0	0	0	0	0	0	0	0	9.97
NCFS1.5Nb	0	0	2.94	0	0	25.03	60.5	0	1.48	0	0	0	0	0	0	0	0	0	0	0	0	0	0	10.05
NCFS3Nb	0	0	2.91	0	0	24.94	59.34	0	2.93	0	0	0	0	0	0	0	0	0	0	0	0	0	0	9.88
AISI430	0	0.42	0.41	0	0	16.3	0	0.076	0.015	0.007	0	0.08	0	0	0.006	0.035	0	0	0	0	0	0	0	82.651
AISI430	0	0.42	0.41	0	0	16.3	0	0.076	0.015	0.007	0	0.08	0	0	0.006	0.035	0	0	0	0	0	0	0	82.651
AISI430	0	0.42	0.41	0	0	16.3	0	0.076	0.015	0.007	0	0.08	0	0	0.006	0.035	0	0	0	0	0	0	0	82.651
AISI441	0	0.4	0.59	0	0	17.53	0	0	0.41	0.172	0	0	0	0	0.07	0	0	0	0	0	0	0	0	80.828
AISI441	0	0.4	0.59	0	0	17.53	0	0	0.41	0.172	0	0	0	0	0.07	0	0	0	0	0	0	0	0	80.828
AISI441	0	0.4	0.59	0	0	17.53	0	0	0.41	0.172	0	0	0	0	0.07	0	0	0	0	0	0	0	0	80.828
Crofer22H	0	0.44	0.25	0	0	23	0	0	0.5	0.1	0	0	0	0	0.01	1.9	0	0	0	0	0	0.07	0	73.73
Crofer22H	0	0.44	0.25	0	0	23	0	0	0.5	0.1	0	0	0	0	0.01	1.9	0	0	0	0	0	0.07	0	73.73
Crofer22H	0	0.44	0.25	0	0	23	0	0	0.5	0.1	0	0	0	0	0.01	1.9	0	0	0	0	0	0.07	0	73.73
Ni base	0	0	0	0	0	6	87.45	0.05	0	0.05	0	0	0	0	6.3	0.05	0	0	0	0.05	0.05	0	0	0

Table A.1 The first data set is collected for prediction (continue).

Type	C	Mn	Si	P	S	Cr	Ni	Mo	Nb	Ti	Cu	V	O	N	Al	W	Ag	B	Re	Ta	Co	La	Se	Fe
Ni base	0	0	0	0	0	6	87.45	0.05	0	0.05	0	0	0	0	6.3	0.05	0	0	0	0.05	0.05	0	0	0
Ti-6Al-7Nb	0.02	0	0	0	0	0	0	0	7.27	86.1063	0	0	0.18	0.0058	6.39	0	0	0	0	0	0	0	0	0.026
Ti-6Al-7Nb	0.02	0	0	0	0	0	0	0	7.27	86.1063	0	0	0.18	0.0058	6.39	0	0	0	0	0	0	0	0	0.026
Ti-6Al-7Nb	0.02	0	0	0	0	0	0	0	7.27	86.1063	0	0	0.18	0.0058	6.39	0	0	0	0	0	0	0	0	0.026
AISI 430	0.042	0.326	0.295	0.018	0	16.92	0.155	0	0	0	0	0	0	0	0	0	0	0	0	0	0	0	0	82.244
AISI 430	0.042	0.326	0.295	0.018	0	16.92	0.155	0	0	0	0	0	0	0	0	0	0	0	0	0	0	0	0	82.244
AISI 430	0.042	0.326	0.295	0.018	0	16.92	0.155	0	0	0	0	0	0	0	0	0	0	0	0	0	0	0	0	82.244
AISI 430	0.042	0.326	0.295	0.018	0	16.92	0.155	0	0	0	0	0	0	0	0	0	0	0	0	0	0	0	0	82.244
AISI 430	0.042	0.326	0.295	0.018	0	16.92	0.155	0	0	0	0	0	0	0	0	0	0	0	0	0	0	0	0	82.244
AISI 430	0.042	0.326	0.295	0.018	0	16.92	0.155	0	0	0	0	0	0	0	0	0	0	0	0	0	0	0	0	82.244
AISI 430	0.042	0.326	0.295	0.018	0	16.92	0.155	0	0	0	0	0	0	0	0	0	0	0	0	0	0	0	0	82.244
AISI 430	0.042	0.326	0.295	0.018	0	16.92	0.155	0	0	0	0	0	0	0	0	0	0	0	0	0	0	0	0	82.244
AISI 441	0.015	0.3	0.6	0.03	0	18.5	0.3	0.25	0.5	0.18	0.3	0	0	0	0.015	0	0	0	0	0	0	0	0	78.96
AISI 441	0.015	0.3	0.6	0.03	0	18.5	0.3	0.25	0.5	0.18	0.3	0	0	0	0.015	0	0	0	0	0	0	0	0	78.96
AISI 441	0.015	0.3	0.6	0.03	0	18.5	0.3	0.25	0.5	0.18	0.3	0	0	0	0.015	0	0	0	0	0	0	0	0	78.96
AISI 441	0.015	0.3	0.6	0.03	0	18.5	0.3	0.25	0.5	0.18	0.3	0	0	0	0.015	0	0	0	0	0	0	0	0	78.96
AISI 441	0.03	1	1	0.04	0.015	18	0.5	0	0.65	0.35	0	0	0	0	0	0	0	0	0	0	0	0	0	78.415
AISI 441	0.03	1	1	0.04	0.015	18	0.5	0	0.65	0.35	0	0	0	0	0	0	0	0	0	0	0	0	0	78.415
AISI 441	0.03	1	1	0.04	0.015	18	0.5	0	0.65	0.35	0	0	0	0	0	0	0	0	0	0	0	0	0	78.415
AISI 441	0.03	1	1	0.04	0.015	18	0.5	0	0.65	0.35	0	0	0	0	0	0	0	0	0	0	0	0	0	78.415
AISI 441	0.03	1	1	0.04	0.015	18	0.5	0	0.65	0.35	0	0	0	0	0	0	0	0	0	0	0	0	0	78.415
AISI 441	0.03	1	1	0.04	0.015	18	0.5	0	0.65	0.35	0	0	0	0	0	0	0	0	0	0	0	0	0	78.415
Fe11Cr0.5Ti	0.022	0.21	0.47	0	0	10.38	0	0	0	0.46	0	0	0	0	0	0	0	0	0	0	0	0	0	88.458
Fe11Cr0.5Ti	0.022	0.21	0.47	0	0	10.38	0	0	0	0.46	0	0	0	0	0	0	0	0	0	0	0	0	0	88.458
Fe18Cr0.5Ti	0.022	0.21	0.47	0	0	17.41	0	0	0	0.46	0	0	0	0	0	0	0	0	0	0	0	0	0	81.428
Fe18Cr0.5Ti	0.022	0.21	0.47	0	0	17.41	0	0	0	0.46	0	0	0	0	0	0	0	0	0	0	0	0	0	81.428
AISI 304	0.0466	1.37	0.46	0.028	0.0006	18.07	8.11	0	0	0	0	0	0	0.0322	0	0	0	0	0	0	0	0	0	71.8826
AISI 304	0.0466	1.37	0.46	0.028	0.0006	18.07	8.11	0	0	0	0	0	0	0.0322	0	0	0	0	0	0	0	0	0	71.8826
AISI 304	0.0466	1.37	0.46	0.028	0.0006	18.07	8.11	0	0	0	0	0	0	0.0322	0	0	0	0	0	0	0	0	0	71.8826
AISI 304	0.0466	1.37	0.46	0.028	0.0006	18.07	8.11	0	0	0	0	0	0	0.0322	0	0	0	0	0	0	0	0	0	71.8826
AISI 304	0.0466	1.37	0.46	0.028	0.0006	18.07	8.11	0	0	0	0	0	0	0.0322	0	0	0	0	0	0	0	0	0	71.8826
AISI 304	0.0466	1.37	0.46	0.028	0.0006	18.07	8.11	0	0	0	0	0	0	0.0322	0	0	0	0	0	0	0	0	0	71.8826
AISI 439	0.006	0.18	0.42	0.033	0.001	17.01	0.23	0	0.17	0.15	0	0	0	0.0122	0	0	0	0	0	0	0	0	0	81.7878
AISI 439	0.006	0.18	0.42	0.033	0.001	17.01	0.23	0	0.17	0.15	0	0	0	0.0122	0	0	0	0	0	0	0	0	0	81.7878
AISI 439	0.006	0.18	0.42	0.033	0.001	17.01	0.23	0	0.17	0.15	0	0	0	0.0122	0	0	0	0	0	0	0	0	0	81.7878
AISI 439	0.006	0.18	0.42	0.033	0.001	17.01	0.23	0	0.17	0.15	0	0	0	0.0122	0	0	0	0	0	0	0	0	0	81.7878
AISI 439	0.006	0.18	0.42	0.033	0.001	17.01	0.23	0	0.17	0.15	0	0	0	0.0122	0	0	0	0	0	0	0	0	0	81.7878
AISI 439	0.006	0.18	0.42	0.033	0.001	17.01	0.23	0	0.17	0.15	0	0	0	0.0122	0	0	0	0	0	0	0	0	0	81.7878
F18TNb/AISI 441	0.01	0.24	0.6	0	0	17.83	0.1	0.01	0.55	0.13	0	0	0	0	0.006	0	0	0	0	0	0	0	0	80.524
F18TNb/AISI 441	0.01	0.24	0.6	0	0	17.83	0.1	0.01	0.55	0.13	0	0	0	0	0.006	0	0	0	0	0	0	0	0	80.524
F18MT/AISI 444	0	0.42	0.42	0	0	17.6	0.1	2.04	0.28	0.16	0	0	0	0	0	0	0	0	0	0	0	0	0	78.98
F18MT/AISI 444	0	0.42	0.42	0	0	17.6	0.1	2.04	0.28	0.16	0	0	0	0	0	0	0	0	0	0	0	0	0	78.98
AISI 304L	0.008	0.9	0.13	0.008	0.0025	18.5	8.3	0	0.01	0	0.36	0.02	0	0.0055	0	0	0	0.0008	0	0.05	0.05	0	0	71.6552
AISI 304L	0.008	0.9	0.13	0.008	0.0025	18.5	8.3	0	0.01	0	0.36	0.02	0	0.0055	0	0	0	0.0008	0	0.05	0.05	0	0	71.6552
AISI 304L	0.008	0.9	0.13	0.008	0.0025	18.5	8.3	0	0.01	0	0.36	0.02	0	0.0055	0	0	0	0.0008	0	0.05	0.05	0	0	71.6552

Table A.1 The first data set is collected for prediction (continue).

Type	C	Mn	Si	P	S	Cr	Ni	Mo	Nb	Ti	Cu	V	O	N	Al	W	Ag	B	Re	Ta	Co	La	Se	Fe
AISI 348	0.052	1.61	0.42	0.017	0.003	17.45	10.94	0	0.83	0	0	0	0	0.018	0	0	0	0.0007	0	0.005	0.023	0	0	68.6313
AISI 348	0.052	1.61	0.42	0.017	0.003	17.45	10.94	0	0.83	0	0	0	0	0.018	0	0	0	0.0007	0	0.005	0.023	0	0	68.6313
AISI 348	0.052	1.61	0.42	0.017	0.003	17.45	10.94	0	0.83	0	0	0	0	0.018	0	0	0	0.0007	0	0.005	0.023	0	0	68.6313
Iron	0.011	0.035	0.035	0.005	0.0094	0.01	0.018	0.005	0.005	0	0.023	0	0	0	0.015	0	0	0	0	0	0	0	0	99.8286
Iron	0.011	0.035	0.035	0.005	0.0094	0.01	0.018	0.005	0.005	0	0.023	0	0	0	0.015	0	0	0	0	0	0	0	0	99.8286
Iron	0.011	0.035	0.035	0.005	0.0094	0.01	0.018	0.005	0.005	0	0.023	0	0	0	0.015	0	0	0	0	0	0	0	0	99.8286
Iron	0.011	0.035	0.035	0.005	0.0094	0.01	0.018	0.005	0.005	0	0.023	0	0	0	0.015	0	0	0	0	0	0	0	0	99.8286
Iron	0.011	0.035	0.035	0.005	0.0094	0.01	0.018	0.005	0.005	0	0.023	0	0	0	0.015	0	0	0	0	0	0	0	0	99.8286
Iron	0.011	0.035	0.035	0.005	0.0094	0.01	0.018	0.005	0.005	0	0.023	0	0	0	0.015	0	0	0	0	0	0	0	0	99.8286

Table A.1 The first data set is collected for prediction (continue)**.**

Type	t (hr)	T (°C)	pO_2 (atm)	pH_2O (atm)	k_p ($g^2/cm^4.s$)	Spallation
AISI 430	500	650	41.45078	0	9.48E-14	0
AISI 430	1000	650	41.45078	0	5.63E-14	0
AISI 630	500	650	41.45078	0	6.48E-15	0
AISI 630	1000	650	41.45078	0	5.14E-15	0
AISI 347 H	500	650	41.45078	0	3.13E-15	1
AISI 347 H	1000	650	41.45078	0	1.27E-13	1
AISI 316 LN	500	650	41.45078	0	5.34E-15	1
AISI 316 LN	1000	650	41.45078	0	4.17E-13	1
Fe22Cr	100	700	0.21	0	4.5E-15	0
Fe22Cr	100	750	0.21	0	3.6E-14	0
Fe22Cr	100	800	0.21	0	1.3E-13	0
Fe22Cr	100	850	0.21	0	3.7E-13	1
Fe22Cr	40	900	0.21	0	1.3E-12	1
330Cb	144	900	0.21	0	1.4E-09	1
0.12B	500	800	0.21	0	0	0
0.12B	500	900	0.21	0	0	0
0.12B2Si	500	800	0.21	0	0	0
0.12B2Si	500	900	0.21	0	0	0
0.12B2Si	500	1000	0.21	0	0	1
0.12B9Ni	500	900	0.21	0	0	0
DD32	500	900	0.21	0	1.26E-14	0
DD32	500	1000	0.21	0	1.8E-14	0
ANSI 310	48	700	0.21	0	5.79E-14	0
ANSI 310	48	750	0.21	0	9.33E-12	0
ANSI 310	48	800	0.21	0	1.02E-10	0
GTD111	96	900	0.21	0	0	0
GTD111	452	900	0.21	0	0	1
Ti36.7Al1.9W0.5Si	240	750	0.21	0	5.4E-14	0
Ti36.7Al1.9W0.5Si	240	850	0.21	0	7.3E-13	1
Ti36.7Al1.9W0.5Si	240	950	0.21	0	3.7E-12	1
Ti36.7Al1.9W0.5Si	240	750	0.2	0	4.6E-14	0
Ti36.7Al1.9W0.5Si	240	850	0.2	0	1.9E-13	0
Ti36.7Al1.9W0.5Si	240	950	0.2	0	1.1E-12	0
Ferritic ss	6.8	600	0.21	0	4.4E-14	0
Ferritic ss	207	600	0.21	0	1.7E-15	0
Ferritic ss	190.5	700	0.21	0	8E-15	0
Ferritic ss	22	800	0.21	0	1E-12	1
Ferritic ss	33.2	600	0	0.025	5.6E-12	0
Ferritic ss	3.6	700	0	0.025	1.5E-11	0
Ferritic ss	216	800	0	0.025	8.5E-14	1
iron	180	650	1	0	6.64E-10	0
iron	180	700	1	0	2.06E-09	1
iron	180	750	1	0	9.1E-09	1
F 20 T	140	849.85	0	0.11	1.26E-12	0
F 20 T	260	849.85	0	0.11	1.17E-12	0

Table A.1 The first data set is collected for prediction (continue)**.**

Type	t (hr)	T (°C)	pO_2 (atm)	pH_2O (atm)	k_p ($g^2/cm^4.s$)	Spallation
F 20 T	500	849.85	0	0.11	1.06E-12	0
F 20 T	760	849.85	0	0.11	9.1E-13	0
F 20 T	1000	849.85	0	0.11	8.21E-13	0
F 20 T	140	849.85	1	0	3.34E-12	0
F 20 T	260	849.85	1	0	3.39E-12	0
F 20 T	500	849.85	1	0	3.47E-12	0
F 20 T	760	849.85	1	0	4.16E-12	0
F 20 T	1000	849.85	1	0	4.34E-12	0
F 20 T	140	849.85	0.21	0.01	2.31E-12	0
F 20 T	260	849.85	0.21	0.01	2.11E-12	0
F 20 T	500	849.85	0.21	0.01	2.15E-12	0
F 20 T	760	849.85	0.21	0.01	1.89E-12	0
F 20 T	1000	849.85	0.21	0.01	1.61E-12	0
TUS 220M	140	849.85	0	0.11	2.35E-13	0
TUS 220M	260	849.85	0	0.11	3.01E-13	0
TUS 220M	500	849.85	0	0.11	2.63E-13	0
TUS 220M	760	849.85	0	0.11	2.6E-13	0
TUS 220M	1000	849.85	0	0.11	2.61E-13	0
TUS 220M	140	849.85	1	0	2.65E-12	0
TUS 220M	260	849.85	1	0	3.51E-12	0
TUS 220M	500	849.85	1	0	6.21E-12	0
TUS 220M	760	849.85	1	0	1.09E-11	0
TUS 220M	1000	849.85	1	0	1.7E-11	0
TUS 220M	140	849.85	0.21	0.01	1.75E-12	0
TUS 220M	260	849.85	0.21	0.01	2.02E-12	0
TUS 220M	500	849.85	0.21	0.01	2.29E-12	0
TUS 220M	760	849.85	0.21	0.01	2.34E-12	0
TUS 220M	1000	849.85	0.21	0.01	2.4E-12	0
AL 453	140	849.85	0	0.11	7.36E-13	0
AL 453	260	849.85	0	0.11	5.52E-13	0
AL 453	500	849.85	0	0.11	3.95E-13	0
AL 453	760	849.85	0	0.11	3.22E-13	0
AL 453	1000	849.85	0	0.11	2.87E-13	0
AL 453	140	849.85	1	0	3.58E-12	0
AL 453	260	849.85	1	0	2.71E-12	0
AL 453	500	849.85	1	0	1.99E-12	0
AL 453	760	849.85	1	0	1.6E-12	0
AL 453	1000	849.85	1	0	1.37E-12	0
AL 453	140	849.85	0.21	0.01	2.14E-12	0
AL 453	260	849.85	0.21	0.01	1.67E-12	0
AL 453	500	849.85	0.21	0.01	1.3E-12	0
AL 453	760	849.85	0.21	0.01	1.04E-12	0
AL 453	1000	849.85	0.21	0.01	9.45E-13	0
Crofer 22 APU	140	849.85	0	0.11	2.33E-13	0
Crofer 22 APU	260	849.85	0	0.11	1.9E-13	0

Table A.1 The first data set is collected for prediction (continue)**.**

Type	t (hr)	T (°C)	pO_2 (atm)	pH_2O (atm)	k_p ($g^2/cm^4.s$)	Spallation
Crofer 22 APU	500	849.85	0	0.11	1.57E-13	0
Crofer 22 APU	760	849.85	0	0.11	1.32E-13	0
Crofer 22 APU	1000	849.85	0	0.11	1.14E-13	0
Crofer 22 APU	140	849.85	1	0	9.34E-13	0
Crofer 22 APU	260	849.85	1	0	1.51E-12	0
Crofer 22 APU	500	849.85	1	0	1.2E-12	0
Crofer 22 APU	760	849.85	1	0	1.85E-12	0
Crofer 22 APU	1000	849.85	1	0	1.65E-12	0
Crofer 22 APU	140	849.85	0.21	0.01	1.57E-13	0
Crofer 22 APU	260	849.85	0.21	0.01	1.76E-13	0
Crofer 22 APU	500	849.85	0.21	0.01	1.92E-13	0
Crofer 22 APU	760	849.85	0.21	0.01	1.91E-13	0
Crofer 22 APU	1000	849.85	0.21	0.01	1.83E-13	0
Crofer 22 H	140	849.85	0	0.11	1.58E-13	0
Crofer 22 H	260	849.85	0	0.11	1.5E-13	0
Crofer 22 H	500	849.85	0	0.11	1.39E-13	0
Crofer 22 H	760	849.85	0	0.11	1.36E-13	0
Crofer 22 H	1000	849.85	0	0.11	1.14E-13	0
Crofer 22 H	140	849.85	1	0	5.43E-13	0
Crofer 22 H	260	849.85	1	0	6.52E-13	0
Crofer 22 H	500	849.85	1	0	7.32E-13	0
Crofer 22 H	760	849.85	1	0	6.45E-13	0
Crofer 22 H	1000	849.85	1	0	7.62E-13	0
Crofer 22 H	140	849.85	0.21	0.01	2.79E-13	0
Crofer 22 H	260	849.85	0.21	0.01	3.69E-13	0
Crofer 22 H	500	849.85	0.21	0.01	3.52E-13	0
Crofer 22 H	760	849.85	0.21	0.01	3.22E-13	0
Crofer 22 H	1000	849.85	0.21	0.01	2.95E-13	0
Sanergy HT	140	849.85	0	0.11	1.24E-13	0
Sanergy HT	260	849.85	0	0.11	9.94E-14	0
Sanergy HT	500	849.85	0	0.11	7.81E-14	0
Sanergy HT	760	849.85	0	0.11	7.24E-14	0
Sanergy HT	1000	849.85	0	0.11	6.51E-14	0
Sanergy HT	140	849.85	1	0	2.11E-12	0
Sanergy HT	260	849.85	1	0	4.68E-12	0
Sanergy HT	500	849.85	1	0	1.43E-11	0
Sanergy HT	760	849.85	1	0	6.07E-11	0
Sanergy HT	1000	849.85	1	0	7.06E-11	0
Sanergy HT	140	849.85	0.21	0.01	1.28E-12	0
Sanergy HT	260	849.85	0.21	0.01	1.43E-12	0
Sanergy HT	500	849.85	0.21	0.01	2.44E-12	0
Sanergy HT	760	849.85	0.21	0.01	4.72E-12	0
Sanergy HT	1000	849.85	0.21	0.01	2.59E-11	0
E-Brite	140	849.85	0	0.11	5.34E-14	0
E-Brite	260	849.85	0	0.11	4.4E-14	0

Table A.1 The first data set is collected for prediction (continue)**.**

Type	t (hr)	T (°C)	pO_2 (atm)	pH_2O (atm)	k_p ($g^2/cm^4.s$)	Spallation
E-Brite	500	849.85	0	0.11	4.26E-14	0
E-Brite	760	849.85	0	0.11	3.93E-14	0
E-Brite	1000	849.85	0	0.11	3.91E-14	0
E-Brite	140	849.85	1	0	2.79E-13	0
E-Brite	260	849.85	1	0	3.1E-13	0
E-Brite	500	849.85	1	0	3.26E-13	0
E-Brite	760	849.85	1	0	3.43E-13	0
E-Brite	1000	849.85	1	0	3.32E-13	0
E-Brite	140	849.85	0.21	0.01	4.5E-13	0
E-Brite	260	849.85	0.21	0.01	4.25E-13	0
E-Brite	500	849.85	0.21	0.01	2.97E-13	0
E-Brite	760	849.85	0.21	0.01	2.6E-13	0
E-Brite	1000	849.85	0.21	0.01	2.36E-13	0
AL 29 4C	140	849.85	0	0.11	3.51E-14	0
AL 29 4C	260	849.85	0	0.11	6.78E-14	0
AL 29 4C	500	849.85	0	0.11	7.81E-14	0
AL 29 4C	760	849.85	0	0.11	8.56E-14	0
AL 29 4C	1000	849.85	0	0.11	9.8E-14	0
AL 29 4C	140	849.85	1	0	1.57E-13	0
AL 29 4C	260	849.85	1	0	2.05E-13	0
AL 29 4C	500	849.85	1	0	2.28E-13	0
AL 29 4C	760	849.85	1	0	2.8E-13	0
AL 29 4C	1000	849.85	1	0	3.71E-13	0
AL 29 4C	140	849.85	0.21	0.01	4.5E-13	0
AL 29 4C	260	849.85	0.21	0.01	4.71E-13	0
AL 29 4C	500	849.85	0.21	0.01	3.52E-13	0
AL 29 4C	760	849.85	0.21	0.01	2.9E-13	0
AL 29 4C	1000	849.85	0.21	0.01	2.87E-13	0
Cu15Ni15Ag	24	600	0.21	0	4.4E-10	0
Cu15Ni15Ag	24	700	0.21	0	2.4E-09	0
Cu25Ni25Ag	24	600	0.21	0	2.6E-10	0
Cu25Ni25Ag	24	700	0.21	0	9.8E-10	0
NCFS	100	1000	0.21	0	6.8E-09	0
NCFS1.5Nb	100	1000	0.21	0	7.9E-09	1
NCFS3Nb	100	1000	0.21	0	1.2E-08	1
AISI430	2000	650	0.21	0	0	0
AISI430	2000	700	0.21	0	0	0
AISI430	2000	750	0.21	0	4.7E-15	0
AISI441	2000	650	0.21	0	0	0
AISI441	2000	700	0.21	0	0	0
AISI441	2000	750	0.21	0	1.1E-14	0
Crofer22H	2000	650	0.21	0	0	0
Crofer22H	2000	700	0.21	0	0	0
Crofer22H	2000	750	0.21	0	3.2E-15	0
Ni base	1925	800	0.21	0	2E-07	0

Table A.1 The first data set is collected for prediction (continue)**.**

Type	t (hr)	T (°C)	pO_2 (atm)	pH_2O (atm)	k_p ($g^2/cm^4.s$)	Spallation
Ni base	1925	900	0.21	0	4E-08	0
Ti-6Al-7Nb	72	600	0.21	0	4.1E-11	0
Ti-6Al-7Nb	72	700	0.21	0	5.8E-10	0
Ti-6Al-7Nb	72	800	0.21	0	3.19E-09	0
AISI 430	24	800	0.2	0	0	0
AISI 430	48	800	0.2	0	0	1
AISI 430	72	800	0.2	0	0	1
AISI 430	96	800	0.2	0	1.07E-13	1
AISI 430	24	800	0	0.18	0	0
AISI 430	48	800	0	0.18	0	0
AISI 430	72	800	0	0.18	0	0
AISI 430	96	800	0	0.18	7.33E-14	1
AISI 441	10	900	0.2	0	0	0
AISI 441	100	800	0	0	0	0
AISI 441	100	800	0	0.2	0	0
AISI 441	100	800	0.2	0	0	0
AISI 441	50	850	0.2	0	9.7E-13	0
AISI 441	50	900	0.2	0	1.7E-12	0
AISI 441	50	950	0.2	0	6E-12	0
AISI 441	50	850	0.000001	0	1.6E-09	0
AISI 441	50	900	0.000001	0	8.9E-10	0
AISI 441	50	950	0.000001	0	7.4E-11	0
Fe11Cr0.5Ti	100	800	0.21	0	9.03E-16	0
Fe11Cr0.5Ti	100	800	0.21	0	6.6E-15	1
Fe18Cr0.5Ti	100	800	0.21	0	1.14E-16	0
Fe18Cr0.5Ti	100	800	0.21	0	1.4E-15	0
AISI 304	50	850	1	0	1.3E-13	0
AISI 304	50	900	1	0	6.2E-12	0
AISI 304	50	950	1	0	1.2E-09	1
AISI 304	50	850	1.46E-20	0.000005	1.6E-13	0
AISI 304	50	900	1.38E-19	0.000005	3E-13	0
AISI 304	50	950	1.46E-18	0.000005	6.4E-13	0
AISI 439	50	850	1	0	3.2E-13	0
AISI 439	50	900	1	0	1.4E-12	0
AISI 439	50	950	1	0	2.5E-12	0
AISI 439	50	850	1.46E-20	0.000005	2.9E-13	0
AISI 439	50	900	1.38E-19	0.000005	1.5E-12	0
AISI 439	50	950	1.46E-18	0.000005	2.6E-12	1
F18TNb/AISI 441	100	800	0.2	0	0	0
F18TNb/AISI 441	200	800	0.2	0	0	1
F18MT/AISI 444	100	800	0	0.02	0	0
F18MT/AISI 444	200	800	0	0.02	0	1
AISI 304L	1.5	1100	0	1	0	1
AISI 304L	1.5	1200	0	1	0	1
AISI 304L	1.5	1300	0	1	0	1

Table A.1 The first data set is collected for prediction (continue)**.**

Type	t (hr)	T (°C)	pO_2 (atm)	pH_2O (atm)	k_p ($g^2/cm^4.s$)	Spallation
AISI 348	1.5	1100	0	1	0	1
AISI 348	1.5	1200	0	1	0	1
AISI 348	1.5	1300	0	1	0	1
Iron	50	650	1	0	8.8E-08	1
Iron	50	700	1	0	2.06E-07	1
Iron	50	750	1	0	1.47E-07	1
Iron	50	650	0	1	6.64E-10	0
Iron	50	700	0	1	2.06E-09	0
Iron	50	750	0	1	9.1E-09	0

Table A.1 The first data set is collected for prediction (continue)**.**

Type	t (hr)	T (°C)	pO_2 (atm)	pH_2O (atm)	FeO_3	FeO	Fe_2O_3	Fe_3O_4	$(Fe,Cr)_3O_4$	Mn_3O_4	Cr_2O_3	$(Cr,Mn,Fe)_3O_4$	CoO	Al_2O_3	WO_3	NiO	SiO_2	Co_3O_4
AISI 430	500	650	41.45078	0	0	0	0	0	0	1	1	0	0	0	0	0	0	0
AISI 430	1000	650	41.45078	0	0	0	0	0	0	1	1	0	0	0	0	0	0	0
AISI 630	500	650	41.45078	0	0	0	0	0	0	0	1	0	0	0	0	0	0	0
AISI 630	1000	650	41.45078	0	0	0	0	0	0	0	1	0	0	0	0	0	0	0
AISI 347 H	500	650	41.45078	0	0	0	0	0	0	0	1	0	0	0	0	0	0	0
AISI 347 H	1000	650	41.45078	0	0	0	0	1	0	0	1	0	0	0	0	0	0	0
AISI 316 LN	500	650	41.45078	0	0	0	0	1	0	0	1	0	0	0	0	0	0	0
AISI 316 LN	1000	650	41.45078	0	0	0	0	1	0	0	1	0	0	0	0	0	0	0
Fe22Cr	100	700	0.21	0	0	0	0	0	0	0	1	0	0	0	0	0	0	0
Fe22Cr	100	750	0.21	0	0	0	0	0	0	0	1	0	0	0	0	0	0	0
Fe22Cr	100	800	0.21	0	1	0	0	0	0	0	1	0	0	0	0	0	0	0
Fe22Cr	100	850	0.21	0	1	0	0	0	0	0	1	0	0	0	0	0	0	0
Fe22Cr	40	900	0.21	0	1	0	0	0	0	0	1	0	0	0	0	0	0	0
330Cb	144	900	0.21	0	0	0	0	0	0	0	1	0	0	0	0	0	0	0
0.12B	500	800	0.21	0	0	0	0	0	0	0	0	0	1	1	1	0	0	1
0.12B	500	900	0.21	0	0	0	0	0	0	0	0	0	1	1	0	0	0	1
0.12B2Si	500	800	0.21	0	0	0	0	0	0	0	0	0	1	1	1	0	1	0
0.12B2Si	500	900	0.21	0	0	0	0	0	0	0	0	0	1	1	1	0	1	0
0.12B2Si	500	1000	0.21	0	0	0	0	0	0	0	0	0	1	1	1	0	1	0
0.12B9Ni	500	900	0.21	0	0	0	0	0	0	0	0	0	1	1	1	1	0	0
DD32	500	900	0.21	0	0	0	0	0	0	0	1	0	1	1	0	1	0	0
DD32	500	1000	0.21	0	0	0	0	0	0	0	0	0	0	1	0	1	0	0
ANSI 310	48	700	0.21	0	0	0	0	0	0	0	1	1	0	0	0	0	0	0
ANSI 310	48	750	0.21	0	0	0	0	0	0	0	1	1	0	0	0	0	0	0
ANSI 310	48	800	0.21	0	0	0	0	0	0	0	1	1	0	0	0	0	0	0
GTD111	96	900	0.21	0	0	0	0	0	0	0	1	0	0	1	0	0	0	0
GTD111	452	900	0.21	0	0	0	0	0	0	0	1	0	0	1	1	1	0	0
Ti36.7Al1.9W0.5Si	240	750	0.21	0	0	0	0	0	0	0	0	0	0	1	0	0	0	0
Ti36.7Al1.9W0.5Si	240	850	0.21	0	0	0	0	0	0	0	0	0	0	1	0	0	0	0
Ti36.7Al1.9W0.5Si	240	950	0.21	0	0	0	0	0	0	0	0	0	0	1	0	0	0	0
Ti36.7Al1.9W0.5Si	240	750	0.2	0	0	0	0	0	0	0	0	0	0	1	0	0	0	0
Ti36.7Al1.9W0.5Si	240	850	0.2	0	0	0	0	0	0	0	0	0	0	1	0	0	0	0
Ti36.7Al1.9W0.5Si	240	950	0.2	0	0	0	0	0	0	0	0	0	0	1	0	0	0	0
Ferritic ss	6.8	600	0.21	0	0	0	0	0	0	0	1	0	0	0	0	0	0	0
Ferritic ss	207	600	0.21	0	0	0	0	0	0	0	1	0	0	0	0	0	0	0
Ferritic ss	190.5	700	0.21	0	0	0	0	0	0	0	1	0	0	0	0	0	0	0
Ferritic ss	22	800	0.21	0	0	0	1	0	0	0	1	0	0	0	0	0	0	0
Ferritic ss	33.2	600	0	0.025	0	1	0	0	1	0	0	0	0	0	0	0	0	0
Ferritic ss	3.6	700	0	0.025	0	1	0	0	1	0	0	0	0	0	0	0	0	0
Ferritic ss	216	800	0	0.025	0	0	0	0	0	0	1	0	0	0	0	0	0	0
iron	180	650	1	0	0	1	1	1	0	0	0	0	0	0	0	0	0	0
iron	180	700	1	0	0	1	1	1	0	0	0	0	0	0	0	0	0	0
iron	180	750	1	0	0	0	1	1	0	0	0	0	0	0	0	0	0	0

Table A.1 The first data set is collected for prediction (continue).

Type	t (hr)	T (°C)	pO_2 (atm)	pH_2O (atm)	FeO_3	FeO	Fe_2O_3	Fe_3O_4	$(Fe,Cr)_3O_4$	Mn_3O_4	Cr_2O_3	$(Cr,Mn,Fe)_3O_4$	CoO	Al_2O_3	WO_3	NiO	SiO_2	Co_3O_4
F 20 T	140	849.85	0	0.11	0	0	0	0	0	0	1	1	0	0	0	0	1	0
F 20 T	260	849.85	0	0.11	0	0	0	0	0	0	1	1	0	0	0	0	1	0
F 20 T	500	849.85	0	0.11	0	0	0	0	0	0	1	1	0	0	0	0	1	0
F 20 T	760	849.85	0	0.11	0	0	0	0	0	0	1	1	0	0	0	0	1	0
F 20 T	1000	849.85	0	0.11	0	0	0	0	0	0	1	1	0	0	0	0	1	0
F 20 T	140	849.85	1	0	0	0	0	0	0	0	1	1	0	0	0	0	1	0
F 20 T	260	849.85	1	0	0	0	0	0	0	0	1	1	0	0	0	0	1	0
F 20 T	500	849.85	1	0	0	0	0	0	0	0	1	1	0	0	0	0	1	0
F 20 T	760	849.85	1	0	0	0	0	0	0	0	1	1	0	0	0	0	1	0
F 20 T	1000	849.85	1	0	0	0	0	0	0	0	1	1	0	0	0	0	1	0
F 20 T	140	849.85	0.21	0.01	0	0	0	0	0	0	1	1	0	0	0	0	1	0
F 20 T	260	849.85	0.21	0.01	0	0	0	0	0	0	1	1	0	0	0	0	1	0
F 20 T	500	849.85	0.21	0.01	0	0	0	0	0	0	1	1	0	0	0	0	1	0
F 20 T	760	849.85	0.21	0.01	0	0	0	0	0	0	1	1	0	0	0	0	1	0
F 20 T	1000	849.85	0.21	0.01	0	0	0	0	0	0	1	1	0	0	0	0	1	0
TUS 220M	140	849.85	0	0.11	0	0	0	0	0	0	1	1	0	0	0	0	0	0
TUS 220M	260	849.85	0	0.11	0	0	0	0	0	0	1	1	0	0	0	0	0	0
TUS 220M	500	849.85	0	0.11	0	0	0	0	0	0	1	1	0	0	0	0	0	0
TUS 220M	760	849.85	0	0.11	0	0	0	0	0	0	1	1	0	0	0	0	0	0
TUS 220M	1000	849.85	0	0.11	0	0	0	0	0	0	1	1	0	0	0	0	0	0
TUS 220M	140	849.85	1	0	0	0	0	0	0	0	1	1	0	0	0	0	0	0
TUS 220M	260	849.85	1	0	0	0	0	0	0	0	1	1	0	0	0	0	0	0
TUS 220M	500	849.85	1	0	0	0	0	0	0	0	1	1	0	0	0	0	0	0
TUS 220M	760	849.85	1	0	0	0	0	0	0	0	1	1	0	0	0	0	0	0
TUS 220M	1000	849.85	1	0	0	0	0	0	0	0	1	1	0	0	0	0	0	0
TUS 220M	140	849.85	0.21	0.01	0	0	0	0	0	0	1	1	0	0	0	0	0	0
TUS 220M	260	849.85	0.21	0.01	0	0	0	0	0	0	1	1	0	0	0	0	0	0
TUS 220M	500	849.85	0.21	0.01	0	0	0	0	0	0	1	1	0	0	0	0	0	0
TUS 220M	760	849.85	0.21	0.01	0	0	0	0	0	0	1	1	0	0	0	0	0	0
TUS 220M	1000	849.85	0.21	0.01	0	0	0	0	0	0	1	1	0	0	0	0	0	0
AL 453	140	849.85	0	0.11	0	0	0	0	0	0	1	1	0	1	0	0	1	0
AL 453	260	849.85	0	0.11	0	0	0	0	0	0	1	1	0	1	0	0	1	0
AL 453	500	849.85	0	0.11	0	0	0	0	0	0	1	1	0	1	0	0	1	0
AL 453	760	849.85	0	0.11	0	0	0	0	0	0	1	1	0	1	0	0	1	0
AL 453	1000	849.85	0	0.11	0	0	0	0	0	0	1	1	0	1	0	0	1	0
AL 453	140	849.85	1	0	0	0	0	0	0	0	1	1	0	1	0	0	1	0
AL 453	260	849.85	1	0	0	0	0	0	0	0	1	1	0	1	0	0	1	0
AL 453	500	849.85	1	0	0	0	0	0	0	0	1	1	0	1	0	0	1	0
AL 453	760	849.85	1	0	0	0	0	0	0	0	1	1	0	1	0	0	1	0
AL 453	1000	849.85	1	0	0	0	0	0	0	0	1	1	0	1	0	0	1	0
AL 453	140	849.85	0.21	0.01	0	0	0	0	0	0	1	1	0	1	0	0	1	0
AL 453	260	849.85	0.21	0.01	0	0	0	0	0	0	1	1	0	1	0	0	1	0
AL 453	500	849.85	0.21	0.01	0	0	0	0	0	0	1	1	0	1	0	0	1	0

Table A.1 The first data set is collected for prediction (continue).

Type	t (hr)	T (°C)	pO_2 (atm)	pH_2O (atm)	FeO_3	FeO	Fe_2O_3	Fe_3O_4	$(Fe,Cr)_3O_4$	Mn_3O_4	Cr_2O_3	$(Cr,Mn,Fe)_3O_4$	CoO	Al_2O_3	WO_3	NiO	SiO_2	Co_3O_4
AL 453	760	849.85	0.21	0.01	0	0	0	0	0	0	1	1	0	1	0	0	1	0
AL 453	1000	849.85	0.21	0.01	0	0	0	0	0	0	1	1	0	1	0	0	1	0
Crofer 22 APU	140	849.85	0	0.11	0	0	0	0	0	0	1	1	0	0	0	0	0	0
Crofer 22 APU	260	849.85	0	0.11	0	0	0	0	0	0	1	1	0	0	0	0	0	0
Crofer 22 APU	500	849.85	0	0.11	0	0	0	0	0	0	1	1	0	0	0	0	0	0
Crofer 22 APU	760	849.85	0	0.11	0	0	0	0	0	0	1	1	0	0	0	0	0	0
Crofer 22 APU	1000	849.85	0	0.11	0	0	0	0	0	0	1	1	0	0	0	0	0	0
Crofer 22 APU	140	849.85	1	0	0	0	0	0	0	0	1	1	0	0	0	0	0	0
Crofer 22 APU	260	849.85	1	0	0	0	0	0	0	0	1	1	0	0	0	0	0	0
Crofer 22 APU	500	849.85	1	0	0	0	0	0	0	0	1	1	0	0	0	0	0	0
Crofer 22 APU	760	849.85	1	0	0	0	0	0	0	0	1	1	0	0	0	0	0	0
Crofer 22 APU	1000	849.85	1	0	0	0	0	0	0	0	1	1	0	0	0	0	0	0
Crofer 22 APU	140	849.85	0.21	0.01	0	0	0	0	0	0	1	1	0	0	0	0	0	0
Crofer 22 APU	260	849.85	0.21	0.01	0	0	0	0	0	0	1	1	0	0	0	0	0	0
Crofer 22 APU	500	849.85	0.21	0.01	0	0	0	0	0	0	1	1	0	0	0	0	0	0
Crofer 22 APU	760	849.85	0.21	0.01	0	0	0	0	0	0	1	1	0	0	0	0	0	0
Crofer 22 APU	1000	849.85	0.21	0.01	0	0	0	0	0	0	1	1	0	0	0	0	0	0
Crofer 22 H	140	849.85	0	0.11	0	0	0	0	0	0	1	1	0	0	0	0	0	0
Crofer 22 H	260	849.85	0	0.11	0	0	0	0	0	0	1	1	0	0	0	0	0	0
Crofer 22 H	500	849.85	0	0.11	0	0	0	0	0	0	1	1	0	0	0	0	0	0
Crofer 22 H	760	849.85	0	0.11	0	0	0	0	0	0	1	1	0	0	0	0	0	0
Crofer 22 H	1000	849.85	0	0.11	0	0	0	0	0	0	1	1	0	0	0	0	0	0
Crofer 22 H	140	849.85	1	0	0	0	0	0	0	0	1	1	0	0	0	0	0	0
Crofer 22 H	260	849.85	1	0	0	0	0	0	0	0	1	1	0	0	0	0	0	0
Crofer 22 H	500	849.85	1	0	0	0	0	0	0	0	1	1	0	0	0	0	0	0
Crofer 22 H	760	849.85	1	0	0	0	0	0	0	0	1	1	0	0	0	0	0	0
Crofer 22 H	1000	849.85	1	0	0	0	0	0	0	0	1	1	0	0	0	0	0	0
Crofer 22 H	140	849.85	0.21	0.01	0	0	0	0	0	0	1	1	0	0	0	0	0	0
Crofer 22 H	260	849.85	0.21	0.01	0	0	0	0	0	0	1	1	0	0	0	0	0	0
Crofer 22 H	500	849.85	0.21	0.01	0	0	0	0	0	0	1	1	0	0	0	0	0	0
Crofer 22 H	760	849.85	0.21	0.01	0	0	0	0	0	0	1	1	0	0	0	0	0	0
Crofer 22 H	1000	849.85	0.21	0.01	0	0	0	0	0	0	1	1	0	0	0	0	0	0
Sanergy HT	140	849.85	0	0.11	0	0	0	0	0	0	1	1	0	0	0	0	0	0
Sanergy HT	260	849.85	0	0.11	0	0	0	0	0	0	1	1	0	0	0	0	0	0
Sanergy HT	500	849.85	0	0.11	0	0	0	0	0	0	1	1	0	0	0	0	0	0
Sanergy HT	760	849.85	0	0.11	0	0	0	0	0	0	1	1	0	0	0	0	0	0
Sanergy HT	1000	849.85	0	0.11	0	0	0	0	0	0	1	1	0	0	0	0	0	0
Sanergy HT	140	849.85	1	0	0	0	0	0	0	0	1	1	0	0	0	0	0	0
Sanergy HT	260	849.85	1	0	0	0	0	0	0	0	1	1	0	0	0	0	0	0
Sanergy HT	500	849.85	1	0	0	0	0	0	0	0	1	1	0	0	0	0	0	0
Sanergy HT	760	849.85	1	0	0	0	0	0	0	0	1	1	0	0	0	0	0	0
Sanergy HT	1000	849.85	1	0	0	0	0	0	0	0	1	1	0	0	0	0	0	0
Sanergy HT	140	849.85	0.21	0.01	0	0	0	0	0	0	1	1	0	0	0	0	0	0

Table A.1 The first data set is collected for prediction (continue).

Type	t (hr)	T (°C)	pO_2 (atm)	pH_2O (atm)	FeO_3	FeO	Fe_2O_3	Fe_3O_4	$(Fe,Cr)_3O_4$	Mn_3O_4	Cr_2O_3	$(Cr,Mn,Fe)_3O_4$	CoO	Al_2O_3	WO_3	NiO	SiO_2	Co_3O_4
Sanergy HT	260	849.85	0.21	0.01	0	0	0	0	0	0	1	1	0	0	0	0	0	0
Sanergy HT	500	849.85	0.21	0.01	0	0	0	0	0	0	1	1	0	0	0	0	0	0
Sanergy HT	760	849.85	0.21	0.01	0	0	0	0	0	0	1	1	0	0	0	0	0	0
Sanergy HT	1000	849.85	0.21	0.01	0	0	0	0	0	0	1	1	0	0	0	0	0	0
E-Brite	140	849.85	0	0.11	0	0	0	0	0	0	1	1	0	0	0	0	1	0
E-Brite	260	849.85	0	0.11	0	0	0	0	0	0	1	1	0	0	0	0	1	0
E-Brite	500	849.85	0	0.11	0	0	0	0	0	0	1	1	0	0	0	0	1	0
E-Brite	760	849.85	0	0.11	0	0	0	0	0	0	1	1	0	0	0	0	1	0
E-Brite	1000	849.85	0	0.11	0	0	0	0	0	0	1	1	0	0	0	0	1	0
E-Brite	140	849.85	1	0	0	0	0	0	0	0	1	1	0	0	0	0	1	0
E-Brite	260	849.85	1	0	0	0	0	0	0	0	1	1	0	0	0	0	1	0
E-Brite	500	849.85	1	0	0	0	0	0	0	0	1	1	0	0	0	0	1	0
E-Brite	760	849.85	1	0	0	0	0	0	0	0	1	1	0	0	0	0	1	0
E-Brite	1000	849.85	1	0	0	0	0	0	0	0	1	1	0	0	0	0	1	0
E-Brite	140	849.85	0.21	0.01	0	0	0	0	0	0	1	1	0	0	0	0	1	0
E-Brite	260	849.85	0.21	0.01	0	0	0	0	0	0	1	1	0	0	0	0	1	0
E-Brite	500	849.85	0.21	0.01	0	0	0	0	0	0	1	1	0	0	0	0	1	0
E-Brite	760	849.85	0.21	0.01	0	0	0	0	0	0	1	1	0	0	0	0	1	0
E-Brite	1000	849.85	0.21	0.01	0	0	0	0	0	0	1	1	0	0	0	0	1	0
AL 29 4C	140	849.85	0	0.11	0	0	0	0	0	0	1	1	0	0	0	0	0	0
AL 29 4C	260	849.85	0	0.11	0	0	0	0	0	0	1	1	0	0	0	0	0	0
AL 29 4C	500	849.85	0	0.11	0	0	0	0	0	0	1	1	0	0	0	0	0	0
AL 29 4C	760	849.85	0	0.11	0	0	0	0	0	0	1	1	0	0	0	0	0	0
AL 29 4C	1000	849.85	0	0.11	0	0	0	0	0	0	1	1	0	0	0	0	0	0
AL 29 4C	140	849.85	1	0	0	0	0	0	0	0	1	1	0	0	0	0	0	0
AL 29 4C	260	849.85	1	0	0	0	0	0	0	0	1	1	0	0	0	0	0	0
AL 29 4C	500	849.85	1	0	0	0	0	0	0	0	1	1	0	0	0	0	0	0
AL 29 4C	760	849.85	1	0	0	0	0	0	0	0	1	1	0	0	0	0	0	0
AL 29 4C	1000	849.85	1	0	0	0	0	0	0	0	1	1	0	0	0	0	0	0
AL 29 4C	140	849.85	0.21	0.01	0	0	0	0	0	0	1	1	0	0	0	0	0	0
AL 29 4C	260	849.85	0.21	0.01	0	0	0	0	0	0	1	1	0	0	0	0	0	0
AL 29 4C	500	849.85	0.21	0.01	0	0	0	0	0	0	1	1	0	0	0	0	0	0
AL 29 4C	760	849.85	0.21	0.01	0	0	0	0	0	0	1	1	0	0	0	0	0	0
AL 29 4C	1000	849.85	0.21	0.01	0	0	0	0	0	0	1	1	0	0	0	0	0	0
Cu15Ni15Ag	24	600	0.21	0	0	0	0	0	0	0	0	0	0	0	0	1	0	0
Cu15Ni15Ag	24	700	0.21	0	0	0	0	0	0	0	0	0	0	0	0	1	0	0
Cu25Ni25Ag	24	600	0.21	0	0	0	0	0	0	0	0	0	0	0	0	1	0	0
Cu25Ni25Ag	24	700	0.21	0	0	0	0	0	0	0	0	0	0	0	0	1	0	0
NCFS	100	1000	0.21	0	0	0	0	0	0	0	1	0	0	0	0	0	1	0
NCFS1.5Nb	100	1000	0.21	0	0	0	0	0	0	0	1	0	0	0	0	0	1	0
NCFS3Nb	100	1000	0.21	0	0	0	0	0	0	0	1	0	0	0	0	0	1	0
AISI430	2000	650	0.21	0	0	0	0	0	0	0	1	0	0	0	0	0	1	0
AISI430	2000	700	0.21	0	0	0	0	0	0	0	1	0	0	0	0	0	1	0

Table A.1 The first data set is collected for prediction (continue)**.**

Type	t (hr)	T (°C)	pO_2 (atm)	pH_2O (atm)	FeO_3	FeO	Fe_2O_3	Fe_3O_4	$(Fe,Cr)_3O_4$	Mn_3O_4	Cr_2O_3	$(Cr,Mn,Fe)_3O_4$	CoO	Al_2O_3	WO_3	NiO	SiO_2	Co_3O_4
AISI430	2000	750	0.21	0	0	0	0	0	0	0	1	0	0	0	0	0	1	0
AISI441	2000	650	0.21	0	0	0	0	0	0	0	1	0	0	0	0	0	1	0
AISI441	2000	700	0.21	0	0	0	0	0	0	0	1	0	0	0	0	0	1	0
AISI441	2000	750	0.21	0	0	0	0	0	0	0	1	0	0	0	0	0	1	0
Crofer22H	2000	650	0.21	0	0	0	0	0	0	0	1	0	0	0	0	0	0	0
Crofer22H	2000	700	0.21	0	0	0	0	0	0	0	1	0	0	0	0	0	0	0
Crofer22H	2000	750	0.21	0	0	0	0	0	0	0	1	0	0	0	0	0	1	0
Ni base	1925	800	0.21	0	0	0	0	0	0	0	1	0	0	1	0	1	0	0
Ni base	1925	900	0.21	0	0	0	0	0	0	0	0	0	0	1	0	1	0	0
Ti-6Al-7Nb	72	600	0.21	0	0	0	0	0	0	0	0	0	0	0	0	0	0	0
Ti-6Al-7Nb	72	700	0.21	0	0	0	0	0	0	0	0	0	0	0	0	0	0	0
Ti-6Al-7Nb	72	800	0.21	0	0	0	0	0	0	0	0	0	0	1	0	0	0	0
AISI 430	24	800	0.2	0	0	0	0	0	0	0	1	0	0	0	0	0	0	0
AISI 430	48	800	0.2	0	0	0	0	0	0	0	1	0	0	0	0	0	0	0
AISI 430	72	800	0.2	0	0	0	0	0	0	0	1	0	0	0	0	0	0	0
AISI 430	96	800	0.2	0	0	0	0	0	0	0	1	0	0	0	0	0	0	0
AISI 430	24	800	0	0.18	0	0	0	0	0	0	1	0	0	0	0	0	0	0
AISI 430	48	800	0	0.18	0	0	0	0	0	0	1	0	0	0	0	0	0	0
AISI 430	72	800	0	0.18	0	0	0	0	0	0	1	0	0	0	0	0	0	0
AISI 430	96	800	0	0.18	0	0	0	0	0	0	1	0	0	0	0	0	0	0
AISI 441	10	900	0.2	0	0	0	0	0	0	0	1	0	0	0	0	0	0	0
AISI 441	100	800	0	0	0	0	0	0	0	0	1	1	0	0	0	0	0	0
AISI 441	100	800	0	0.2	0	0	0	0	0	0	1	1	0	0	0	0	0	0
AISI 441	100	800	0.2	0	0	0	0	0	0	0	1	1	0	0	0	0	0	0
AISI 441	50	850	0.2	0	0	0	0	0	0	0	1	1	0	0	0	0	0	0
AISI 441	50	900	0.2	0	0	0	0	0	0	0	1	1	0	0	0	0	0	0
AISI 441	50	950	0.2	0	0	0	0	0	0	0	1	1	0	0	0	0	0	0
AISI 441	50	850	0.000001	0	0	0	0	0	0	0	1	0	0	0	0	0	0	0
AISI 441	50	900	0.000001	0	0	0	0	0	0	0	1	0	0	0	0	0	1	0
AISI 441	50	950	0.000001	0	0	0	0	0	0	0	1	0	0	0	0	0	1	0
Fe11Cr0.5Ti	100	800	0.21	0	0	0	0	0	0	0	0	0	0	0	0	0	0	0
Fe11Cr0.5Ti	100	800	0.21	0	0	0	1	0	0	0	0	0	0	0	0	0	0	0
Fe18Cr0.5Ti	100	800	0.21	0	0	0	0	0	0	0	0	0	0	0	0	0	0	0
Fe18Cr0.5Ti	100	800	0.21	0	0	0	0	0	0	0	1	0	0	0	0	0	0	0
AISI 304	50	850	1	0	0	0	0	0	1	1	0	0	0	0	0	0	0	0
AISI 304	50	900	1	0	0	0	0	0	1	1	0	0	0	0	0	0	0	0
AISI 304	50	950	1	0	0	0	1	0	0	0	0	0	0	0	0	0	1	0
AISI 304	50	850	1.46E-20	0.000005	0	0	0	0	0	0	1	0	0	0	0	0	0	0
AISI 304	50	900	1.38E-19	0.000005	0	0	0	0	0	0	1	0	0	0	0	0	0	0
AISI 304	50	950	1.46E-18	0.000005	0	0	0	0	0	0	1	0	0	0	0	0	0	0
AISI 439	50	850	1	0	0	0	0	0	0	1	1	0	0	0	0	0	0	0
AISI 439	50	900	1	0	0	0	0	0	0	1	1	0	0	0	0	0	0	0
AISI 439	50	950	1	0	0	0	0	0	0	1	1	0	0	0	0	0	0	0

Table A.1 The first data set is collected for prediction (continue)**.**

Type	t (hr)	T (°C)	pO_2 (atm)	pH_2O (atm)	FeO_3	FeO	Fe_2O_3	Fe_3O_4	$(Fe,Cr)_3O_4$	Mn_3O_4	Cr_2O_3	$(Cr,Mn,Fe)_3O_4$	CoO	Al_2O_3	WO_3	NiO	SiO_2	Co_3O_4
AISI 439	50	850	1.46E-20	0.000005	0	0	0	0	0	0	1	0	0	0	0	0	0	0
AISI 439	50	900	1.38E-19	0.000005	0	0	0	0	0	0	1	0	0	0	0	0	0	0
AISI 439	50	950	1.46E-18	0.000005	0	0	0	0	0	0	1	0	0	0	0	0	0	0
F18TNb/AISI 441	100	800	0.2	0	0	0	0	0	0	0	1	0	0	0	0	0	0	0
F18TNb/AISI 441	200	800	0.2	0	0	0	0	0	0	0	1	0	0	0	0	0	0	0
F18MT/AISI 444	100	800	0	0.02	0	0	0	0	0	0	1	0	0	0	0	0	0	0
F18MT/AISI 444	200	800	0	0.02	0	0	0	0	0	0	1	0	0	0	0	0	0	0
AISI 304L	1.5	1100	0	1	0	0	1	1	1	0	0	0	0	0	0	0	0	0
AISI 304L	1.5	1200	0	1	0	0	1	1	1	0	0	0	0	0	0	0	0	0
AISI 304L	1.5	1300	0	1	0	0	1	1	1	0	0	0	0	0	0	0	0	0
AISI 348	1.5	1100	0	1	0	0	1	1	1	0	0	0	0	0	0	0	0	0
AISI 348	1.5	1200	0	1	0	0	1	1	1	0	0	0	0	0	0	0	0	0
AISI 348	1.5	1300	0	1	0	0	1	1	1	0	0	0	0	0	0	0	0	0
Iron	50	650	1	0	0	1	1	1	0	0	0	0	0	0	0	0	0	0
Iron	50	700	1	0	0	1	1	1	0	0	0	0	0	0	0	0	0	0
Iron	50	750	1	0	0	1	1	1	0	0	0	0	0	0	0	0	0	0
Iron	50	650	0	1	0	1	1	1	0	0	0	0	0	0	0	0	0	0
Iron	50	700	0	1	0	1	1	1	0	0	0	0	0	0	0	0	0	0
Iron	50	750	0	1	0	1	1	1	0	0	0	0	0	0	0	0	0	0

Table A.1 The first data set is collected for prediction (continue)**.**

Type	$CoWO_4$	$CrTaO_4$	$NiCr_2O_4$	$NiAl_2O_4$	$CoAl_2O_4$	TiO_2	$MnTiO_3$	Ni_5TiO_7	Cr_2TiO_5	$CrWO_4$	$W_{20}O_{58}$	Ta_2O_5	CuO	Cu_2O	Nb_2O_5	$(Ni,Co)Al_2O_4$	$NiTiO_3$	$(Mn,Cr)_3O_4$
AISI 430	0	0	0	0	0	0	0	0	0	0	0	0	0	0	0	0	0	0
AISI 430	0	0	0	0	0	0	0	0	0	0	0	0	0	0	0	0	0	0
AISI 630	0	0	0	0	0	0	0	0	0	0	0	0	0	0	0	0	0	0
AISI 630	0	0	0	0	0	0	0	0	0	0	0	0	0	0	0	0	0	0
AISI 347 H	0	0	0	0	0	0	0	0	0	0	0	0	0	0	0	0	0	0
AISI 347 H	0	0	0	0	0	0	0	0	0	0	0	0	0	0	0	0	0	0
AISI 316 LN	0	0	0	0	0	0	0	0	0	0	0	0	0	0	0	0	0	0
AISI 316 LN	0	0	0	0	0	0	0	0	0	0	0	0	0	0	0	0	0	0
Fe22Cr	0	0	0	0	0	0	0	0	0	0	0	0	0	0	0	0	0	0
Fe22Cr	0	0	0	0	0	0	0	0	0	0	0	0	0	0	0	0	0	0
Fe22Cr	0	0	0	0	0	0	0	0	0	0	0	0	0	0	0	0	0	0
Fe22Cr	0	0	0	0	0	0	0	0	0	0	0	0	0	0	0	0	0	0
Fe22Cr	0	0	0	0	0	0	0	0	0	0	0	0	0	0	0	0	0	0
330Cb	0	0	0	0	0	0	0	0	0	0	0	0	0	0	0	0	0	1
0.12B	1	0	0	0	0	0	0	0	0	0	0	0	0	0	0	0	0	0
0.12B	1	0	0	0	0	0	0	0	0	0	0	0	0	0	0	0	0	0
0.12B2Si	0	0	0	0	0	0	0	0	0	0	0	0	0	0	0	0	0	0
0.12B2Si	0	0	0	0	0	0	0	0	0	0	0	0	0	0	0	0	0	0
0.12B2Si	0	0	0	0	0	0	0	0	0	0	0	0	0	0	0	0	0	0
0.12B9Ni	0	0	0	0	0	0	0	0	0	0	0	0	0	0	0	0	0	0
DD32	0	1	1	1	1	0	0	0	0	0	1	0	0	0	0	0	0	0
DD32	0	1	1	1	1	0	0	0	0	0	1	0	0	0	0	0	0	0
ANSI 310	0	0	0	0	0	0	0	0	0	0	0	0	0	0	0	0	0	0
ANSI 310	0	0	0	0	0	0	0	0	0	0	0	0	0	0	0	0	0	0
ANSI 310	0	0	0	0	0	0	0	0	0	0	0	0	0	0	0	0	0	0
GTD111	0	1	1	0	0	1	0	1	1	1	0	0	0	0	0	0	0	0
GTD111	0	1	1	0	0	1	0	1	1	1	0	1	0	0	0	0	0	0
Ti36.7Al1.9W0.5Si	0	0	0	0	0	1	0	0	0	0	0	0	0	0	0	0	0	0
Ti36.7Al1.9W0.5Si	0	0	0	0	0	1	0	0	0	0	0	0	0	0	0	0	0	0
Ti36.7Al1.9W0.5Si	0	0	0	0	0	1	0	0	0	0	0	0	0	0	0	0	0	0
Ti36.7Al1.9W0.5Si	0	0	0	0	0	1	0	0	0	0	0	0	0	0	0	0	0	0
Ti36.7Al1.9W0.5Si	0	0	0	0	0	1	0	0	0	0	0	0	0	0	0	0	0	0
Ti36.7Al1.9W0.5Si	0	0	0	0	0	1	0	0	0	0	0	0	0	0	0	0	0	0
Ferritic ss	0	0	0	0	0	0	0	0	0	0	0	0	0	0	0	0	0	0
Ferritic ss	0	0	0	0	0	0	0	0	0	0	0	0	0	0	0	0	0	0
Ferritic ss	0	0	0	0	0	0	0	0	0	0	0	0	0	0	0	0	0	0
Ferritic ss	0	0	0	0	0	0	0	0	0	0	0	0	0	0	0	0	0	0
Ferritic ss	0	0	0	0	0	0	0	0	0	0	0	0	0	0	0	0	0	0
Ferritic ss	0	0	0	0	0	0	0	0	0	0	0	0	0	0	0	0	0	0
Ferritic ss	0	0	0	0	0	0	0	0	0	0	0	0	0	0	0	0	0	0
iron	0	0	0	0	0	0	0	0	0	0	0	0	0	0	0	0	0	0
iron	0	0	0	0	0	0	0	0	0	0	0	0	0	0	0	0	0	0
iron	0	0	0	0	0	0	0	0	0	0	0	0	0	0	0	0	0	0

Table A.1 The first data set is collected for prediction (continue).

Type	$CoWO_4$	$CrTaO_4$	$NiCr_2O_4$	$NiAl_2O_4$	$CoAl_2O_4$	TiO_2	$MnTiO_3$	Ni_5TiO_7	Cr_2TiO_5	$CrWO_4$	$W_{20}O_{58}$	Ta_2O_5	CuO	Cu_2O	Nb_2O_5	$(Ni,Co)Al_2O_4$	$NiTiO_3$	$(Mn,Cr)_3O_4$
F 20 T	0	0	0	0	0	0	1	0	0	0	0	0	0	0	0	0	0	0
F 20 T	0	0	0	0	0	0	1	0	0	0	0	0	0	0	0	0	0	0
F 20 T	0	0	0	0	0	0	1	0	0	0	0	0	0	0	0	0	0	0
F 20 T	0	0	0	0	0	0	1	0	0	0	0	0	0	0	0	0	0	0
F 20 T	0	0	0	0	0	0	1	0	0	0	0	0	0	0	0	0	0	0
F 20 T	0	0	0	0	0	0	0	0	0	0	0	0	0	0	0	0	0	0
F 20 T	0	0	0	0	0	0	0	0	0	0	0	0	0	0	0	0	0	0
F 20 T	0	0	0	0	0	0	0	0	0	0	0	0	0	0	0	0	0	0
F 20 T	0	0	0	0	0	0	0	0	0	0	0	0	0	0	0	0	0	0
F 20 T	0	0	0	0	0	0	0	0	0	0	0	0	0	0	0	0	0	0
F 20 T	0	0	0	0	0	1	0	0	0	0	0	0	0	0	0	0	0	0
F 20 T	0	0	0	0	0	1	0	0	0	0	0	0	0	0	0	0	0	0
F 20 T	0	0	0	0	0	1	0	0	0	0	0	0	0	0	0	0	0	0
F 20 T	0	0	0	0	0	1	0	0	0	0	0	0	0	0	0	0	0	0
F 20 T	0	0	0	0	0	1	0	0	0	0	0	0	0	0	0	0	0	0
TUS 220M	0	0	0	0	0	0	0	0	0	0	0	0	0	0	0	0	0	0
TUS 220M	0	0	0	0	0	0	0	0	0	0	0	0	0	0	0	0	0	0
TUS 220M	0	0	0	0	0	0	0	0	0	0	0	0	0	0	0	0	0	0
TUS 220M	0	0	0	0	0	0	0	0	0	0	0	0	0	0	0	0	0	0
TUS 220M	0	0	0	0	0	0	0	0	0	0	0	0	0	0	0	0	0	0
TUS 220M	0	0	0	0	0	0	0	0	0	0	0	0	0	0	0	0	0	0
TUS 220M	0	0	0	0	0	0	0	0	0	0	0	0	0	0	0	0	0	0
TUS 220M	0	0	0	0	0	0	0	0	0	0	0	0	0	0	0	0	0	0
TUS 220M	0	0	0	0	0	0	0	0	0	0	0	0	0	0	0	0	0	0
TUS 220M	0	0	0	0	0	0	0	0	0	0	0	0	0	0	0	0	0	0
TUS 220M	0	0	0	0	0	1	0	0	0	0	0	0	0	0	0	0	0	0
TUS 220M	0	0	0	0	0	1	0	0	0	0	0	0	0	0	0	0	0	0
TUS 220M	0	0	0	0	0	1	0	0	0	0	0	0	0	0	0	0	0	0
TUS 220M	0	0	0	0	0	1	0	0	0	0	0	0	0	0	0	0	0	0
TUS 220M	0	0	0	0	0	1	0	0	0	0	0	0	0	0	0	0	0	0
AL 453	0	0	0	0	0	0	0	0	0	0	0	0	0	0	0	0	0	0
AL 453	0	0	0	0	0	0	0	0	0	0	0	0	0	0	0	0	0	0
AL 453	0	0	0	0	0	0	0	0	0	0	0	0	0	0	0	0	0	0
AL 453	0	0	0	0	0	0	0	0	0	0	0	0	0	0	0	0	0	0
AL 453	0	0	0	0	0	0	0	0	0	0	0	0	0	0	0	0	0	0
AL 453	0	0	0	0	0	0	0	0	0	0	0	0	0	0	0	0	0	0
AL 453	0	0	0	0	0	0	0	0	0	0	0	0	0	0	0	0	0	0
AL 453	0	0	0	0	0	0	0	0	0	0	0	0	0	0	0	0	0	0
AL 453	0	0	0	0	0	0	0	0	0	0	0	0	0	0	0	0	0	0
AL 453	0	0	0	0	0	0	0	0	0	0	0	0	0	0	0	0	0	0
AL 453	0	0	0	0	0	0	0	0	0	0	0	0	0	0	0	0	0	0
AL 453	0	0	0	0	0	0	0	0	0	0	0	0	0	0	0	0	0	0
AL 453	0	0	0	0	0	0	0	0	0	0	0	0	0	0	0	0	0	0

Table A.1 The first data set is collected for prediction (continue).

Type	$CoWO_4$	$CrTaO_4$	$NiCr_2O_4$	$NiAl_2O_4$	$CoAl_2O_4$	TiO_2	$MnTiO_3$	Ni_5TiO_7	Cr_2TiO_5	$CrWO_4$	$W_{20}O_{58}$	Ta_2O_5	CuO	Cu_2O	Nb_2O_5	$(Ni,Co)Al_2O_4$	$NiTiO_3$	$(Mn,Cr)_3O_4$
AL 453	0	0	0	0	0	0	0	0	0	0	0	0	0	0	0	0	0	0
AL 453	0	0	0	0	0	0	0	0	0	0	0	0	0	0	0	0	0	0
Crofer 22 APU	0	0	0	0	0	0	0	0	0	0	0	0	0	0	0	0	0	0
Crofer 22 APU	0	0	0	0	0	0	0	0	0	0	0	0	0	0	0	0	0	0
Crofer 22 APU	0	0	0	0	0	0	0	0	0	0	0	0	0	0	0	0	0	0
Crofer 22 APU	0	0	0	0	0	0	0	0	0	0	0	0	0	0	0	0	0	0
Crofer 22 APU	0	0	0	0	0	0	0	0	0	0	0	0	0	0	0	0	0	0
Crofer 22 APU	0	0	0	0	0	0	0	0	0	0	0	0	0	0	0	0	0	0
Crofer 22 APU	0	0	0	0	0	0	0	0	0	0	0	0	0	0	0	0	0	0
Crofer 22 APU	0	0	0	0	0	0	0	0	0	0	0	0	0	0	0	0	0	0
Crofer 22 APU	0	0	0	0	0	0	0	0	0	0	0	0	0	0	0	0	0	0
Crofer 22 APU	0	0	0	0	0	0	0	0	0	0	0	0	0	0	0	0	0	0
Crofer 22 APU	0	0	0	0	0	0	0	0	0	0	0	0	0	0	0	0	0	0
Crofer 22 APU	0	0	0	0	0	0	0	0	0	0	0	0	0	0	0	0	0	0
Crofer 22 APU	0	0	0	0	0	0	0	0	0	0	0	0	0	0	0	0	0	0
Crofer 22 APU	0	0	0	0	0	0	0	0	0	0	0	0	0	0	0	0	0	0
Crofer 22 APU	0	0	0	0	0	0	0	0	0	0	0	0	0	0	0	0	0	0
Crofer 22 H	0	0	0	0	0	0	0	0	0	0	0	0	0	0	0	0	0	0
Crofer 22 H	0	0	0	0	0	0	0	0	0	0	0	0	0	0	0	0	0	0
Crofer 22 H	0	0	0	0	0	0	0	0	0	0	0	0	0	0	0	0	0	0
Crofer 22 H	0	0	0	0	0	0	0	0	0	0	0	0	0	0	0	0	0	0
Crofer 22 H	0	0	0	0	0	0	0	0	0	0	0	0	0	0	0	0	0	0
Crofer 22 H	0	0	0	0	0	0	0	0	0	0	0	0	0	0	0	0	0	0
Crofer 22 H	0	0	0	0	0	0	0	0	0	0	0	0	0	0	0	0	0	0
Crofer 22 H	0	0	0	0	0	0	0	0	0	0	0	0	0	0	0	0	0	0
Crofer 22 H	0	0	0	0	0	0	0	0	0	0	0	0	0	0	0	0	0	0
Crofer 22 H	0	0	0	0	0	0	0	0	0	0	0	0	0	0	0	0	0	0
Crofer 22 H	0	0	0	0	0	0	0	0	0	0	0	0	0	0	0	0	0	0
Crofer 22 H	0	0	0	0	0	0	0	0	0	0	0	0	0	0	0	0	0	0
Crofer 22 H	0	0	0	0	0	0	0	0	0	0	0	0	0	0	0	0	0	0
Crofer 22 H	0	0	0	0	0	0	0	0	0	0	0	0	0	0	0	0	0	0
Crofer 22 H	0	0	0	0	0	0	0	0	0	0	0	0	0	0	0	0	0	0
Sanergy HT	0	0	0	0	0	0	0	0	0	0	0	0	0	0	0	0	0	0
Sanergy HT	0	0	0	0	0	0	0	0	0	0	0	0	0	0	0	0	0	0
Sanergy HT	0	0	0	0	0	0	0	0	0	0	0	0	0	0	0	0	0	0
Sanergy HT	0	0	0	0	0	0	0	0	0	0	0	0	0	0	0	0	0	0
Sanergy HT	0	0	0	0	0	0	0	0	0	0	0	0	0	0	0	0	0	0
Sanergy HT	0	0	0	0	0	0	0	0	0	0	0	0	0	0	0	0	0	0
Sanergy HT	0	0	0	0	0	0	0	0	0	0	0	0	0	0	0	0	0	0
Sanergy HT	0	0	0	0	0	0	0	0	0	0	0	0	0	0	0	0	0	0
Sanergy HT	0	0	0	0	0	0	0	0	0	0	0	0	0	0	0	0	0	0
Sanergy HT	0	0	0	0	0	0	0	0	0	0	0	0	0	0	0	0	0	0
Sanergy HT	0	0	0	0	0	0	0	0	0	0	0	0	0	0	0	0	0	0

Table A.1 The first data set is collected for prediction (continue).

Type	$CoWO_4$	$CrTaO_4$	$NiCr_2O_4$	$NiAl_2O_4$	$CoAl_2O_4$	TiO_2	$MnTiO_3$	Ni_5TiO_7	Cr_2TiO_5	$CrWO_4$	$W_{20}O_{58}$	Ta_2O_5	CuO	Cu_2O	Nb_2O_5	$(Ni,Co)Al_2O_4$	$NiTiO_3$	$(Mn,Cr)_3O_4$
Sanergy HT	0	0	0	0	0	0	0	0	0	0	0	0	0	0	0	0	0	0
Sanergy HT	0	0	0	0	0	0	0	0	0	0	0	0	0	0	0	0	0	0
Sanergy HT	0	0	0	0	0	0	0	0	0	0	0	0	0	0	0	0	0	0
Sanergy HT	0	0	0	0	0	0	0	0	0	0	0	0	0	0	0	0	0	0
E-Brite	0	0	0	0	0	0	0	0	0	0	0	0	0	0	0	0	0	0
E-Brite	0	0	0	0	0	0	0	0	0	0	0	0	0	0	0	0	0	0
E-Brite	0	0	0	0	0	0	0	0	0	0	0	0	0	0	0	0	0	0
E-Brite	0	0	0	0	0	0	0	0	0	0	0	0	0	0	0	0	0	0
E-Brite	0	0	0	0	0	0	0	0	0	0	0	0	0	0	0	0	0	0
E-Brite	0	0	0	0	0	0	0	0	0	0	0	0	0	0	0	0	0	0
E-Brite	0	0	0	0	0	0	0	0	0	0	0	0	0	0	0	0	0	0
E-Brite	0	0	0	0	0	0	0	0	0	0	0	0	0	0	0	0	0	0
E-Brite	0	0	0	0	0	0	0	0	0	0	0	0	0	0	0	0	0	0
E-Brite	0	0	0	0	0	0	0	0	0	0	0	0	0	0	0	0	0	0
E-Brite	0	0	0	0	0	0	0	0	0	0	0	0	0	0	0	0	0	0
E-Brite	0	0	0	0	0	0	0	0	0	0	0	0	0	0	0	0	0	0
E-Brite	0	0	0	0	0	0	0	0	0	0	0	0	0	0	0	0	0	0
E-Brite	0	0	0	0	0	0	0	0	0	0	0	0	0	0	0	0	0	0
E-Brite	0	0	0	0	0	0	0	0	0	0	0	0	0	0	0	0	0	0
AL 29 4C	0	0	0	0	0	0	0	0	0	0	0	0	0	0	0	0	0	0
AL 29 4C	0	0	0	0	0	0	0	0	0	0	0	0	0	0	0	0	0	0
AL 29 4C	0	0	0	0	0	0	0	0	0	0	0	0	0	0	0	0	0	0
AL 29 4C	0	0	0	0	0	0	0	0	0	0	0	0	0	0	0	0	0	0
AL 29 4C	0	0	0	0	0	0	0	0	0	0	0	0	0	0	0	0	0	0
AL 29 4C	0	0	0	0	0	0	0	0	0	0	0	0	0	0	0	0	0	0
AL 29 4C	0	0	0	0	0	0	0	0	0	0	0	0	0	0	0	0	0	0
AL 29 4C	0	0	0	0	0	0	0	0	0	0	0	0	0	0	0	0	0	0
AL 29 4C	0	0	0	0	0	0	0	0	0	0	0	0	0	0	0	0	0	0
AL 29 4C	0	0	0	0	0	0	0	0	0	0	0	0	0	0	0	0	0	0
AL 29 4C	0	0	0	0	0	0	0	0	0	0	0	0	0	0	0	0	0	0
AL 29 4C	0	0	0	0	0	0	0	0	0	0	0	0	0	0	0	0	0	0
AL 29 4C	0	0	0	0	0	0	0	0	0	0	0	0	0	0	0	0	0	0
AL 29 4C	0	0	0	0	0	0	0	0	0	0	0	0	0	0	0	0	0	0
AL 29 4C	0	0	0	0	0	0	0	0	0	0	0	0	0	0	0	0	0	0
Cu15Ni15Ag	0	0	0	0	0	0	0	0	0	0	0	0	1	1	0	0	0	0
Cu15Ni15Ag	0	0	0	0	0	0	0	0	0	0	0	0	1	1	0	0	0	0
Cu25Ni25Ag	0	0	0	0	0	0	0	0	0	0	0	0	1	1	0	0	0	0
Cu25Ni25Ag	0	0	0	0	0	0	0	0	0	0	0	0	1	1	0	0	0	0
NCFS	0	0	0	0	0	0	0	0	0	0	0	0	0	0	0	0	0	0
NCFS1.5Nb	0	0	0	0	0	0	0	0	0	0	0	0	0	0	1	0	0	0
NCFS3Nb	0	0	0	0	0	0	0	0	0	0	0	0	0	0	1	0	0	0
AISI430	0	0	0	0	0	0	0	0	0	0	0	0	0	0	0	0	0	1
AISI430	0	0	0	0	0	0	0	0	0	0	0	0	0	0	0	0	0	1

Table A.1 The first data set is collected for prediction (continue).

Type	$CoWO_4$	$CrTaO_4$	$NiCr_2O_4$	$NiAl_2O_4$	$CoAl_2O_4$	TiO_2	$MnTiO_3$	Ni_5TiO_7	Cr_2TiO_5	$CrWO_4$	$W_{20}O_{58}$	Ta_2O_5	CuO	Cu_2O	Nb_2O_5	$(Ni,Co)Al_2O_4$	$NiTiO_3$	$(Mn,Cr)_3O_4$
AISI430	0	0	0	0	0	0	0	0	0	0	0	0	0	0	0	0	0	1
AISI441	0	0	0	0	0	1	0	0	0	0	0	0	0	0	0	0	0	1
AISI441	0	0	0	0	0	1	0	0	0	0	0	0	0	0	0	0	0	1
AISI441	0	0	0	0	0	1	0	0	0	0	0	0	0	0	0	0	0	1
Crofer22H	0	0	0	0	0	0	0	0	0	0	0	0	0	0	0	0	0	0
Crofer22H	0	0	0	0	0	0	0	0	0	0	0	0	0	0	0	0	0	1
Crofer22H	0	0	0	0	0	1	0	0	0	0	0	0	0	0	0	0	0	1
Ni base	0	1	1	0	0	0	0	0	0	0	0	0	0	0	0	1	0	0
Ni base	0	1	0	1	0	0	0	0	0	0	0	0	0	0	0	0	1	0
Ti-6Al-7Nb	0	0	0	0	0	1	0	0	0	0	0	0	0	0	0	0	0	0
Ti-6Al-7Nb	0	0	0	0	0	1	0	0	0	0	0	0	0	0	0	0	0	0
Ti-6Al-7Nb	0	0	0	0	0	1	0	0	0	0	0	0	0	0	0	0	0	0
AISI 430	0	0	0	0	0	0	0	0	0	0	0	0	0	0	0	0	0	0
AISI 430	0	0	0	0	0	0	0	0	0	0	0	0	0	0	0	0	0	0
AISI 430	0	0	0	0	0	0	0	0	0	0	0	0	0	0	0	0	0	0
AISI 430	0	0	0	0	0	0	0	0	0	0	0	0	0	0	0	0	0	0
AISI 430	0	0	0	0	0	0	0	0	0	0	0	0	0	0	0	0	0	0
AISI 430	0	0	0	0	0	0	0	0	0	0	0	0	0	0	0	0	0	0
AISI 430	0	0	0	0	0	0	0	0	0	0	0	0	0	0	0	0	0	0
AISI 430	0	0	0	0	0	0	0	0	0	0	0	0	0	0	0	0	0	0
AISI 441	0	0	0	0	0	0	0	0	0	0	0	0	0	0	0	0	0	0
AISI 441	0	0	0	0	0	0	0	0	0	0	0	0	0	0	0	0	0	0
AISI 441	0	0	0	0	0	0	0	0	0	0	0	0	0	0	0	0	0	0
AISI 441	0	0	0	0	0	0	0	0	0	0	0	0	0	0	0	0	0	0
AISI 441	0	0	0	0	0	0	0	0	0	0	0	0	0	0	0	0	0	0
AISI 441	0	0	0	0	0	0	0	0	0	0	0	0	0	0	0	0	0	0
AISI 441	0	0	0	0	0	0	0	0	0	0	0	0	0	0	0	0	0	0
AISI 441	0	0	0	0	0	0	0	0	0	0	0	0	0	0	0	0	0	0
AISI 441	0	0	0	0	0	0	0	0	0	0	0	0	0	0	0	0	0	0
AISI 441	0	0	0	0	0	0	0	0	0	0	0	0	0	0	0	0	0	0
Fe11Cr0.5Ti	0	0	0	0	0	0	0	0	0	0	0	0	0	0	0	0	0	0
Fe11Cr0.5Ti	0	0	0	0	0	0	0	0	0	0	0	0	0	0	0	0	0	0
Fe18Cr0.5Ti	0	0	0	0	0	0	0	0	0	0	0	0	0	0	0	0	0	0
Fe18Cr0.5Ti	0	0	0	0	0	0	0	0	0	0	0	0	0	0	0	0	0	1
AISI 304	0	0	0	0	0	0	0	0	0	0	0	0	0	0	0	0	0	0
AISI 304	0	0	0	0	0	0	0	0	0	0	0	0	0	0	0	0	0	0
AISI 304	0	0	0	0	0	0	0	0	0	0	0	0	0	0	0	0	0	0
AISI 304	0	0	0	0	0	0	0	0	0	0	0	0	0	0	0	0	0	0
AISI 304	0	0	0	0	0	0	0	0	0	0	0	0	0	0	0	0	0	0
AISI 304	0	0	0	0	0	0	0	0	0	0	0	0	0	0	0	0	0	0
AISI 439	0	0	0	0	0	1	0	0	0	0	0	0	0	0	0	0	0	0
AISI 439	0	0	0	0	0	1	0	0	0	0	0	0	0	0	0	0	0	0
AISI 439	0	0	0	0	0	1	0	0	0	0	0	0	0	0	0	0	0	0

Table A.1 The first data set is collected for prediction (continue)**.**

Type	$CoWO_4$	$CrTaO_4$	$NiCr_2O_4$	$NiAl_2O_4$	$CoAl_2O_4$	TiO_2	$MnTiO_3$	Ni_5TiO_7	Cr_2TiO_5	$CrWO_4$	$W_{20}O_{58}$	Ta_2O_5	CuO	Cu_2O	Nb_2O_5	$(Ni,Co)Al_2O_4$	$NiTiO_3$	$(Mn,Cr)_3O_4$
AISI 439	0	0	0	0	0	0	0	0	0	0	0	0	0	0	0	0	0	0
AISI 439	0	0	0	0	0	0	0	0	0	0	0	0	0	0	0	0	0	0
AISI 439	0	0	0	0	0	0	0	0	0	0	0	0	0	0	0	0	0	0
F18TNb/AISI 441	0	0	0	0	0	0	0	0	0	0	0	0	0	0	0	0	0	1
F18TNb/AISI 441	0	0	0	0	0	0	0	0	0	0	0	0	0	0	0	0	0	1
F18MT/AISI 444	0	0	0	0	0	0	0	0	0	0	0	0	0	0	0	0	0	1
F18MT/AISI 444	0	0	0	0	0	0	0	0	0	0	0	0	0	0	0	0	0	1
AISI 304L	0	0	0	0	0	0	0	0	0	0	0	0	0	0	0	0	0	0
AISI 304L	0	0	0	0	0	0	0	0	0	0	0	0	0	0	0	0	0	0
AISI 304L	0	0	0	0	0	0	0	0	0	0	0	0	0	0	0	0	0	0
AISI 348	0	0	0	0	0	0	0	0	0	0	0	0	0	0	0	0	0	0
AISI 348	0	0	0	0	0	0	0	0	0	0	0	0	0	0	0	0	0	0
AISI 348	0	0	0	0	0	0	0	0	0	0	0	0	0	0	0	0	0	0
Iron	0	0	0	0	0	0	0	0	0	0	0	0	0	0	0	0	0	0
Iron	0	0	0	0	0	0	0	0	0	0	0	0	0	0	0	0	0	0
Iron	0	0	0	0	0	0	0	0	0	0	0	0	0	0	0	0	0	0
Iron	0	0	0	0	0	0	0	0	0	0	0	0	0	0	0	0	0	0
Iron	0	0	0	0	0	0	0	0	0	0	0	0	0	0	0	0	0	0
Iron	0	0	0	0	0	0	0	0	0	0	0	0	0	0	0	0	0	0

Table A.2 The second data set is collected for prediction.

Alloy	C	Mn	P	S	Si	Cr	Ni	Mo	N	Ti	Al	La	Nb	V	Cu	W	Se	Fe	T_{in} (°C)	T_{fi} (°C)	CTE (/K)
S20100	0.15	6.5	0.06	0.03	1	17	4.5	0	0.25	0	0	0	0	0	0	0	0	70.51	0	100	0.0000157
S20100	0.15	6.5	0.06	0.03	1	17	4.5	0	0.25	0	0	0	0	0	0	0	0	70.51	0	315	0.0000175
S20100	0.15	6.5	0.06	0.03	1	17	4.5	0	0.25	0	0	0	0	0	0	0	0	70.51	0	538	0.0000184
S20100	0.15	6.5	0.06	0.03	1	17	4.5	0	0.25	0	0	0	0	0	0	0	0	70.51	0	650	0.0000189
S20100	0.15	6.5	0.06	0.03	1	17	4.5	0	0.25	0	0	0	0	0	0	0	0	70.51	0	871	0.0000203
S20200	0.15	8.75	0.06	0.03	1	18	5	0	0	0	0	0	0	0	0	0	0	67.01	0	100	0.0000175
S20200	0.15	8.75	0.06	0.03	1	18	5	0	0	0	0	0	0	0	0	0	0	67.01	0	315	0.0000184
S20200	0.15	8.75	0.06	0.03	1	18	5	0	0	0	0	0	0	0	0	0	0	67.01	0	538	0.0000192
S30100	0.15	2	0.045	0.03	1	17	7	0	0	0	0	0	0	0	0	0	0	72.775	0	315	0.0000172
S30100	0.15	2	0.045	0.03	1	17	7	0	0	0	0	0	0	0	0	0	0	72.775	0	650	0.0000187
S30100	0.15	2	0.045	0.03	1	17	7	0	0	0	0	0	0	0	0	0	0	72.775	20	700	0.0000195
S30100	0.15	2	0.045	0.03	1	17	7	0	0	0	0	0	0	0	0	0	0	72.775	200	800	0.0000194
S30100	0.15	2	0.045	0.03	1	17	7	0	0	0	0	0	0	0	0	0	0	72.775	20	871	0.0000198
S30200	0.15	2	0.045	0.03	0.75	18	9	0	0.1	0	0	0	0	0	0	0	0	69.925	0	315	0.0000178
S30200	0.15	2	0.045	0.03	0.75	18	9	0	0.1	0	0	0	0	0	0	0	0	69.925	0	538	0.0000178
S30200	0.15	2	0.045	0.03	0.75	18	9	0	0.1	0	0	0	0	0	0	0	0	69.925	200	800	0.0000199
S30215	0.15	2	0.045	0.03	2.5	18	9	0	0	0	0	0	0	0	0	0	0	68.275	0	100	0.0000162
S30215	0.15	2	0.045	0.03	2.5	18	9	0	0	0	0	0	0	0	0	0	0	68.275	0	315	0.0000180
S30215	0.15	2	0.045	0.03	2.5	18	9	0	0	0	0	0	0	0	0	0	0	68.275	0	538	0.0000194
S30300	0.15	2	0.2	0.15	1	18	9	0.6	0	0	0	0	0	0	0	0	0	68.9	0	100	0.0000172
S30300	0.15	2	0.2	0.15	1	18	9	0.6	0	0	0	0	0	0	0	0	0	68.9	0	315	0.0000178
S30300	0.15	2	0.2	0.15	1	18	9	0.6	0	0	0	0	0	0	0	0	0	68.9	0	538	0.0000184
S30300	0.15	2	0.2	0.15	1	18	9	0.6	0	0	0	0	0	0	0	0	0	68.9	0	650	0.0000187
S30300	0.15	2	0.2	0.15	1	18	9	0.6	0	0	0	0	0	0	0	0	0	68.9	20	787	0.0000196
s30323	0.15	2	0.2	0.06	1	18	9	0	0	0	0	0	0	0	0	0	0.15	69.59	0	350	0.0000187
S30400	0.08	2	0.045	0.03	0.75	19	9.25	0	0	0	0	0	0	0	0	0	0	68.845	0	100	0.0000172
S30400	0.08	2	0.045	0.03	0.75	19	9.25	0	0	0	0	0	0	0	0	0	0	68.845	0	100	0.0000172
S30400	0.08	2	0.045	0.03	0.75	19	9.25	0	0	0	0	0	0	0	0	0	0	68.845	0	315	0.0000178
S30400	0.08	2	0.045	0.03	0.75	19	9.25	0	0	0	0	0	0	0	0	0	0	68.845	0	538	0.0000184
S30400	0.08	2	0.045	0.03	0.75	19	9.25	0	0	0	0	0	0	0	0	0	0	68.845	0	650	0.0000187
S30400	0.08	2	0.045	0.03	0.75	19	9.25	0	0	0	0	0	0	0	0	0	0	68.845	200	800	0.0000194
S30409	0.07	2	0.045	0.03	0.75	19	9.25	0	0	0	0	0	0	0	0	0	0	68.855	20	600	0.0000190
S30409	0.07	2	0.045	0.03	0.75	19	9.25	0	0	0	0	0	0	0	0	0	0	68.855	20	700	0.0000190
S30409	0.07	2	0.045	0.03	0.75	19	9.25	0	0	0	0	0	0	0	0	0	0	68.855	20	800	0.0000195
S30403	0.03	2	0.045	0.03	0.75	19	10	0	0.1	0	0	0	0	0	0	0	0	68.045	0	650	0.0000187
S30403	0.03	2	0.045	0.03	0.75	19	10	0	0.1	0	0	0	0	0	0	0	0	68.045	200	800	0.0000194
304N	0.08	2	0.045	0.03	0.75	19	9.25	0	0.13	0	0	0	0	0	0	0	0	68.715	200	800	0.0000194
S30500	0.12	2	0.045	0.03	0.75	18	11.75	0	0	0	0	0	0	0	0	0	0	67.305	0	100	0.0000172
S30500	0.12	2	0.045	0.03	0.75	18	11.75	0	0	0	0	0	0	0	0	0	0	67.305	0	315	0.0000178
S30500	0.12	2	0.045	0.03	0.75	18	11.75	0	0	0	0	0	0	0	0	0	0	67.305	0	538	0.0000184
S30500	0.12	2	0.045	0.03	0.75	18	11.75	0	0	0	0	0	0	0	0	0	0	67.305	0	650	0.0000189
S30500	0.12	2	0.045	0.03	0.75	18	11.75	0	0	0	0	0	0	0	0	0	0	67.305	200	800	0.0000199
S30800	0.08	2	0.045	0.03	0.75	20	11	0	0	0	0	0	0	0	0	0	0	66.095	0	100	0.0000172
S30800	0.08	2	0.045	0.03	0.75	20	11	0	0	0	0	0	0	0	0	0	0	66.095	0	315	0.0000178
S30800	0.08	2	0.045	0.03	0.75	20	11	0	0	0	0	0	0	0	0	0	0	66.095	0	538	0.0000184

Table A.2 The second data set is collected for prediction (continue).

Alloy	C	Mn	P	S	Si	Cr	Ni	Mo	N	Ti	Al	La	Nb	V	Cu	W	Se	Fe	T_{in} (°C)	T_{fi} (°C)	CTE (/K)
S30900	0.2	2	0.045	0.03	1	23	13.5	0	0	0	0	0	0	0	0	0	0	60.225	0	100	0.0000150
S30900	0.2	2	0.045	0.03	1	23	13.5	0	0	0	0	0	0	0	0	0	0	60.225	0	315	0.0000166
S30900	0.2	2	0.045	0.03	1	23	13.5	0	0	0	0	0	0	0	0	0	0	60.225	0	538	0.0000172
S30900	0.2	2	0.045	0.03	1	23	13.5	0	0	0	0	0	0	0	0	0	0	60.225	200	800	0.0000182
S30900	0.2	2	0.045	0.03	1	23	13.5	0	0	0	0	0	0	0	0	0	0	60.225	20	1000	0.0000194
s30908	0.08	2	0.045	0.03	0.75	23	13.5	0	0	0	0	0	0	0	0	0	0	60.595	0	650	0.0000180
S31000	0.2	2	0.045	0.03	1.5	25	20.5	0	0	0	0	0	0	0	0	0	0	50.725	0	100	0.0000159
S31000	0.2	2	0.045	0.03	1.5	25	20.5	0	0	0	0	0	0	0	0	0	0	50.725	0	315	0.0000162
S31000	0.2	2	0.045	0.03	1.5	25	20.5	0	0	0	0	0	0	0	0	0	0	50.725	0	538	0.0000170
S31000	0.2	2	0.045	0.03	1.5	25	20.5	0	0	0	0	0	0	0	0	0	0	50.725	200	800	0.0000186
S31000	0.2	2	0.045	0.03	1.5	25	20.5	0	0	0	0	0	0	0	0	0	0	50.725	20	1000	0.0000189
S31000	0.2	2	0.045	0.03	1.5	25	20.5	0	0	0	0	0	0	0	0	0	0	50.725	25	600	0.0000175
S31000	0.2	2	0.045	0.03	1.5	25	20.5	0	0	0	0	0	0	0	0	0	0	50.725	25	700	0.0000178
S31000	0.2	2	0.045	0.03	1.5	25	20.5	0	0	0	0	0	0	0	0	0	0	50.725	25	800	0.0000182
S31000	0.2	2	0.045	0.03	1.5	25	20.5	0	0	0	0	0	0	0	0	0	0	50.725	25	900	0.0000186
310S	0.08	2	0.045	0.03	1.5	25	20.5	0	0	0	0	0	0	0	0	0	0	50.845	25	600	0.0000175
310S	0.08	2	0.045	0.03	1.5	25	20.5	0	0	0	0	0	0	0	0	0	0	50.845	25	700	0.0000178
310S	0.08	2	0.045	0.03	1.5	25	20.5	0	0	0	0	0	0	0	0	0	0	50.845	25	800	0.0000182
310S	0.08	2	0.045	0.03	1.5	25	20.5	0	0	0	0	0	0	0	0	0	0	50.845	25	900	0.0000186
310S	0.08	2	0.045	0.03	1.5	25	20.5	0	0	0	0	0	0	0	0	0	0	50.845	25	1000	0.0000189
S31400	0.25	2	0.045	0.03	2.25	24.5	20.5	0	0	0	0	0	0	0	0	0	0	50.425	0	315	0.0000151
S31400	0.25	2	0.045	0.03	2.25	24.5	20.5	0	0	0	0	0	0	0	0	0	0	50.425	200	800	0.0000202
S31600	0.08	2	0.045	0.03	0.75	17	12	2.5	0.1	0	0	0	0	0	0	0	0	65.495	0	100	0.0000159
S31600	0.08	2	0.045	0.03	0.75	17	12	2.5	0.1	0	0	0	0	0	0	0	0	65.495	0	315	0.0000162
S31600	0.08	2	0.045	0.03	0.75	17	12	2.5	0.1	0	0	0	0	0	0	0	0	65.495	0	538	0.0000175
S31600	0.08	2	0.045	0.03	0.75	17	12	2.5	0.1	0	0	0	0	0	0	0	0	65.495	0	650	0.0000180
S31600	0.08	2	0.045	0.03	0.75	17	12	2.5	0.1	0	0	0	0	0	0	0	0	65.495	200	800	0.0000196
316L	0.03	2	0.045	0.03	0.75	17	12	2.5	0.1	0	0	0	0	0	0	0	0	65.545	20	600	0.0000180
316L	0.03	2	0.045	0.03	0.75	17	12	2.5	0.1	0	0	0	0	0	0	0	0	65.545	0	650	0.0000173
316L	0.03	2	0.045	0.03	0.75	17	12	2.5	0.1	0	0	0	0	0	0	0	0	65.545	20	700	0.0000185
316L	0.03	2	0.045	0.03	0.75	17	12	2.5	0.1	0	0	0	0	0	0	0	0	65.545	20	800	0.0000190
316L	0.03	2	0.045	0.03	0.75	17	12	2.5	0.1	0	0	0	0	0	0	0	0	65.545	200	800	0.0000196
316N	0.08	2	0.045	0.03	0.75	17	12	2.5	0.13	0	0	0	0	0	0	0	0	65.465	200	800	0.0000194
316LN	0.03	2	0.045	0.03	0.75	17	12	2.5	0.13	0	0	0	0	0	0	0	0	65.515	200	800	0.0000194
S31700	0.08	2	0.045	0.03	0.75	19	13	3.5	0	0	0	0	0	0	0	0	0	61.595	0	100	0.0000159
S31700	0.08	2	0.045	0.03	0.75	19	13	3.5	0	0	0	0	0	0	0	0	0	61.595	0	315	0.0000162
S31700	0.08	2	0.045	0.03	0.75	19	13	3.5	0	0	0	0	0	0	0	0	0	61.595	0	538	0.0000175
S31700	0.08	2	0.045	0.03	0.75	19	13	3.5	0	0	0	0	0	0	0	0	0	61.595	0	650	0.0000185
S31700	0.08	2	0.045	0.03	0.75	19	13	3.5	0	0	0	0	0	0	0	0	0	61.595	200	800	0.0000195
S31703	0.03	2	0.045	0.03	0.75	19	13	3.5	0	0	0	0	0	0	0	0	0	61.645	0	538	0.0000181
S31703	0.03	2	0.045	0.03	0.75	19	13	3.5	0	0	0	0	0	0	0	0	0	61.645	30	600	0.0000180
S31703	0.03	2	0.045	0.03	0.75	19	13	3.5	0	0	0	0	0	0	0	0	0	61.645	30	700	0.0000185
S32100	0.08	2	0.045	0.03	0.75	18	10.5	0	0	0	0	0	0	0	0	0	0	68.595	0	100	0.0000166
S32100	0.08	2	0.045	0.03	0.75	18	10.5	0	0	0	0	0	0	0	0	0	0	68.595	0	315	0.0000172
S32100	0.08	2	0.045	0.03	0.75	18	10.5	0	0	0	0	0	0	0	0	0	0	68.595	0	538	0.0000185

Table A.2 The second data set is collected for prediction (continue).

Alloy	C	Mn	P	S	Si	Cr	Ni	Mo	N	Ti	Al	La	Nb	V	Cu	W	Se	Fe	T_{in} (°C)	T_{fi} (°C)	CTE (/K)
S32100	0.08	2	0.045	0.03	0.75	18	10.5	0	0	0	0	0	0	0	0	0	0	68.595	0	650	0.0000193
S32100	0.08	2	0.045	0.03	0.75	18	10.5	0	0	0	0	0	0	0	0	0	0	68.595	0	871	0.0000202
S32100	0.08	2	0.045	0.03	0.75	18	10.5	0	0	0	0	0	0	0	0	0	0	68.595	200	800	0.0000195
S34700	0.08	2	0.045	0.03	0.75	18	11	0	0	0	0	0	0	0	0	0	0	68.095	0	100	0.0000166
S34700	0.08	2	0.045	0.03	0.75	18	11	0	0	0	0	0	0	0	0	0	0	68.095	0	315	0.0000172
S34700	0.08	2	0.045	0.03	0.75	18	11	0	0	0	0	0	0	0	0	0	0	68.095	0	538	0.0000186
S38400	0.08	2	0.045	0.03	1	16	18	0	0	0	0	0	0	0	0	0	0	62.845	0	100	0.0000172
S38400	0.08	2	0.045	0.03	1	16	18	0	0	0	0	0	0	0	0	0	0	62.845	0	315	0.0000178
S38400	0.08	2	0.045	0.03	1	16	18	0	0	0	0	0	0	0	0	0	0	62.845	0	538	0.0000184
S38400	0.08	2	0.045	0.03	1	16	18	0	0	0	0	0	0	0	0	0	0	62.845	0	350	0.0000187
S40300	0.15	1	0.04	0.03	0.5	12.25	0.6	0	0	0	0	0	0	0	0	0	0	85.43	200	800	0.0000128
S40500	0.08	1	0.04	0.03	1	13	0.6	0	0	0	0	0	0	0	0	0	0	84.25	0	100	0.0000108
S40500	0.08	1	0.04	0.03	1	13	0.6	0	0	0	0	0	0	0	0	0	0	84.25	0	315	0.0000116
S40500	0.08	1	0.04	0.03	1	13	0.6	0	0	0	0	0	0	0	0	0	0	84.25	0	538	0.0000121
S40500	0.08	1	0.04	0.03	1	13	0.6	0	0	0	0	0	0	0	0	0	0	84.25	0	650	0.0000130
S40500	0.08	1	0.04	0.03	1	13	0.6	0	0	0	0	0	0	0	0	0	0	84.25	25	700	0.0000123
S40500	0.08	1	0.04	0.03	1	13	0.6	0	0	0	0	0	0	0	0	0	0	84.25	25	800	0.0000127
S40500	0.08	1	0.04	0.03	1	13	0.6	0	0	0	0	0	0	0	0	0	0	84.25	25	900	0.0000130
S42900	0.12	1	0.04	0.03	1	15	0	0	0	0	0	0	0	0	0	0	0	82.81	0	100	0.0000103
S43000	0.12	1	0.04	0.03	1	17	0.75	0	0	0	0	0	0	0	0	0	0	80.06	0	315	0.0000110
S43000	0.12	1	0.04	0.03	1	17	0.75	0	0	0	0	0	0	0	0	0	0	80.06	0	538	0.0000114
S43000	0.12	1	0.04	0.03	1	17	0.75	0	0	0	0	0	0	0	0	0	0	80.06	0	650	0.0000118
S43000	0.12	1	0.04	0.03	1	17	0.75	0	0	0	0	0	0	0	0	0	0	80.06	200	800	0.0000128
S43020	0.12	1.25	0.06	0.15	1	17	0.75	0.6	0	0	0	0	0	0	0	0	0	79.07	0	100	0.0000104
S43020	0.12	1.25	0.06	0.15	1	17	0.75	0.6	0	0	0	0	0	0	0	0	0	79.07	0	315	0.0000110
S43020	0.12	1.25	0.06	0.15	1	17	0.75	0.6	0	0	0	0	0	0	0	0	0	79.07	0	538	0.0000114
S43400	0.12	1	0.04	0.03	1	17	0	1	0	0	0	0	0	0	0	0	0	79.81	0	315	0.0000110
S43400	0.12	1	0.04	0.03	1	17	0	1	0	0	0	0	0	0	0	0	0	79.81	200	800	0.0000126
S43600	0.12	1	0.04	0.03	1	17	0	1	0	0	0	0	0	0	0	0	0	79.81	0	100	0.0000093
S43035	0.03	1	0.04	0.03	1	18	0.5	0	0	0	0	0	0	0	0	0	0	79.4	0	100	0.0000104
S43035	0.03	1	0.04	0.03	1	18	0.5	0	0	0	0	0	0	0	0	0	0	79.4	0	315	0.0000110
S43035	0.03	1	0.04	0.03	1	18	0.5	0	0	0	0	0	0	0	0	0	0	79.4	0	538	0.0000114
S44400	0.025	1	0.04	0.03	1	18.5	1	2.125	0	0	0	0	0	0	0	0	0	76.28	0	100	0.0000100
S44400	0.025	1	0.04	0.03	1	18.5	1	2.125	0	0	0	0	0	0	0	0	0	76.28	0	315	0.0000106
S44400	0.025	1	0.04	0.03	1	18.5	1	2.125	0	0	0	0	0	0	0	0	0	76.28	0	538	0.0000114
S44600	0.2	1.5	0.04	0.03	1	25	0.75	0	0	0	0	0	0	0	0	0	0	71.48	0	100	0.0000104
S44600	0.2	1.5	0.04	0.03	1	25	0.75	0	0	0	0	0	0	0	0	0	0	71.48	0	315	0.0000108
S44600	0.2	1.5	0.04	0.03	1	25	0.75	0	0	0	0	0	0	0	0	0	0	71.48	0	538	0.0000112
S41000	0.115	1	0.04	0.03	1	12.25	0.75	0	0	0	0	0	0	0	0	0	0	84.815	0	315	0.0000114
S41000	0.115	1	0.04	0.03	1	12.25	0.75	0	0	0	0	0	0	0	0	0	0	84.815	0	538	0.0000116
S41000	0.115	1	0.04	0.03	1	12.25	0.75	0	0	0	0	0	0	0	0	0	0	84.815	0	650	0.0000116
S41000	0.115	1	0.04	0.03	1	12.25	0.75	0	0	0	0	0	0	0	0	0	0	84.815	700	1000	0.0000127
S41000	0.115	1	0.04	0.03	1	12.25	0.75	0	0	0	0	0	0	0	0	0	0	84.815	200	800	0.0000128
S41400	0.15	1	0.04	0.03	1	12.25	1.875	0	0	0	0	0	0	0	0	0	0	83.655	0	100	0.0000104
S41400	0.15	1	0.04	0.03	1	12.25	1.875	0	0	0	0	0	0	0	0	0	0	83.655	0	315	0.0000110

Table A.2 The second data set is collected for prediction (continue).

Alloy	C	Mn	P	S	Si	Cr	Ni	Mo	N	Ti	Al	La	Nb	V	Cu	W	Se	Fe	T_{in} (°C)	T_{fi} (°C)	CTE (/K)
S41400	0.15	1	0.04	0.03	1	12.25	1.875	0	0	0	0	0	0	0	0	0	0	83.655	0	538	0.0000121
S41400	0.15	1	0.04	0.03	1	12.25	1.875	0	0	0	0	0	0	0	0	0	0	83.655	0	650	0.0000121
S41600	0.15	1.25	0.06	0.15	1	13	0	0.6	0	0	0	0	0	0	0	0	0	83.79	0	100	0.0000099
S41600	0.15	1.25	0.06	0.15	1	13	0	0.6	0	0	0	0	0	0	0	0	0	83.79	0	315	0.0000110
S41600	0.15	1.25	0.06	0.15	1	13	0	0.6	0	0	0	0	0	0	0	0	0	83.79	0	538	0.0000116
S41600	0.15	1.25	0.06	0.15	1	13	0	0.6	0	0	0	0	0	0	0	0	0	83.79	0	650	0.0000117
S41600	0.15	1.25	0.06	0.15	1	13	0	0.6	0	0	0	0	0	0	0	0	0	83.79	20	787	0.0000124
S42000	0.15	1	0.04	0.03	1	13	0.75	0.5	0	0	0	0	0	0	0	0	0	83.53	0	100	0.0000103
S42000	0.15	1	0.04	0.03	1	13	0.75	0.5	0	0	0	0	0	0	0	0	0	83.53	0	315	0.0000108
S42000	0.15	1	0.04	0.03	1	13	0.75	0.5	0	0	0	0	0	0	0	0	0	83.53	0	538	0.0000117
S42000	0.15	1	0.04	0.03	1	13	0.75	0.5	0	0	0	0	0	0	0	0	0	83.53	0	650	0.0000122
S42200	0.225	1	0.025	0.025	0.5	11.75	0.75	1.075	0	0	0	0	0	0	0	0	0	84.65	0	100	0.0000112
S42200	0.225	1	0.025	0.025	0.5	11.75	0.75	1.075	0	0	0	0	0	0	0	0	0	84.65	0	315	0.0000114
S42200	0.225	1	0.025	0.025	0.5	11.75	0.75	1.075	0	0	0	0	0	0	0	0	0	84.65	0	538	0.0000119
S42200	0.225	1	0.025	0.025	0.5	11.75	0.75	1.075	0	0	0	0	0	0	0	0	0	84.65	21	649	0.0000121
S43100	0.2	1	0.04	0.03	1	16	1.875	0	0	0	0	0	0	0	0	0	0	79.855	0	100	0.0000102
S43100	0.2	1	0.04	0.03	1	16	1.875	0	0	0	0	0	0	0	0	0	0	79.855	0	315	0.0000121
S43100	0.2	1	0.04	0.03	1	16	1.875	0	0	0	0	0	0	0	0	0	0	79.855	0	650	0.0000122
S44002	0.675	1	0.04	0.03	1	17	0	0.75	0	0	0	0	0	0	0	0	0	79.505	0	100	0.0000102
S44004	1.075	1	0.04	0.03	1	17	0	0.75	0	0	0	0	0	0	0	0	0	79.105	0	100	0.0000103
S21900	0.08	9	0.06	0.03	1	20.25	6.5	0	0.0275	0	0	0	0	0	0	0	0	63.0525	200	800	0.0000200
S21900	0.08	9	0.06	0.03	1	20.25	6.5	0	0.0275	0	0	0	0	0	0	0	0	63.0525	27	760	0.0000200
S21900	0.08	9	0.06	0.03	1	20.25	6.5	0	0.0275	0	0	0	0	0	0	0	0	63.0525	27	871	0.0000202
S21900	0.08	9	0.06	0.03	1	20.25	6.5	0	0.0275	0	0	0	0	0	0	0	0	63.0525	27	982	0.0000205
S20910	0.06	7.75	0.04	0.03	0.75	22	12.5	2.25	0.3	0	0	0	0.2	0.2	0	0	0	54.32	21	649	0.0000189
S20910	0.06	7.75	0.04	0.03	0.75	22	12.5	2.25	0.3	0	0	0	0	0	0	0	0	54.32	21	760	0.0000194
S20910	0.06	7.75	0.04	0.03	0.75	22	12.5	2.25	0.3	0	0	0	0	0	0	0	0	54.32	21	871	0.0000200
S24100	0.15	12.5	0.06	0.03	1	18	1.5	0	0.325	0	0	0	0	0	0	0	0	66.435	0	100	0.0000161
S24100	0.15	12.5	0.06	0.03	1	18	1.5	0	0.325	0	0	0	0	0	0	0	0	66.435	0	315	0.0000174
S24100	0.15	12.5	0.06	0.03	1	18	1.5	0	0.325	0	0	0	0	0	0	0	0	66.435	0	538	0.0000188
S30431	0.06	2	0.04	0.14	1	17.5	10	0	0	0	0	0	0	0	1.85	0	0	69.26	25	538	0.0000186
S30431	0.06	2	0.04	0.14	1	17.5	10	0	0	0	0	0	0	0	0	0	0	69.26	25	649	0.0000190
S30430	0.1	2	0.045	0.03	1	0	18	9	0	0	0	0	0	0	3.5	0	0	69.825	0	100	0.0000172
S30430	0.1	2	0.045	0.03	1	0	18	9	0	0	0	0	0	0	0	0	0	69.825	0	315	0.0000178
S30430	0.1	2	0.045	0.03	1	0	18	9	0	0	0	0	0	0	0	0	0	69.825	0	650	0.0000187
N08028	0.03	2.5	0.03	0.03	1	27	31	3.5	0	0	0	0	0	0	1	0	0	34.91	20	100	0.0000149
N08028	0.03	2.5	0.03	0.03	1	27	31	3.5	0	0	0	0	0	0	0	0	0	34.91	20	200	0.0000155
N08028	0.03	2.5	0.03	0.03	1	27	31	3.5	0	0	0	0	0	0	0	0	0	34.91	20	400	0.0000166
N08028	0.03	2.5	0.03	0.03	1	27	31	3.5	0	0	0	0	0	0	0	0	0	34.91	21	427	0.0000167
N08926	0.02	2	0.03	0.01	0.5	20	25	6.5	0.2	0	0	0	0	0	1	0	0	45.74	25	427	0.0000164
N08926	0.02	2	0.03	0.01	0.5	20	25	6.5	0.2	0	0	0	0	0	0	0	0	45.74	25	649	0.0000169
S31200	0.03	2	0.045	0.03	1	25	5	1.6	0.17	0	0	0	0	0	0	0	0	65.125	20	100	0.0000140
S32760	0.03	1	0.03	0.01	1	25	7	3.5	0.25	0	0	0	0	0	0.75	0.75	0	62.18	20	100	0.0000111
S32760	0.03	1	0.03	0.01	1	25	7	3.5	0.25	0	0	0	0	0	0	0	0	62.18	20	300	0.0000120
S31500	0.03	1.6	0.03	0.03	1.7	18.5	4.75	2.75	0	0	0	0	0	0	0	0	0	70.61	20	100	0.0000122

Table A.2 The second data set is collected for prediction (continue).

Alloy	C	Mn	P	S	Si	Cr	Ni	Mo	N	Ti	Al	La	Nb	V	Cu	W	Se	Fe	T_{in} (°C)	T_{fi} (°C)	CTE (/K)
S31803	0.03	2	0.03	0.02	1	22	5.5	3	0.14	0	0	0	0	0	0	0	0	66.28	20	100	0.0000135
S31803	0.03	2	0.03	0.02	1	22	5.5	3	0.14	0	0	0	0	0	0	0	0	66.28	20	200	0.0000140
S31803	0.03	2	0.03	0.02	1	22	5.5	3	0.14	0	0	0	0	0	0	0	0	66.28	20	300	0.0000146
S32205	0.03	2	0.03	0.02	1	22	5.5	3	0.107	0	0	0	0	0	0	0	0	66.313	20	100	0.0000135
S32205	0.03	2	0.03	0.02	1	22	5.5	3	0.107	0	0	0	0	0	0	0	0	66.313	20	200	0.0000140
S32205	0.03	2	0.03	0.02	1	22	5.5	3	0.107	0	0	0	0	0	0	0	0	66.313	20	300	0.0000146
S32304	0.03	2.5	0.04	0.03	1	23	4.25	0.325	0.128	0	0	0	0	0	0.325	0	0	68.697	20	100	0.0000130
S32304	0.03	2.5	0.04	0.03	1	23	4.25	0.325	0.128	0	0	0	0	0	0	0	0	68.697	20	200	0.0000135
S32304	0.03	2.5	0.04	0.03	1	23	4.25	0.325	0.128	0	0	0	0	0	0	0	0	68.697	20	300	0.0000140
S32550	0.04	1.5	0.04	0.03	1	25.5	5.5	3.4	0.175	0	0	0	0	0	2	0	0	62.815	23	400	0.0000135
S32550	0.04	1.5	0.04	0.03	1	25.5	5.5	3.4	0.175	0	0	0	0	0	0	0	0	62.815	23	500	0.0000138
S32750	0.03	1.2	0.035	0.02	0.8	25	7	4	0.28	0	0	0	0	0	0	0	0	61.635	20	300	0.0000140
S32750	0.03	1.2	0.035	0.02	0.8	25	7	4	0.28	0	0	0	0	0	0	0	0	61.635	20	400	0.0000145
S32950	0.03	2	0.035	0.01	0.6	27.5	4.35	1.75	0.25	0	0	0	0	0	0	0	0	63.475	24	538	0.0000133
S32950	0.03	2	0.035	0.01	0.6	27.5	4.35	1.75	0.25	0	0	0	0	0	0	0	0	63.475	24	649	0.0000145
S32950	0.03	2	0.035	0.01	0.6	27.5	4.35	1.75	0.25	0	0	0	0	0	0	0	0	63.475	24	760	0.0000147
S32950	0.03	2	0.035	0.01	0.6	27.5	4.35	1.75	0.25	0	0	0	0	0	0	0	0	63.475	24	816	0.0000147
S13800	0.05	0.2	0.01	0.008	0.1	12.75	7	2.25	0.01	0	1.125	0	0	0	0	0	0	77.622	0	315	0.0000112
S13800	0.05	0.2	0.01	0.008	0.1	12.75	7	0	0	0	0	0	0	0	0	0	0	79.882	0	538	0.0000119
S15500	0.07	1	0.04	0.03	1	14.75	4.5	0	0	0	0	0	0.3	0	3.5	0	0	78.61	0	315	0.0000114
S15500	0.07	1	0.04	0.03	1	14.75	4.5	0	0	0	0	0	0	0	0	0	0	78.61	21	483	0.0000131
S46500	0.02	0.25	0.015	0.01	0.25	11.75	11	1	0.01	1.65	0	0	0	0	0	0	0	75.695	21	600	0.0000131
Crofer22 APU	0	0.4	0	0	0.02	22.78	0	0	0	0.07	0.006	0.086	0	0	0	0	0	76.8	30	800	0.0000119
F18TNb	0	0.12	0	0	0.46	19.4	0	1.7	0	0.12	0.02	0	0.17	0	0	0	0	78.32	30	800	0.0000128
E-Brite	0	0.04	0	0	0.19	24.1	0	0.96	0	0.01	0.02	0	0	0	0	0	0	74.71	30	800	0.0000190
SUS430	0.12	1	0.04	0.03	0.75	17	0	0	0	0	0	0	0	0	0	0	0	81.06	400	850	0.0000127
Crofer22 APU	0.03	0.55	0.05	0.02	0.5	22	0	0	0	0.115	0.5	0.12	0	0	0.5	0	0	76.85	600	1000	0.0000120
Ni85.4MoW11.3	0	0	0	0	0	0	85.4	3.3	0	0	0	0	0	0	0	11.3	0	11.3	0	600	0.0000130
Ni85.1Mo4.6W10.3	0	0	0	0	0	0	85.1	4.6	0	0	0	0	0	0	0	10.3	0	10.3	0	600	0.0000135
Ni85.3Mo5.9W8.8	0	0	0	0	0	0	85.3	5.9	0	0	0	0	0	0	0	8.8	0	8.8	0	600	0.0000130
Ni84.3Mo8.9W6.8	0	0	0	0	0	0	84.3	8.9	0	0	0	0	0	0	0	6.8	0	6.8	0	600	0.0000127
Ni84.4Mo10.7W4.9	0	0	0	0	0	0	84.4	10.7	0	0	0	0	0	0	0	4.9	0	4.9	0	600	0.0000117
Ni84.1Mo11.8W4.1	0	0	0	0	0	0	84.1	11.8	0	0	0	0	0	0	0	4.1	0	4.1	0	600	0.0000125
Ni85.2Mo12.7W2.1	0	0	0	0	0	0	85.2	12.7	0	0	0	0	0	0	0	2.1	0	2.1	0	600	0.0000121
Sanergy HT	0.05	0.5	0	0	0.03	22	0	1	0	0.04	0	0	0.75	0	0	0	0	76.42	550	900	0.0000145
Sanergy HT	0.05	0.5	0	0	0.03	22	0	1	0	0.04	0	0	0.75	0	0	0	0	76.42	100	900	0.0000129
Sanergy HT	0.05	0.5	0	0	0.03	22	0	1	0	0.04	0	0	0.75	0	0	0	0	76.42	600	900	0.0000117

Table A.3 The third data set is collected for prediction.

Oxide	Ti	Al	Cr	Fe	Ni	Co	Cu	Si	Y	Mn	Zn	Ta	Nb	Zr	W	Mg	T_{in} (°C)	T_{fi} (°C)	CTE (/K)
TiO2	1	0	0	0	0	0	0	0	0	0	0	0	0	0	0	0	20	600	0.000007
Al2O3	0	2	0	0	0	0	0	0	0	0	0	0	0	0	0	0	20	1000	0.0000084
Cr2O3	0	0	2	0	0	0	0	0	0	0	0	0	0	0	0	0	100	1000	0.0000073
FeO	0	0	0	1	0	0	0	0	0	0	0	0	0	0	0	0	100	1000	0.0000122
NiO	0	0	0	0	1	0	0	0	0	0	0	0	0	0	0	0	20	1000	0.0000171
Fe2O3	0	0	0	2	0	0	0	0	0	0	0	0	0	0	0	0	20	900	0.0000149
CoO	0	0	0	0	0	1	0	0	0	0	0	0	0	0	0	0	20	900	0.000015
Cu2O	0	0	0	0	0	0	2	0	0	0	0	0	0	0	0	0	20	750	0.0000043
SiO2	0	0	0	0	0	0	0	1	0	0	0	0	0	0	0	0			0.0000123
SiO2	0	0	0	0	0	0	0	1	2	0	0	0	0	0	0	0	30	1450	7.06E-06
Y2Si2O7	0	0	0	0	0	0	0	2	2	0	0	0	0	0	0	0	30	1450	3.96E-06
Y3Al5O12	0	5	0	0	0	0	0	0	3	0	0	0	0	0	0	0	30	1450	9.16E-06
Si2Al6O13	0	6	0	0	0	0	0	2	0	0	0	0	0	0	0	0	30	1000	4.56E-06
CuO	0	0	0	0	0	0	1	0	0	0	0	0	0	0	0	0	25	900	9.59E-06
CuO	0	0	0	0	0	0	1	0	0	0	0	0	0	0	0	0			0.0000093
NiCr2O4	0	0	2	0	1	0	0	0	0	0	0	0	0	0	0	0	25	900	0.0000076
MnCr2O4	0	0	2	0	0	0	0	0	0	1	0	0	0	0	0	0	25	900	0.0000072
CoCr2O4	0	0	2	0	0	1	0	0	0	0	0	0	0	0	0	0	25	900	0.0000074
Mn1.5Co1.5O4	0	0	0	0	0	1.5	0	0	0	1.5	0	0	0	0	0	0	0	800	0.0000097
Co2MnO4	0	0	0	0	0	2	0	0	0	1	0	0	0	0	0	0	20	800	0.0000097
MgAl2O4	0	2	0	0	0	0	0	0	0	0	0	0	0	0	0	1	20	1020	0.0000088
MgAl2O4	0	2	0	0	0	0	0	0	0	0	0	0	0	0	0	1	25	1000	0.000009
MnAl2O4	0	2	0	0	0	0	0	0	0	1	0	0	0	0	0	0	25	700	0.0000079
CoAl2O4	0	2	0	0	0	1	0	0	0	0	0	0	0	0	0	0	20	1020	0.0000087
NiAl2O4	0	2	0	0	1	0	0	0	0	0	0	0	0	0	0	0	20	1010	0.0000081
ZnAl2O4	0	2	0	0	0	0	0	0	0	0	1	0	0	0	0	0	20	1020	0.0000099
ZnAl2O4	0	2	0	0	0	0	0	0	0	0	1	0	0	0	0	0	25	1000	0.0000087
MgCr2O4	0	0	2	0	0	0	0	0	0	0	0	0	0	0	0	1	20	1020	0.0000075
MgCr2O4	0	0	2	0	0	0	0	0	0	0	0	0	0	0	0	1	20	1027	0.0000072
CoCr2O4	0	0	2	0	0	1	0	0	0	0	0	0	0	0	0	0	20	12020	0.0000073
ZnCr2O4	0	0	2	0	0	0	0	0	0	0	1	0	0	0	0	0	20	12020	0.0000075
Mn3O4	0	0	0	0	0	0	0	0	0	3	0	0	0	0	0	0	50	1000	0.0000088
NiMn2O4	0	0	0	0	1	0	0	0	0	2	0	0	0	0	0	0	25	675	0.0000085
Cu1.4Mn1.6O4	0	0	0	0	0	0	1.4	0	0	1.6	0	0	0	0	0	0	25	600	0.0000139
MgFe2O4	0	0	0	2	0	0	0	0	0	0	0	0	0	0	0	1	100	1000	0.0000115
MgFe2O4	0	0	0	2	0	0	0	0	0	0	0	0	0	0	0	1	20	1027	0.0000123
CoFe2O4	0	0	0	2	0	1	0	0	0	0	0	0	0	0	0	0	50	650	0.0000149
Co3O4	0	0	0	0	0	3	0	0	0	0	0	0	0	0	0	0	25	800	0.0000093
SiO2	0	0	0	0	0	0	0	1	0	0	0	0	0	0	0	0	25	70	3.8E-07
Al2O3	0	2	0	0	0	0	0	0	0	0	0	0	0	0	0	0	25	70	2.04E-06
Ta2O5	0	0	0	0	0	0	0	0	0	0	0	2	0	0	0	0	25	70	2.45E-06
Nb2O5	0	0	0	0	0	0	0	0	0	0	0	0	2	0	0	0	25	70	1.52E-06
Al2TiO5	1	2	0	0	0	0	0	0	0	0	0	0	0	0	0	0	25	1350	6.8E-07
ZrTiO4	1	0	0	0	0	0	0	0	0	0	0	0	0	1	0	0	25	1350	8.29E-06
Fe2O3	0	0	0	2	0	0	0	0	0	0	0	0	0	0	0	0	100	1000	1.145E-05

Table A.3 The third data set is collected for prediction (continue).

Oxide	Ti	Al	Cr	Fe	Ni	Co	Cu	Si	Y	Mn	Zn	Ta	Nb	Zr	W	Mg	T_{in} (°C)	T_{fi} (°C)	CTE (/K)
Fe2SiO4	0	0	0	2	0	0	0	1	0	0	0	0	0	0	0	0	100	1000	1.114E-05
Fe3O4	0	0	0	3	0	0	0	0	0	0	0	0	0	0	0	0	100	1000	1.286E-05
FeO	0	0	0	1	0	0	0	0	0	0	0	0	0	0	0	0	100	1000	1.462E-05
WO3	0	0	0	0	0	0	0	0	0	0	0	0	0	0	1	0			0.00001
WO3	0	0	0	0	0	0	0	0	0	0	0	0	0	0	1	0	25	330	0.000013
WO3	0	0	0	0	0	0	0	0	0	0	0	0	0	0	1	0	330	710	0.00001
CoWO4	0	0	0	0	0	1	0	0	0	0	0	0	0	0	1	0		800	0.0000115

Table A.4 The data for PBR calculation

Type	t (hr)	T (°C)	pO_2 (atm)	pH_2O (atm)	Metal volume / surface area (mm)	Oxide volume / surface area (mm)	PBR	Spallation from experiment	Spallation form PBR
Fe22Cr	100	700	0.21	0	0.35	0.4	1.142857	No	No
Fe22Cr	100	750	0.21	0	0.35	0.4	1.142857	No	No
Fe22Cr	100	800	0.21	0	0.35	0.4	1.142857	No	No
Fe22Cr	100	850	0.21	0	0.35	0.4	1.142857	Yes	No
Fe22Cr	40	900	0.21	0	0.35	0.4	1.142857	Yes	No
330Cb	144	900	0.21	0	1.5	0.001	0.000667	Yes	Yes
0.12B	500	800	0.21	0	2	0.023	0.0115	No	Yes
0.12B	500	900	0.21	0	2	0.126	0.063	No	Yes
0.12B2Si	500	800	0.21	0	2	0.072	0.036	No	Yes
0.12B2Si	500	900	0.21	0	2	0.058	0.029	No	Yes
0.12B9Ni	500	900	0.21	0	2	0.242	0.121	No	Yes
DD32	500	900	0.21	0	4	0.009	0.00225	No	Yes
DD32	500	1000	0.21	0	4	0.017	0.00425	No	Yes
GTD111	452	900	0.21	0	9	0.023	0.002556	Yes	Yes
iron	180	650	1	0	2	0.0185	0.00925	No	Yes
iron	180	700	1	0	2	0.059	0.0295	Yes	Yes
iron	180	750	1	0	2	0.014	0.007	Yes	Yes
NCFS	100	1000	0.21	0	3	0.005	0.001667	No	Yes
NCFS1.5Nb	100	1000	0.21	0	3	0.008	0.002667	Yes	Yes
NCFS3Nb	100	1000	0.21	0	3	0.0078	0.0026	Yes	Yes
AISI430	2000	650	0.21	0	0.0003	0.0006	2	No	No
AISI430	2000	700	0.21	0	0.0003	0.0006	2	No	No
AISI430	2000	750	0.21	0	0.0003	0.0006	2	No	No
AISI441	2000	650	0.21	0	0.0003	0.0007	2.333333	No	Yes
AISI441	2000	700	0.21	0	0.0003	0.0007	2.333333	No	Yes
AISI441	2000	750	0.21	0	0.0003	0.0007	2.333333	No	Yes
Crofer22H	2000	650	0.21	0	0.0003	0.0005	1.666667	No	No
Crofer22H	2000	700	0.21	0	0.0003	0.0005	1.666667	No	No
Crofer22H	2000	750	0.21	0	0.0003	0.0005	1.666667	No	No
Ni base	1925	800	0.21	0	5	0.018	0.0036	No	Yes
Ni base	1925	900	0.21	0	5	0.018	0.0036	No	Yes
AISI 441	10	900	0.2	0	1.47	0.0008	0.000544	No	Yes
AISI 441	100	800	0	0	1	0.00245	0.00245	No	Yes
AISI 441	100	800	0	0.2	1	0.00234	0.00234	No	Yes
AISI 441	100	800	0.2	0	1	0.00225	0.00225	No	Yes
Fe11Cr0.5Ti	100	800	0.21	0	1.2	0.00226	0.001883	No	Yes
Fe11Cr0.5Ti	100	900	0.21	0	1.2	0.74	0.616667	Yes	Yes
Fe18Cr0.5Ti	100	800	0.21	0	1.2	2.772	0.001283	No	Yes
Fe18Cr0.5Ti	100	900	0.21	0	1.2	4.536	0.0021	No	Yes
F18TNb/AISI 441	100	800	0.2	0	2	0.0065	0.00325	No	Yes
F18TNb/AISI 441	200	800	0.2	0	2	0.001	0.0005	Yes	Yes
F18MT/AISI 444	100	800	0	0.02	1.2	0.009	0.0075	No	Yes
F18MT/AISI 444	200	800	0	0.02	1.2	0.0011	0.000917	Yes	Yes
								Accuracy	41.86 %

Table A.5 The thermal expansion coefficient (CTE) data obtained from thermal expansion coefficient (CTE) of alloys and oxides prediction model.

No.	Type of alloy	CTE of alloy (/K)	CTE of oxide (/K)	Spallation
0	AISI 430	1.23E-05	7.5936E-06	0
1	AISI 430	1.23E-05	7.5936E-06	0
2	AISI 630	1.3E-05	7.5936E-06	0
3	AISI 630	1.3E-05	7.5936E-06	0
8	Fe22Cr	1.22E-05	7.5936E-06	0
9	Fe22Cr	1.22E-05	7.5936E-06	0
10	Fe22Cr	1.22E-05	7.5936E-06	0
14	0.12B	1.53E-05	8.2423E-06	0
15	0.12B	1.53E-05	8.3424E-06	0
16	0.12B2Si	1.5E-05	8.2423E-06	0
17	0.12B2Si	1.5E-05	8.3424E-06	0
19	0.12B9Ni	1.53E-05	8.3905E-06	0
20	DD32	1.5E-05	6.7318E-06	0
21	DD32	1.5E-05	6.7318E-06	0
22	ANSI 310	1.52E-05	7.5936E-06	0
23	ANSI 310	1.52E-05	7.5936E-06	0
24	ANSI 310	1.52E-05	7.5936E-06	0
25	GTD111	1.52E-05	6.1829E-06	0
27	Ti36.7Al1.9W0.5Si	1.52E-05	6.875E-06	0
30	Ti36.7Al1.9W0.5Si	1.52E-05	6.875E-06	0
31	Ti36.7Al1.9W0.5Si	1.52E-05	6.7318E-06	0
32	Ti36.7Al1.9W0.5Si	1.52E-05	6.7318E-06	0
33	Ferritic ss	1.33E-05	0.000007325	0
34	Ferritic ss	1.33E-05	0.000007325	0
35	Ferritic ss	1.34E-05	7.5936E-06	0
37	Ferritic ss	1.33E-05	1.09803E-05	0
38	Ferritic ss	1.34E-05	7.5936E-06	0
40	iron	1.48E-05	1.31403E-05	0
43	F 20 T	1.34E-05	6.7229E-06	0
44	F 20 T	1.34E-05	6.7229E-06	0
45	F 20 T	1.34E-05	6.7229E-06	0
46	F 20 T	1.34E-05	6.7229E-06	0
47	F 20 T	1.34E-05	6.7229E-06	0
48	F 20 T	1.34E-05	7.5676E-06	0
49	F 20 T	1.34E-05	7.5676E-06	0
50	F 20 T	1.34E-05	7.5676E-06	0
51	F 20 T	1.34E-05	7.5676E-06	0
52	F 20 T	1.34E-05	7.5676E-06	0
53	F 20 T	1.34E-05	6.7318E-06	0
54	F 20 T	1.34E-05	6.7318E-06	0
55	F 20 T	1.34E-05	6.7318E-06	0
56	F 20 T	1.34E-05	6.7318E-06	0
57	F 20 T	1.34E-05	6.7318E-06	0

Table A.5 The thermal expansion coefficient (CTE) data obtained from thermal expansion coefficient (CTE) of alloys and oxides prediction model. (continue)

No.	Type of alloy	CTE of alloy (/K)	CTE of oxide (/K)	Spallation
58	TUS 220M	1.36E-05	7.5676E-06	0
59	TUS 220M	1.36E-05	7.5676E-06	0
60	TUS 220M	1.36E-05	7.5676E-06	0
61	TUS 220M	1.36E-05	7.5676E-06	0
62	TUS 220M	1.36E-05	7.5676E-06	0
63	TUS 220M	1.36E-05	7.5676E-06	0
64	TUS 220M	1.36E-05	7.5676E-06	0
65	TUS 220M	1.36E-05	7.5676E-06	0
66	TUS 220M	1.36E-05	7.5676E-06	0
67	TUS 220M	1.36E-05	7.5676E-06	0
68	TUS 220M	1.36E-05	6.7318E-06	0
69	TUS 220M	1.36E-05	6.7318E-06	0
70	TUS 220M	1.36E-05	6.7318E-06	0
71	TUS 220M	1.36E-05	6.7318E-06	0
72	TUS 220M	1.36E-05	6.7318E-06	0
73	AL 453	1.34E-05	7.5676E-06	0
74	AL 453	1.34E-05	7.5676E-06	0
75	AL 453	1.34E-05	7.5676E-06	0
76	AL 453	1.34E-05	7.5676E-06	0
77	AL 453	1.34E-05	7.5676E-06	0
78	AL 453	1.34E-05	7.5676E-06	0
79	AL 453	1.34E-05	7.5676E-06	0
80	AL 453	1.34E-05	7.5676E-06	0
81	AL 453	1.34E-05	7.5676E-06	0
82	AL 453	1.34E-05	7.5676E-06	0
83	AL 453	1.34E-05	7.5676E-06	0
84	AL 453	1.34E-05	7.5676E-06	0
85	AL 453	1.34E-05	7.5676E-06	0
86	AL 453	1.34E-05	7.5676E-06	0
87	AL 453	1.34E-05	7.5676E-06	0
88	Crofer 22 APU	1.2E-05	7.5676E-06	0
89	Crofer 22 APU	1.2E-05	7.5676E-06	0
90	Crofer 22 APU	1.2E-05	7.5676E-06	0
91	Crofer 22 APU	1.2E-05	7.5676E-06	0
92	Crofer 22 APU	1.2E-05	7.5676E-06	0
93	Crofer 22 APU	1.2E-05	7.5676E-06	0
94	Crofer 22 APU	1.2E-05	7.5676E-06	0
95	Crofer 22 APU	1.2E-05	7.5676E-06	0
96	Crofer 22 APU	1.2E-05	7.5676E-06	0
97	Crofer 22 APU	1.2E-05	7.5676E-06	0
98	Crofer 22 APU	1.2E-05	7.5676E-06	0
99	Crofer 22 APU	1.2E-05	7.5676E-06	0
100	Crofer 22 APU	1.2E-05	7.5676E-06	0

Table A.5 The thermal expansion coefficient (CTE) data obtained from thermal expansion coefficient (CTE) of alloys and oxides prediction model. (continue)

No.	Type of alloy	CTE of alloy (/K)	CTE of oxide (/K)	Spallation
101	Crofer 22 APU	1.2E-05	7.5676E-06	0
102	Crofer 22 APU	1.2E-05	7.5676E-06	0
103	Crofer 22 H	1.4E-05	7.5676E-06	0
104	Crofer 22 H	1.4E-05	7.5676E-06	0
105	Crofer 22 H	1.4E-05	7.5676E-06	0
106	Crofer 22 H	1.4E-05	7.5676E-06	0
107	Crofer 22 H	1.4E-05	7.5676E-06	0
108	Crofer 22 H	1.4E-05	7.5676E-06	0
109	Crofer 22 H	1.4E-05	7.5676E-06	0
110	Crofer 22 H	1.4E-05	7.5676E-06	0
111	Crofer 22 H	1.4E-05	7.5676E-06	0
112	Crofer 22 H	1.4E-05	7.5676E-06	0
113	Crofer 22 H	1.4E-05	7.5676E-06	0
114	Crofer 22 H	1.4E-05	7.5676E-06	0
115	Crofer 22 H	1.4E-05	7.5676E-06	0
116	Crofer 22 H	1.4E-05	7.5676E-06	0
117	Crofer 22 H	1.4E-05	7.5676E-06	0
118	Sanergy HT	1.35E-05	7.5676E-06	0
119	Sanergy HT	1.35E-05	7.5676E-06	0
120	Sanergy HT	1.35E-05	7.5676E-06	0
121	Sanergy HT	1.35E-05	7.5676E-06	0
122	Sanergy HT	1.35E-05	7.5676E-06	0
123	Sanergy HT	1.35E-05	7.5676E-06	0
124	Sanergy HT	1.35E-05	7.5676E-06	0
125	Sanergy HT	1.35E-05	7.5676E-06	0
126	Sanergy HT	1.35E-05	7.5676E-06	0
127	Sanergy HT	1.35E-05	7.5676E-06	0
128	Sanergy HT	1.35E-05	7.5676E-06	0
129	Sanergy HT	1.35E-05	7.5676E-06	0
130	Sanergy HT	1.35E-05	7.5676E-06	0
131	Sanergy HT	1.35E-05	7.5676E-06	0
132	Sanergy HT	1.35E-05	7.5676E-06	0
133	E-Brite	1.44E-05	7.5676E-06	0
134	E-Brite	1.44E-05	7.5676E-06	0
135	E-Brite	1.44E-05	7.5676E-06	0
136	E-Brite	1.44E-05	7.5676E-06	0
137	E-Brite	1.44E-05	7.5676E-06	0
138	E-Brite	1.44E-05	7.5676E-06	0
139	E-Brite	1.44E-05	7.5676E-06	0
140	E-Brite	1.44E-05	7.5676E-06	0
141	E-Brite	1.44E-05	7.5676E-06	0
142	E-Brite	1.44E-05	7.5676E-06	0
143	E-Brite	1.44E-05	7.5676E-06	0

Table A.5 The thermal expansion coefficient (CTE) data obtained from thermal expansion coefficient (CTE) of alloys and oxides prediction model. (continue)

No.	Type of alloy	CTE of alloy (/K)	CTE of oxide (/K)	Spallation
144	E-Brite	1.44E-05	7.5676E-06	0
145	E-Brite	1.44E-05	7.5676E-06	0
146	E-Brite	1.44E-05	7.5676E-06	0
147	E-Brite	1.44E-05	7.5676E-06	0
148	AL 29 4C	1.45E-05	7.5676E-06	0
149	AL 29 4C	1.45E-05	7.5676E-06	0
150	AL 29 4C	1.45E-05	7.5676E-06	0
151	AL 29 4C	1.45E-05	7.5676E-06	0
152	AL 29 4C	1.45E-05	7.5676E-06	0
153	AL 29 4C	1.45E-05	7.5676E-06	0
154	AL 29 4C	1.45E-05	7.5676E-06	0
155	AL 29 4C	1.45E-05	7.5676E-06	0
156	AL 29 4C	1.45E-05	7.5676E-06	0
157	AL 29 4C	1.45E-05	7.5676E-06	0
158	AL 29 4C	1.45E-05	7.5676E-06	0
159	AL 29 4C	1.45E-05	7.5676E-06	0
160	AL 29 4C	1.45E-05	7.5676E-06	0
161	AL 29 4C	1.45E-05	7.5676E-06	0
162	AL 29 4C	1.45E-05	7.5676E-06	0
163	Cu15Ni15Ag	1.35E-05	5.7242E-06	0
164	Cu15Ni15Ag	1.38E-05	6.3078E-06	0
165	Cu25Ni25Ag	1.35E-05	5.7242E-06	0
166	Cu25Ni25Ag	1.38E-05	6.3078E-06	0
167	NCFS	1.42E-05	7.5676E-06	0
170	AISI430	1.23E-05	7.3846E-06	0
171	AISI430	1.23E-05	7.3846E-06	0
172	AISI430	1.23E-05	7.3846E-06	0
173	AISI441	1.31E-05	6.875E-06	0
174	AISI441	1.31E-05	6.875E-06	0
175	AISI441	1.31E-05	6.875E-06	0
176	Crofer22H	1.26E-05	7.5936E-06	0
177	Crofer22H	1.26E-05	7.3846E-06	0
178	Crofer22H	1.26E-05	7.3846E-06	0
179	Ni base	1.53E-05	6.875E-06	0
180	Ni base	1.53E-05	6.875E-06	0
181	Ti-6Al-7Nb	1.5E-05	6.154E-06	0
182	Ti-6Al-7Nb	1.53E-05	6.875E-06	0
183	Ti-6Al-7Nb	1.53E-05	6.875E-06	0
184	AISI 430	1.23E-05	7.5936E-06	0
188	AISI 430	1.23E-05	7.5936E-06	0
189	AISI 430	1.23E-05	7.5936E-06	0
190	AISI 430	1.23E-05	7.5936E-06	0
192	AISI 441	1.31E-05	7.5676E-06	0

Table A.5 The thermal expansion coefficient (CTE) data obtained from thermal expansion coefficient (CTE) of alloys and oxides prediction model. (continue)

No.	Type of alloy	CTE of alloy (/K)	CTE of oxide (/K)	Spallation
193	AISI 441	1.31E-05	1.14886E-05	0
194	AISI 441	1.31E-05	1.14886E-05	0
195	AISI 441	1.31E-05	1.14886E-05	0
196	AISI 441	1.23E-05	1.07965E-05	0
197	AISI 441	1.23E-05	1.07965E-05	0
198	AISI 441	1.23E-05	1.07965E-05	0
199	AISI 441	1.23E-05	1.07965E-05	0
200	AISI 441	1.23E-05	7.5676E-06	0
201	AISI 441	1.23E-05	7.5676E-06	0
202	Fe11Cr0.5Ti	1.24E-05	0	0
204	Fe18Cr0.5Ti	1.23E-05	7.5936E-06	0
205	Fe18Cr0.5Ti	1.23E-05	7.5936E-06	0
206	AISI 304	1.31E-05	7.5676E-06	0
207	AISI 304	1.31E-05	7.5676E-06	0
209	AISI 304	1.31E-05	7.5676E-06	0
210	AISI 304	1.31E-05	7.5676E-06	0
211	AISI 304	1.31E-05	7.5676E-06	0
212	AISI 439	1.24E-05	6.7318E-06	0
213	AISI 439	1.24E-05	6.7318E-06	0
214	AISI 439	1.24E-05	6.7318E-06	0
215	AISI 439	1.24E-05	7.5676E-06	0
216	AISI 439	1.24E-05	7.5676E-06	0
218	F18TNb/AISI 441	1.23E-05	7.3846E-06	0
220	F18MT/AISI 444	1.22E-05	7.3846E-06	0
231	Iron	1.46E-05	1.15385E-05	0
232	Iron	1.46E-05	1.15385E-05	0
233	Iron	1.46E-05	1.15385E-05	0
4	AISI 347 H	1.31E-05	1.36198E-05	1
5	AISI 347 H	1.31E-05	1.36198E-05	1
6	AISI 316 LN	1.75E-05	1.36198E-05	1
7	AISI 316 LN	1.75E-05	1.36198E-05	1
11	Fe22Cr	1.22E-05	1.08324E-05	1
12	Fe22Cr	1.22E-05	1.08324E-05	1
13	330Cb	1.31E-05	7.3906E-06	1
18	0.12B2Si	1.5E-05	8.3424E-06	1
26	GTD111	1.52E-05	6.1829E-06	1
28	Ti36.7Al1.9W0.5Si	1.52E-05	6.7318E-06	1
29	Ti36.7Al1.9W0.5Si	1.52E-05	6.7318E-06	1
36	Ferritic ss	1.34E-05	7.5936E-06	1
39	Ferritic ss	1.34E-05	7.5936E-06	1
41	iron	1.48E-05	1.31403E-05	1
42	iron	1.48E-05	1.31403E-05	1
168	NCFS1.5Nb	1.42E-05	7.5676E-06	1

Table A.5 The thermal expansion coefficient (CTE) data obtained from thermal expansion coefficient (CTE) of alloys and oxides prediction model. (continue)

No.	Type of alloy	CTE of alloy (/K)	CTE of oxide (/K)	Spallation
169	NCFS3Nb	1.42E-05	7.5676E-06	1
185	AISI 430	1.23E-05	7.5936E-06	1
186	AISI 430	1.23E-05	7.5936E-06	1
187	AISI 430	1.23E-05	7.5936E-06	1
191	AISI 430	1.23E-05	7.5936E-06	1
203	Fe11Cr0.5Ti	1.24E-05	0	1
208	AISI 304	1.31E-05	7.5676E-06	1
217	AISI 439	1.24E-05	7.5676E-06	1
219	F18TNb/AISI 441	1.23E-05	7.3846E-06	1
221	F18MT/AISI 444	1.22E-05	7.3846E-06	1
222	AISI 304L	1.3E-05	1.14231E-05	1
223	AISI 304L	1.3E-05	1.14231E-05	1
224	AISI 304L	1.3E-05	1.14231E-05	1
225	AISI 348	1.32E-05	1.14231E-05	1
226	AISI 348	1.32E-05	1.14231E-05	1
227	AISI 348	1.32E-05	1.14231E-05	1
228	Iron	1.46E-05	1.15385E-05	1
229	Iron	1.46E-05	1.15385E-05	1
230	Iron	1.46E-05	1.15385E-05	1

Appendix B

Python code for M1 the spallation of oxide prediction model.

```
#M1 Spallation prediction model

#Import data
import pandas as pd
iM12_data = pd.read_excel(r'D:\File\College\Y4_project\Raw Data
23042023.xlsx','Alloy Data')
iM12_data = iM12_data.fillna(0)
rM12_data = pd.DataFrame(iM12_data,
columns=['C','Mn','Si','P','S','Cr','Ni','Mo','Nb','Ti','Cu','V','O','N
','Al','W','Ag','B','Re','Ta','Co','La','Se','Fe','t','T','Tin','Tfi','
p','pO2','pH2O','kp','FeO3','FeO','Fe2O3','Fe3O4','(Fe,Cr)3O4','Mn3O4',
'Cr2O3','(Cr,Mn,Fe)3O4','CoO','Al2O3','WO3','NiO','SiO2','Co3O4','CoWO4
','CrTaO4','NiCr2O4','NiAl2O4','CoAl2O4','TiO2','MnTiO3','Ni5TiO7','Cr2
TiO5','CrWO4','W20O58','Ta2O5','CuO','Cu2O','Nb2O5','(Ni,Co)Al2O4','NiT
iO3','(Mn,Cr)3O4','Spallation'])

#Define X and Y
import numpy as np
x_M1 =
rM12_data[['C','Mn','Si','P','S','Cr','Ni','Mo','Nb','Ti','Cu','V','O',
'N','Al','W','Ag','B','Re','Ta','Co','La','Fe','t','T','pO2','pH2O']]
y_M1 = np.ravel(rM12_data[['Spallation']])

#Split data
from  sklearn.model_selection import train_test_split
x_M1_train, x_M1_test, y_M1_train, y_M1_test = train_test_split(x_M1,
y_M1, test_size = 0.3, random_state= 3)

#Import Ml algorithms
from sklearn.tree import DecisionTreeClassifier
modelM1 = DecisionTreeClassifier()
from sklearn.ensemble import RandomForestClassifier
modelM1 = RandomForestClassifier()
from sklearn.neighbors import KNeighborsClassifier
modelM1 = KNeighborsClassifier(n_neighbors = 2, p=1)
from sklearn.neural_network import MLPClassifier
modelM1 = MLPClassifier(solver = 'lbfgs',max_iter = 1e10, random_state
=1)

#Training Ml algorithms
modelM1.fit(x_M1_train,y_M1_train)
yp_M1_train = modelM1.predict(x_M1_train)
yp_M1_test = modelM1.predict(x_M1_test)
yp_M1_all = modelM1.predict(x_M1)

#Check quality of model
from sklearn.metrics import classification_report
```

Python code for M1 the spallation of oxide prediction model. (continue)

```
print('[M1] Spallation prediction model')
print("Training set")
print(classification_report(y_M1_train, yp_M1_train, digits=4))
print("Test set")
print(classification_report(y_M1_test, yp_M1_test, digits=4))
print("All data set")
print(classification_report(y_M1, yp_M1_all, digits=4))
```

Python code for M2 the types of oxide prediction model.

```
#M2 Type of oxide prediction model

#Import data
import pandas as pd
iM12_data = pd.read_excel(r'D:\File\College\Y4_project\Raw Data
23042023.xlsx','Alloy Data')
iM12_data = iM12_data.fillna(0)
rM12_data = pd.DataFrame(iM12_data,
columns=['C','Mn','Si','P','S','Cr','Ni','Mo','Nb','Ti','Cu','V','O','N
','Al','W','Ag','B','Re','Ta','Co','La','Se','Fe','t','T','Tin','Tfi','
p','pO2','pH2O','kp','FeO3','FeO','Fe2O3','Fe3O4','(Fe,Cr)3O4','Mn3O4',
'Cr2O3','(Cr,Mn,Fe)3O4','CoO','Al2O3','WO3','NiO','SiO2','Co3O4','CoWO4
','CrTaO4','NiCr2O4','NiAl2O4','CoAl2O4','TiO2','MnTiO3','Ni5TiO7','Cr2
TiO5','CrWO4','W20O58','Ta2O5','CuO','Cu2O','Nb2O5','(Ni,Co)Al2O4','NiT
iO3','(Mn,Cr)3O4','Spallation'])

#Define X and Y
import numpy as np
x_M2 =
rM12_data[['C','Mn','Si','P','S','Cr','Ni','Mo','Nb','Ti','Cu','V','O',
'N','Al','W','Ag','B','Re','Ta','Co','La','Fe','t','T','pO2','pH2O']]
y_M2 =
rM12_data[['FeO3','FeO','Fe2O3','Fe3O4','(Fe,Cr)3O4','Mn3O4','Cr2O3','(
Cr,Mn,Fe)3O4','CoO','Al2O3','WO3','NiO','SiO2','Co3O4','CoWO4','CrTaO4'
,'NiCr2O4','NiAl2O4','CoAl2O4','TiO2','MnTiO3','Ni5TiO7','Cr2TiO5','CrW
O4','W20O58','Ta2O5','CuO','Cu2O','Nb2O5','(Ni,Co)Al2O4','NiTiO3','(Mn,
Cr)3O4']]

#Split data
from  sklearn.model_selection import train_test_split
x_M2_train, x_M2_test, y_M2_train, y_M2_test = train_test_split(x_M2,
y_M2, test_size = 0.3, random_state= 3)

#Import Ml algorithms
from sklearn.tree import DecisionTreeClassifier
modelM2 = DecisionTreeClassifier(random_state=1)
```

Python code for M2 the types of oxide prediction model. (continue)

```
from sklearn.ensemble import RandomForestClassifier
modelM2 = RandomForestClassifier(random_state=1)
from sklearn.neighbors import KNeighborsClassifier
modelM2 = KNeighborsClassifier(n_neighbors = 2, p=1)
from sklearn.neural_network import MLPClassifier
modelM2 = MLPClassifier(solver = 'lbfgs',max_iter = 1e10, random_state=
1)

#Training Ml algorithms
modelM2.fit(x_M2_train,y_M2_train)
yp_M2_train = modelM2.predict(x_M2_train)
yp_M2_test = modelM2.predict(x_M2_test)
yp_M2_all = modelM2.predict(x_M2)

#Check quality of model
from sklearn.metrics import classification_report
from sklearn import metrics
print('[M2] Type of oxide prediction model')
print("Training set")
print(classification_report(y_M2_train, yp_M2_train, digits=4))
print("Test set")
print(classification_report(y_M2_test, yp_M2_test, digits=4))
print("All data set")
print(classification_report(y_M2, yp_M2_all, digits=4))
```

Python code for M3 the thermal expansion coefficient of alloy prediction model.

```
#M3 CTE of alloy prediction model
#Import data
import pandas as pd
iM3_data = pd.read_excel(r'D:\File\College\Y4_project\Raw Data CTE
14042023.xlsx','CTE alloy')
iM3_data = iM3_data.fillna(0)
rM3_data = pd.DataFrame(iM3_data,
columns=['C','Mn','P','S','Si','Cr','Ni','Mo','N','Ti','Al','La','Nb','
V','Cu','W','Se','Fe','Tin','Tfi','CTE'])
#Define X and Y
import numpy as np
x_M3 =
rM3_data[['C','Mn','P','S','Si','Cr','Ni','Mo','N','Ti','Al','La','Nb',
'V','Cu','W','Se','Fe','Tin','Tfi']]
y_M3 = np.ravel(rM3_data[['CTE']])
#Split data
from  sklearn.model_selection import train_test_split
x_M3_train, x_M3_test, y_M3_train, y_M3_test = train_test_split(x_M3,
y_M3, test_size = 0.3, random_state= 3)
```

Python code for M3 the thermal expansion coefficient of alloy prediction model. (continue)

```
#Import Ml algorithms
from sklearn.ensemble import RandomForestRegressor
modelM3 = RandomForestRegressor(random_state= 1)
from sklearn.tree import DecisionTreeRegressor
modelM3 = DecisionTreeRegressor(random_state= 1)
from sklearn.neighbors import KNeighborsRegressor
modelM3 = KNeighborsRegressor(n_neighbors = 2, p=1)
from sklearn.neural_network import MLPRegressor
modelM3 = MLPRegressor(random_state= 1)
#training Ml algorithms
modelM3.fit(x_M3_train,y_M3_train)
yp_M3_train = modelM3.predict(x_M3_train)
yp_M3_all = modelM3.predict(x_M3)
yp_M3_test = modelM3.predict(x_M3_test)
#Check quality of model
from sklearn.metrics import mean_absolute_percentage_error
from sklearn.metrics import r2_score
print('[M3] CTE of alloy prediction model')
print("Training set")
print("MAPE: ", mean_absolute_percentage_error(y_M3_train,
yp_M3_train))
print("R2: ", r2_score(y_M3_train, yp_M3_train))
print("Test set")
print("MAPE: ", mean_absolute_percentage_error(y_M3_test, yp_M3_test))
print("R2: ", r2_score(y_M3_test, yp_M3_test))
print("All data set")
print("MAPE: ", mean_absolute_percentage_error(y_M3, yp_M3_all))
print("R2: ", r2_score(y_M3, yp_M3_all))
```

Python code for M4 the thermal expansion coefficient of oxide prediction model.

```
#M4 CTE of oxide prediction model
#Import data
import pandas as pd
iM4_data = pd.read_excel(r'D:\File\College\Y4_project\Raw Data CTE
14042023.xlsx','CTE oxide')
iM4_data = iM4_data.fillna(0)
rM4_data = pd.DataFrame(iM4_data,
columns=['Ti','Al','Cr','Fe','Ni','Co','Cu','Si','Y','Mn','Zn','Ta','Nb
','Zr','Mg','Tin','Tfi','CTE'])
#Define X and Y
import numpy as np
x_M4 =
rM4_data[['Ti','Al','Cr','Fe','Ni','Co','Cu','Si','Y','Mn','Zn','Ta','N
b','Zr','Mg','Tin','Tfi']]
```

Python code for M4 the thermal expansion coefficient of oxide prediction model. (continue)

```
y_M4 = np.ravel(rM4_data[['CTE']])
#Split data
from  sklearn.model_selection import train_test_split
x_M4_train, x_M4_test, y_M4_train, y_M4_test = train_test_split(x_M4,
y_M4, test_size = 0.3, random_state= 3)
#Import Ml algorithms
from sklearn.ensemble import RandomForestRegressor
modelM4 = RandomForestRegressor(random_state= 1)
from sklearn.tree import DecisionTreeRegressor
modelM4 = DecisionTreeRegressor(random_state= 1)
from sklearn.neighbors import KNeighborsRegressor
modelM4 = KNeighborsRegressor(n_neighbors = 2, p=1)
from sklearn.neural_network import MLPRegressor
modelM4 = MLPRegressor(random_state= 1)
#Training Ml algorithms
modelM4.fit(x_M4_train,y_M4_train)
yp_M4_train = modelM4.predict(x_M4_train)
yp_M4_test = modelM4.predict(x_M4_test)
yp_M4_all = modelM4.predict(x_M4)
#Check quality of model
from sklearn.metrics import mean_absolute_percentage_error
from sklearn.metrics import r2_score
print('[M4] CTE of oxide prediction model')
print("Training set")
print("MAPE: ", mean_absolute_percentage_error(y_M4_train,
yp_M4_train))
print("R2: ", r2_score(y_M4_train, yp_M4_train))
print("Test set")
print("MAPE: ", mean_absolute_percentage_error(y_M4_test, yp_M4_test))
print("R2: ", r2_score(y_M4_test, yp_M4_test))
print("All data set")
print("MAPE: ", mean_absolute_percentage_error(y_M4, yp_M4_all))
print("R2: ", r2_score(y_M4, yp_M4_all))
```